Winter 2015

CHARACTERIZING AND QUANTIFYING MARINE METHANE GAS SEEPS USING ACOUSTIC OBSERVATIONS AND BUBBLE DISSOLUTION MODELS

Liam Pillsbury
University of New Hampshire, Durham

CHARACTERIZING AND QUANTIFYING MARINE METHANE GAS SEEPS USING

ACOUSTIC OBSERVATIONS AND BUBBLE DISSOLUTION MODELS

BY

LIAM PILLSBURY

Mechanical Engineering (BS), University of New Hampshire, 2013

THESIS

Submitted to the University of New Hampshire
In Partial Fulfillment of
The Requirements for the Degree of

Master of Science
In
Ocean Engineering

December, 2015

This thesis has been examined and approved in partial fulfillment of the requirements for the degree of Master of Science in Ocean Engineering by:

Thesis Director, Thomas C Weber, Associate Professor of Mechanical Engineering

Larry Mayer, Director Center for Coastal and Ocean Mapping

Ruth Varner, Associate Professor of Biogeochemistry

On the 18th of November, 2015

Original approval signatures are on file with the University of New Hampshire Graduate School

ACKNOWLEDGEMENTS

I would like to thank Dr. Thomas Weber for his guidance as my thesis advisor, and for providing me with the opportunity to pursue my interest in Ocean Engineering. I also would like to thank my thesis committee who have helped support and improve this project and the DOE for funding my research.

Additionally, I would like to thank the faculty and staff at CCOM/JHC and my teachers throughout my six year pursuit here at UNH; please know that you have all contributed to my success.

Pillsbury 2015

DEDICATION

I would like to dedicate this thesis to my loving parents, Peggy and David, and my grandmother,

Eileen, who is dear in our hearts. This would not have been possible without your continued

support. I love you, always.

TABLE OF CONTENTS

Pillsbury 2015

LIST OF FIGURES

Pillsbury 2015

LIST OF TABLES

Pillsbury 2015

ABSTRACT

Characterizing and quantifying marine methane gas seeps using acoustic observations and

bubble dissolution models

by

Liam Pillsbury

University of New Hampshire, December, 2015

A method for characterizing and quantifying marine methane gas seeps along the U.S. Western Atlantic Margin was developed and applied to 70 free-gas seeps observed by the R/V Okeanos Explorer in 2012 and 2013, in water depths ranging from 300-2000 meters. Acoustic backscatter from an 18 kHz split-beam echo sounder and a 30 kHz multi-beam echo sounder provided information on the height to which the gas seeps rose from the seafloor. Profiles of the depth-dependent target strength and scattering strength were compared to models of the evolution of rising bubbles to help constrain the ultimate fate of the methane gas. To do so, a refined methodology was developed that decoupled the target strength of a bubble plume from the inherent background noise and reverberation in the ocean. This methodology was particularly useful for acoustically weak (i.e. low signal-to-noise ratio) seeps, and for examining the acoustic trends of seeps as their echo signature approached background noise levels. Comparisons of target strength profiles to models of bubble dissolution demonstrated that the parameters used in the model (e.g. gas transfer rate) are consistent with empirical observations.

Pillsbury 2015

1 INTRODUCTION

1.1 Marine Methane Gas Bubbles

Methane gas is important to study and understand due to its global impact as a greenhouse gas. During the transition period between the Paleocene and Eocene eras (~ 55 MA), a thermal maximum occurred in the atmospheric and oceanic records [Dickens et al, 1977]. Dickens et al (1977) theorize that the cause of this thermal maximum was due to a mass ebbullation of methane gas from the seafloor sediments released by the dissociation of methane hydrate due to increasing ocean temperatures. Once methane reaches the atmosphere, over a 100 year time scale it is roughly 33 times as effective at trapping heat in the atmosphere as the same quantity of carbon dioxide [Shindell et al, 2013]. The reservoirs of methane in the sea floor are estimated to contain over 100 gigatons of carbon, which is 4000 times the amount of natural gas consumed by the United States in 2010 [USGS, 2015]. With the concentration of methane in the atmosphere doubling over the past 150 years [Ehhalt, 1967], the contribution of oceanic methane to the atmosphere is being studied.

Oceanic methane is derived from two separate processes: biogenic and thermogenic methane production [USGS, 2015]. Biogenic methane is produced by bacteria in relatively shallow water areas (<1000 meters). Burial and decomposition of marine organic carbon by bacteria present in anoxic sediments of the seafloor produce methane as a byproduct of decomposition. Thermogenic methane is often found in deeper ocean environments (>1000 meters) or near geothermal features. Thermogenic methane is produced under high pressure and temperature environments by thermal degradation of organic matter and oil in ocean sediments [Schoell,

1

1983]. Biogenic oceanic methane is often found along the continental shelf where the burial rate of organic carbon is large [USGS, 2015]. Some of this methane escapes the sediments or is trapped by geologic features, but more often it is trapped in hydrates within the sediments. Hydrate is an ice crystal structure that forms under large pressures (>50 atm) and low temperatures at the interface between gas and water [USGS, 2015]. Methane hydrate is a type of hydrate that forms between methane gas and seawater. As the oceans warm, the hydrate near the edge of the stability zone (the zone within which the temperature and pressure are sufficient to form hydrate) could become unstable, potentially leading to an increase in methane release from the sediments into the ocean [Johnson et al 2015, USGS, 2015].

There are several methods of methane transport from the sediment to the ocean including local diffusion between sediments and seawater in regions where methane is present, and the release of methane bubbles into the water column. When the ocean is surveyed acoustically, free-gas bubbles, presumed to contain primarily methane gas [USGS, 2015], are observed ebullating from the seafloor and buoyantly rising upward through the water column.
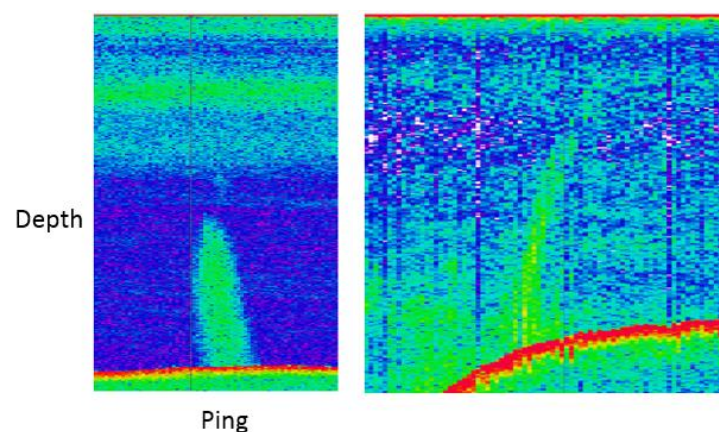
Figure 1: (Left) An 18 kHz EK60 echogram of a methane seep in deep water (2100m).
(Right) An 18 kHz EK60 echogram of a shallow water seep (300m)
Both echograms show the seafloor (red line) and consist of many EK60 pings (columns) along with the inclusion of a methane seep (vertical bright green) and the acoustic scattering layer (shallow horizontal green layer)

2

If the methane bubbles are dissolved in the deep ocean, the methane gas is assumed to be oxidized and stored in the ocean as carbon dioxide [Intergovernmental Panel on Climate Change, 1966], which contributes to ocean acidification and the depletion of oxygen in the ocean [USGS, 2015]. If the bubbles do not dissolve before reaching the surface ocean then they potentially transfer methane to the atmosphere. Understanding the fate and evolution of a bubble in the water column provides insight into the relative importance of these different outcomes (e.g. global warming, ocean acidification, oxygen depletion) [USGS, 2015].

When a bubble releases from the seafloor and starts to buoyantly rise through the water column, several factors affect the size and gas concentration of the bubble. As the hydrostatic pressure decreases with decreasing depth, the bubble size grows to accommodate the increase in volume of the methane gas (e.g. the same number of moles of methane at 2000 meters takes up a smaller volume than the same amount of moles of methane at 1000 meters). As the bubble rises, gas is transferred to and from the surrounding water column through the bubble wall. The gas exchange between the bubble and the ocean is governed in part by the relative gas concentrations in the bubble and in the water column surrounding the bubble. Methane is initially highly concentrated inside the bubble, and methane transfers from the bubble as the bubble works toward equilibrium in the generally under-saturated ocean water. As methane is being transferred out of the bubble, nitrogen, oxygen, and other gasses in aqueous concentration (e.g. carbon dioxide), not originally present in the bubble, are transferred into the bubble. Yamamoto et al (2009) showed that the local effect of methane saturation on the water column surrounding a methane seep could lead to a reduction in the gas exchange rate, causing bubbles that would have previously dissolved quickly to extend their lifetimes and ascend higher in the water column.

3

The rate of gas exchange depends on the difference between the aqueous concentration and the amount of gas inside the bubble, but also depends on the surface area and a fixed parameter (K) called the gas transfer velocity [Liss 1973; Leifer and Patro 2002]. K is parametrized by two distinct definitions; one for a 'clean' bubble with no inhibition on the bubble wall; and the other for a 'dirty' bubble with an inhibiting surfactant covering the bubble [Levich 1962, Jahne et al 1987, Clift et al 1978, Leifer and Patro 2002]. Hydrate coatings, created in the hydrate stability zone, inhibit the transfer of the methane gas by creating an ice shell that coats the bubble until it reaches the upper limit of the hydrate stability zone [Maini and Bishnoi, 1981; Rehder et al, 2002]. Oil coatings have also been observed as inhibitors to gas transfer [Solomon et al, 2009]. The gas transfer rate is also a function of the inclusions of surfactants, or particulate matter, which can cause a bubble with no obvious inhibition (oil or hydrate) to deviate its gas transfer velocity from either the 'clean' or 'dirty' classification [Johnson and Cook, 1981; Weber, 2005].

Two ways to analyze the methane gas flux from a seep include modeling of methane bubble dissolution and quantifying empirical acoustic methane gas seep observations. For modeling of gas bubble dissolution, the sensitivity of the model to certain parameters must be constrained. These parameters include the gas transfer velocity (K), aqueous methane gas concentration and the in-situ environmental parameters (i.e. temperature and salinity). An example output of the methane bubble model for a 5mm radius bubble released at 2100 meters is shown in Figure 2. The other outputs of the model include the bubbles gas fraction of methane, oxygen and nitrogen.

Pillsbury 2015
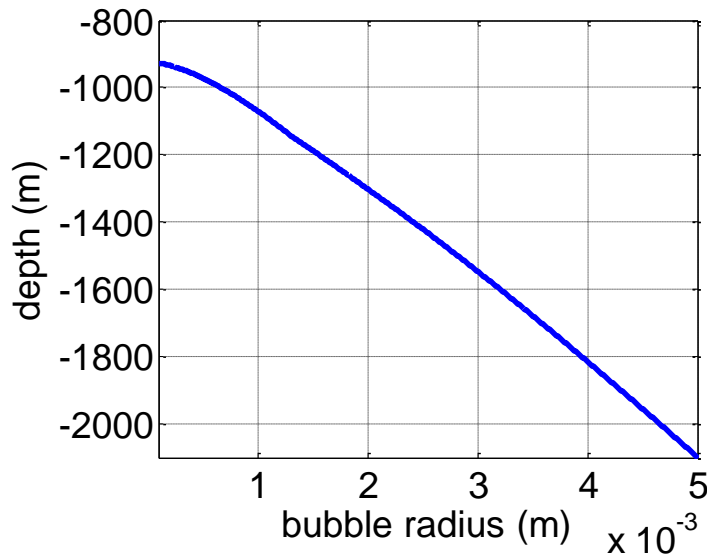
Figure 2: The bubble dissolution model results for a 5mm radius bubble released at 2100 meters and how its radius changes with depth until dissolution at ~900 meters

Another way to attempt a determination of the fate of methane gas from a bubble seep is using empirical acoustic observations (e.g. Figure 1). The seep echograms can be translated to target strength (TS) profiles to analyze the trends of bubble dissolution [e.g. Weber et al 2014, Jerram et al 2015]. The main difficulty associated with empirical observations, at least those using only one frequency, is the ambiguity between the size and number of bubbles.

In this thesis, the modeling and empirical observation approaches are combined. To do so, a TS model [Clay and Medwin, 1977] is added to a bubble evolution model similar to that developed by McGinnis et al (2006), making it possible to predict TS profiles from known, or assumed, source bubble size distributions. Comparisons with empirically observed bubble size distributions [Skarke et al, 2014] is then used to explore the model parameter space and to validate the bubble dissolution model.

5

Pillsbury 2015

2 METHODOLOGY: BUBBLE DISSOLUTION MODEL

As gas bubbles ascend through the ocean's water column, transfer of gasses into and out of the

bubble, along with changes in hydrostatic pressure, determine the size and evolution of the

bubble. Several models have been developed to determine the fate of a methane gas bubble in the

ocean. This study uses a recreation of a model originally compiled by Leifer and Patro (2002)

and later adopted by McGinnis et al (2006) to create a methane bubble dissolution model that

incorporated hydrate coatings. In the present work, an acoustic target strength (TS) model has

been added to this model. This makes it possible to link acoustic observations to bubble size

estimates and methane transport predictions. Recreating the bubble dissolution model also makes

it possible to explore the sensitivity of the model to its input parameters (e.g. aqueous gas

concentrations, temperature, salinity, gas transfer velocity (K)).

2.1 Gas Transfer Model Equations

The bubble dissolution model describes the fate of a gas bubble by calculating the transfer of

gasses into and out of the bubble as it ascends through the water column. Gas transfer includes

release of methane out of the bubble and into the surrounding water column and the transport of

oxygen, nitrogen and carbon dioxide into the bubble. The rate of gas transfer is an effect of the

partial pressure between the bubble's interior pressure and the ambient pressure of the ocean

surrounding the bubble. It is also a factor of rise velocity, presence of surfactants on the bubble

skin, bubble-water contact time, Henry's law coefficient, diffusion coefficient, concentration of

Pillsbury 2015

gas inside the bubble and the surrounding water column, and the local water column parameters

(i.e temperature and salinity). The equation for the rate of change of the bubble radius can be

derived from the modified ideal gas law shown in Equation 2 [Leifer and Patro 2002]. All

calculations are done using SI units [meter, Pascal, Kelvin].

$$P_b V = ZNRT \, , \tag{2}$$

where P_b is internal bubble pressure, V is volume of the bubble ($\frac{4}{3} * pi * r^3$ where r is the

bubble radius), N is number of moles, R is the universal gas constant, T is ambient temperature,

and Z is the compressibility factor calculated from the Peng-Robinson equation of state [Orbey et

al 1998]. The Peng-Robinson equation of state describes the deviation from the ideal gas law,

taking into consideration the compressibility of the non-ideal methane gas. Taking the derivative

of Equation 2 with respect to time yields

$$P_b \frac{dV}{dt} + V \frac{dP_b}{dt} = ZRT \frac{dN}{dt} \, . \tag{3}$$

The internal bubble pressure, P_b, is calculated from

$$P_b = P_{atm} + \rho_{water} * g * z + 2 * \frac{tau}{r} \, , \tag{4}$$

where P_{atm} is the atmospheric pressure, ρ_{water} is the density of seawater at z depth, tau is the

interfacial surface tension of the bubble and g is the gravitational constant.

7

Pillsbury 2015

Combing equations 3 and 4, and substituting $\frac{4}{3} * pi * r^3$ for V yields Equation 5

$$(P_b)\left(4\pi r^2 \frac{dr}{dt}\right) + \frac{4}{3}\pi r^3 \left(\rho_{water} g \frac{dz}{dt} - \frac{dr}{dt}\left(\frac{2tau}{r^2}\right)\right) = ZRT\frac{dN}{dt} \qquad . \tag{5}$$

Equation 5 can be rearranged to solve for the rate of change of the bubble radius [Leifer and Patro 2002]

$$\frac{dr}{dt} = \frac{R*T*[Z_{CH4}\frac{dN_{CH4}}{dt} + Z_{O2}\frac{dN_{O2}}{dt} + Z_{N2}\frac{dN_{N2}}{dt}] - \frac{4*pi*r^3}{3}*\rho_{water}*g*\frac{dz}{dt}}{4*pi*r^2*Pb - \frac{8*pi*r*tau}{3}} \qquad . \tag{6}$$

A Lagrangian particle (bubble) tracking method was used to calculate the dissolution of a methane bubble. By calculating Equation 6 and using the output to determine a new bubble size, the Lagrangian method tracks the evolution of the bubble size by continually calculating the change in radius over very small time steps and subtracting the difference from the previous bubble size until the bubble dissolves.

There are three main parts of Equation 6. The first term includes R*T*Z*dN/dt and describes the rate of change of the amount of gas in the bubble [Equation 7]. The second term describes the change in volume based on the change in hydrostatic pressure (rho*g*dz/dt), while the third term describes the internal bubble pressure (Pb) based on the bubbles radius (r) and surface tension (tau). In Equation 6, dz/dt is the rise velocity of the bubble and is negative for a bubble moving buoyantly upward. dz/dt is controlled by two equations from McGinnis et al (2006) describing the terminal rise velocity of a bubble. dN/dt, the rate of mass transfer in the bubble is

Pillsbury 2015

$$\frac{dN}{dt} = K * 4 * pi * r^2 * (C_{gas} - \frac{P_{b_{gas}}}{H_{gas}}) \text{ , [Liss 1973; Leifer and Patro 2002].} \qquad (7)$$

For each gas constituent shown in Equation 6, Equation 7 describes the rate of mass transfer of that respective gas. Mackay and Shiu (1981) define that at equilibrium $C_{gas_{bubble}} = P_{b_{gas}}/H_{gas}$. This definition helps to understand Equation 7, which is a function of the internal partial bubble gas pressure ($P_{b_{gas}}$), Henrys Law (H_{gas}), and the aqueous gas concentration (C_{gas}). Gasses such as methane (which are highly concentrated inside the bubble) degas, and the bubble dissolves due to the higher concentration of gas in the bubble than in the surrounding ocean. For gasses that are highly concentrated in the ocean (e.g N_2, CO_2, O_2) the dN/dt term is initially positive leading to an increase in the concentration of those gasses in the bubble, albeit a small effect [McGinnis et al 2006].

Figure 3 shows dN/dt as a function of depth for the number of moles of each gas and the bubble's gas fractionation for a dissolving 10 mm diameter methane bubble released at 2100 m. The trends observed in the exchange of nitrogen and oxygen through the bubble wall show an initial increase in the number of moles of each gas constituent inside the bubble. This molar increase continues until the concentrations inside and outside the bubble are in equilibrium. As the bubble continues to dissolve and the internal partial bubble gas pressure increases, the bubble degasses nitrogen and oxygen and the observed molar values decrease [Figure 3].

9

Pillsbury 2015
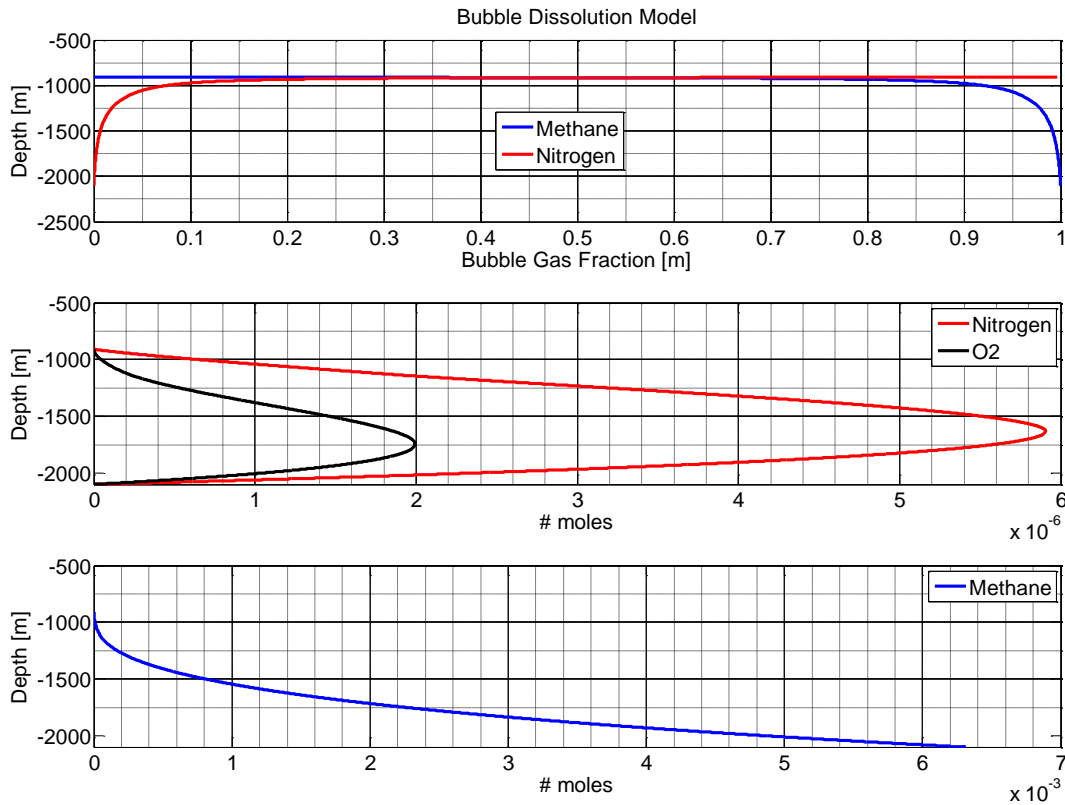
Figure 3: (Top) Shows the gas fraction of a bubble as a function of depth. At this depth there is very little oxygen, leading to a very small input of oxygen (not shown). CO2 is a trace gas and is negligible (also not shown). (Middle and Bottom) Shows the number of moles of each gas as a function of depth

K is the gas transfer velocity shown in Equations 10 and 11, C is the aqueous concentration of the gas, $P_{b_{gas}}$ is the internal bubble pressure for a gas constituent ($P_{b_{gas}}$=P_b* Molar Fraction) and H_{gas} is the Henrys coefficient for that gas constituent. Henrys Law is calculated from Rettich et al (1981).

$$H_{calculated} = H_{atm} * compressibility * \exp(-\frac{V_{mp}(P_b - P_{atm})}{R*T}) \qquad (8)$$

10

Pillsbury 2015

H_{atm} is the Henrys law coefficient for the respective gas at atmospheric conditions, the compressibility factor, different from the Peng-Robinson compressibility, is 1 for ideal gasses and for methane varies between .9 and 1.1 [USGS 2015]. V_{mp} is the partial molar volume at infinite dilution calculated using Equation 9 [Rettich et al 1981]

$$V_{mp} = \frac{\exp(3.541+(1.23e-3)*T)}{(100^3)} \tag{9}$$

Gas transfer velocity (K) for deep water bubble release is governed by Equations 10 and 11 [Clift et al 1978] and is a function of kinematic viscosity, v, and the diffusion coefficient, D. K values account for a generic 'dirty' or 'clean' bubble. A 'clean' bubble has no coating or inhibiting surfactants present on the bubble skin. The 'dirty' bubble classification includes a bubble with any inhibiting surfactant or covering (hydrate, oil, and particles) that affects the transfer of gas through the bubble-water interface. Gas transfer velocity for 'clean bubbles' is governed by equation 10 [Levich 1962] where D is raised to the (1/2)

$$K = 2 * sqrt(\frac{D*\frac{dz}{dt}}{2*pi*r}) . \tag{10}$$

K is raised to the (2/3) to account for the immobilization of the bubbles skin, used by McGinnis et al (2006) to account for the presence of a hydrate coating,

$$K = 0.45 * g^{0.3} * v^{0.3} * r^{-0.1} * \left(\frac{D}{v}\right)^{\frac{2}{3}} . \tag{11}$$

11

In Equations 10 and 11, D is the diffusion coefficient calculated from

$$D = \frac{13.26e-9}{\frac{mu^{1.14}}{V_{b_{Lebas}}^{0.589}}} \text{ , [McGinnis et al, 2006].}$$ (12)

The Lebas molar volume for methane is calculated using

$$V_{b_{Lebas}} = 0.285 * \frac{V_{C_{CH4}}^{1.048}}{0.9} \text{ ,}$$ (13)

where Vc_{CH4} is the critical volume of methane (98.6 cm^3/mole) found from Ambrose et al.

2.2 McGinnis et al (2006) Model Recreation and Parameter Sensitivity Study

The McGinnis et al (2006) single bubble model was derived from the rising fluid bubble model [Wuest et al 1992] which was evolved from the Epstein and Plesset (1950) model for gas transfer from a single, static bubble. The major differences from Wuest et al (1992) applied in the McGinnis et al (2006) model were the parameters for diffusivity and solubility, mass transfer coefficients, and rise velocities using values from the Leifer and Patro (2002) model. McGinnis used acoustic data of methane seeps observed and collected by Rheder et al (2002) and assumptions of a hydrate stability zone described by Maini and Bishnoi (1981) to calibrate his model. The major differences applied in the model in this paper in comparison with the McGinnis et al (2006) model were the calculations for bubble size [Figure 6]. The models are not a perfect match because the McGinnis (2006) model uses the number of moles of each gas (and

Pillsbury 2015

their rate of change) as the sole parameter for estimating bubble size (and its rate of change), while the new model uses Equation 6 from [Leifer and Patro, 2002] which more explicitly incorporates the Z factor from the modified ideal gas law.
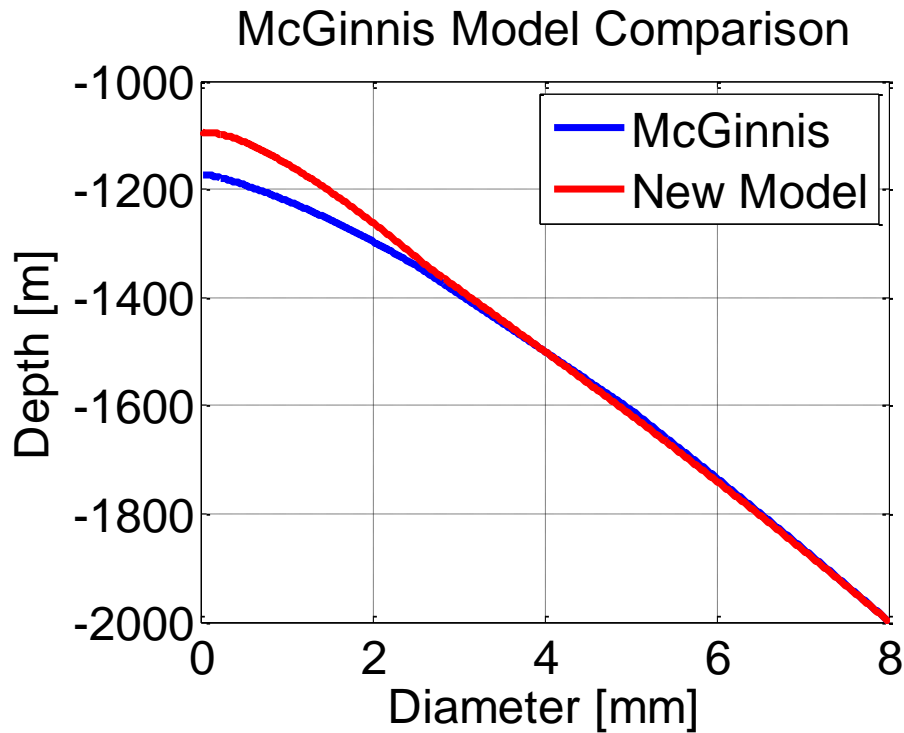
Figure 4: Comparison of the McGinnis (2006) model to the Pillsbury bubble dissolution model created in this study.

The McGinnis methane model is available as a GUI interface created in Python [Greinert and McGinnis, 2009]. The model was constrained by running iterations with each parameter to determine the models sensitivity.

These model calculations were processed using an algorithm developed in the programming language editor Matlab. The model inputs are shown below in Table 1.

Pillsbury 2015

Table 1: Examples of parameters used in the Matlab processing algorithm along with their respective units

Parameter	Value (example)	Unit
Initial bubble radius	5e-3	Meters
Bubble release depth	2000	Meters
Temperature, Salinity	6.5,35	Celsius, PPT
R, g	8.31, 9.81 (constants)	J/(mol K) , m/(s^2)
Initial molar fraction of methane in bubble	100 %	Moles CH4/total moles gas

To determine the McGinnis model's sensitivity to environmental parameters, a sensitivity study was performed. These parameters include temperature, salinity, and dissolved gas concentrations [Figure 5]. The model was run for an eight millimeter diameter bubble released at 2000 meters water depth. Table 2 shows the range of values used in the parameter sensitivity study, as well as the percentage of the dissolution depth of the bubble that was effected by varying the parameter from the maximum to minimum range value. The constants in this study were used based on values from McGinnis et al (2006) as well as literature studies on deep ocean gas concentrations [World Ocean Database (2015), USGS (2015)]. The saturation values show that the dissolved gas concentration constants used in this study were much less than the saturation values, which were calculated based on the pressure inside the bubble and the Henrys law coefficient for the respective gas.

Table 2: Parameter Sensitivity Study Results. The sensitivity percentage is the percent change in dissolution depth from the minimum parameter range to the maximum parameter range.

Parameter	Temperature	Salinity	Methane	CO_2	Oxygen	Nitrogen
Range	0-10 C	28-37 PSU	3E-08-3E-02 mmol/L	1E-05-1 mmol/L	0-1 mmol/L	.005-5 mmol/L
Sensitivity	.45%	2%	.05%	.23%	.35%	5%
Constant	4	35	3e-06 mmol/L	0.01 mmol/L	0.3 mmol/L	0.6 mmol/L
Saturation @2000meters			~387 Mol/L	~6.7e3 Mol/L	~372 Mol/L	~183 Mol/L

The range values for each parameter where evaluated based upon literature values and world ocean data available at the World Ocean Database. The upper and lower limits for temperature, salinity, and oxygen concentrations were found using the maximum and minimum values from CTD casts collected during the acoustic surveys. CO_2 is considered negligible in the methane gas bubble transfer process [McGinnis et al 2006] and Nitrogen was constrained by 2 orders of magnitude on either side of the accepted literature value [World Ocean Database, 2015].

First the dependence on temperature was constrained. As shown in Figure 5B, the model is not sensitive to temperature based on the assumption that at this depth the temperature is cold enough to form a hydrate shell (based on the input depth of GHSZ ~500m). The GHSZ is the gas hydrate stability zone and the upper limit is controlled by the ocean thermocline. A constant of 4

degrees Celsius was used to determine the dependence of other environmental parameters. If modeling bubble dissolution in shallow surface waters, temperature could become a larger factor.

Salinity was four times more sensitive than temperature over the range of values evaluated in this study, but still showed only a two percent effect on the dissolution depth [Figure 5A]. A constant of 35 PSU was used to determine the dependence of other environmental parameters.

Carbon dioxide and oxygen were both constrained by orders of magnitude within the model, shown in Table 2 and Figure 5E, 5F. The model was least sensitive to these gas constituents.

Nitrogen was more sensitive than the other gas constituents (excluding methane), but affected the dissolution depth by only 5% when raised an order of magnitude above the literature values for aqueous nitrogen concentration [Figure 5C].

As shown in Table 2, the methane concentration constant used in this study was 3E-06 mmol/L. This concentration, as a result of diffuse bubble methane saturation, would have to increase by as much as seven orders of magnitude for the dissolution depth of the bubble to be affected; within one order of magnitude from methane saturation [Figure 5D].

Pillsbury 2015
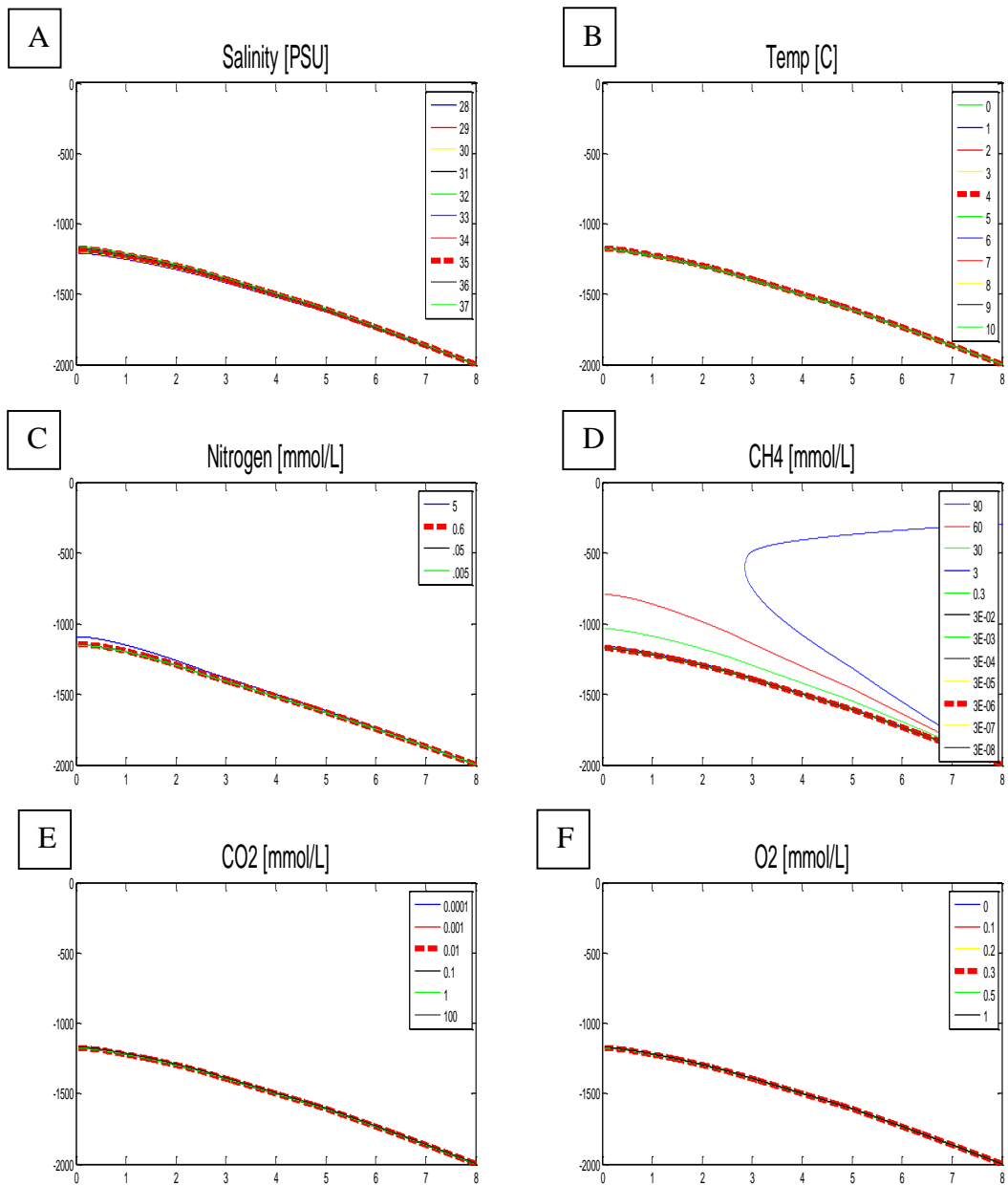
Figure 5: The plots demonstrate the models sensitivity to each parameter (y-axis depth [m], x-axis bubble diameter [mm]). The aqueous concentration of methane is a significant factor when the concentration approaches an order of magnitude from saturation.

17

A recent study by Yamamoto et al (2009), on methane saturation of the water column, determined that if local ocean currents are slow, dissolving methane bubbles can locally saturate the water column with dissolved methane. Saturation would inhibit the dissolution of the methane bubbles and cause the methane to reach higher in the water column, possibly as a source of methane to the mixed layer and the atmosphere [Leifer and Patro 2002].

For methane bubble dissolution studies, the local aqueous methane and nitrogen concentrations, the determination of the upper limit of the hydrate stability zone, and the determination of an accurate (K) gas transfer velocity are the most important parameters; constant values for temperature, salinity, and dissolved O_2, CH_4 and N_2 [Table 2] are used in the modeling of methane gas bubble dissolution. Constraining the bubble model parameters led to a more accurate comparison with the acoustic data.

2.3 Further Considerations of the Gas Transfer Velocity

The gas transfer velocity (K) classification for a 'dirty' bubble has a broad definition and is an area of interest for scientists in determining the effects of the different inhibiting coatings under the classification of a 'dirty' bubble. Leifer and Patro (2002) discussed the effect of a bubble coating and the decrease in circulation of gas inside of the bubble. This effect of the decrease in internal bubble gas circulation caused by the coating inhibits the gas transfer velocity under the classification of a 'dirty' bubble. Hydrate coatings, created in the hydrate stability zone, inhibit the transfer of the methane gas by creating an ice shell that coats the bubble until it reaches the upper limit of the hydrate stability zone [Maini and Bishnoi, 1981; Rehder et al, 2002]. Oil

18

coatings have also been observed as inhibitors to gas transfer [Solomon et al, 2009]. The gas transfer rate is also a function of the inclusions of surfactants, or particulate matter, which can cause a bubble with no obvious inhibition (oil or hydrate) to deviate its gas transfer velocity from the 'clean' classification [Johnson and Cook, 1981; Weber, 2005].

Johnson et al (1981) found that small oceanic bubbles persisted for a much longer duration than experimental results from pure water bubbles. This led to the conclusion that marine particulates were effecting the gas transfer through the bubble wall.

Weber et al (2005) studied the gas transfer rate of oceanic bubbles using acoustic observations of bubbles created in ships wakes and found that the bubbles persisted longer than any model accounted for; with a gas transfer rate approximately 15 times reduced. This difference could be an effect of surfactants covering the bubbles, which would lead the gas transfer rate to deviate from what was previously thought.

However, there is no part of the K value that takes into account the composition of the coating and how the gas transfers through the medium. There is also no account for the differentiation between a bubble coating that dissolves (hydrate) or one that does not (oil, particulates). Figure 6 shows an echogram of a methane seep observed at the Deepwater Horizon Oil Spill which shows oil coated bubbles surviving much longer in the water column than a bubble dissolution model for a 'dirty' bubble would account for.

19
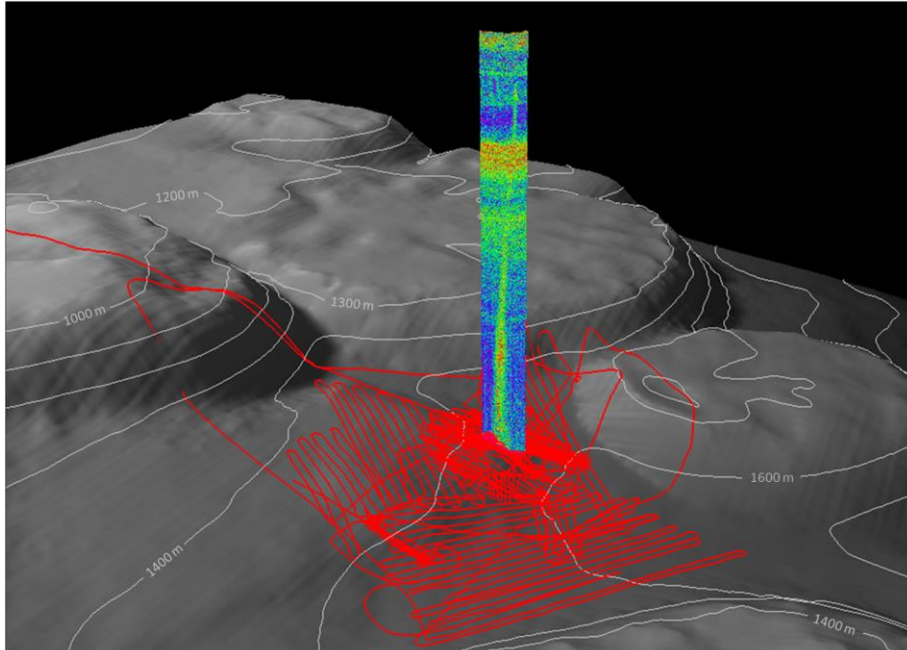
Figure 6: Methane seep echogram observed during the Deepwater Horizon Oil Spill showing a methane plume extending vertically through the deep scattering layer and surviving much longer in the water column than any modeling for a 'dirty' bubble predicts. Hickman, S. H., Hsieh, P. A., Mooney, W. D., Enomoto, C. B., Nelson, P. H., Mayer, L. A., ... & McNutt, M. K. (2012). Scientific basis for safely shutting in the Macondo Well after the April 20, 2010 Deepwater Horizon blowout.*Proceedings of the National Academy of Sciences*, *109*(50), 20268-20273.

This present work reviews the calculations for K and attempts to quantify the possible effects of the different types of coatings that inhibit bubbles gas transfer. This ambiguity of bubble coatings creates difficulties in calibrating a theoretical bubble model to describe the fate of methane gas in marine environments.

2.4 Incorporation of an Acoustic Target Strength Model

Gas bubbles in the ocean are excellent acoustic scatterers, with their loud acoustic response making them observable at great depths (full water column).

Clay and Medwin (1977) developed theoretical equations to determine the target strength of a gas bubble as a function of the total backscattering cross-section (σ) of a bubble, which for single targets is related to TS

$$TS = 10log_{10}(\sigma) \quad . \tag{14}$$

When the wavelength of the incident plane wave (at 18kHz the wavelength is ~ 8cm [Weber et al 2014]) is an order of magnitude larger than the bubble being insonified [Clay and Medwin, 1977], the equation for calculating σ is

$$\sigma = \frac{a^2}{\left[\left(\frac{f_{resonance}}{f}\right)-1\right]^2 + delta^2} \quad . \tag{15}$$

f is the working frequency of the transducer and delta is the damping coefficient due to the energy losses in a vibrating bubble of radius a. The energy losses are a combination of the thermal conductivity and shear viscosity at the bubble wall [Clay and Medwin, 1977]. When a bubble's radius is much smaller than the wavelength of the sound wave, the bubble scatters an omni-directional spherical wave. This is important because the total backscattering cross-section described in Equation 15 is specific to a bubble radiating an omnidirectional spherical wave. There are other theoretical target strength models [Anderson et al, 1950], yet the Clay and Medwin (1977) model has been shown to be accurate in predicting bubble sizes using an 18 kHz EK60 echo-sounder [Weber et al, 2014].

The resonance frequency $f_{resonance}$ is depth, temperature and gas constituent dependent. An example of the target strength as a function of depth and bubble radius is shown in Figure 7. The resonance peaks at four water depths are the respective TS peaks [Figure 7]. The radius of a

21

bubble that would resonate decreases with decreasing water depth. This is caused by the compressibility of the gas in the bubble. For two different sized bubbles to resonate at the same frequency, the mass-spring bubble system influenced by the compressibility of the methane gas must respond in the same oscillatory nature. For a bubble under large pressure the compressibility (not Peng-Robinson's in this case) decreases, leading to an increase in the stiffness of the 'spring'. This would lead to a larger bubble (at depth) resonating at the same frequency a smaller bubble would resonate at a shallower depth, due to the change in stiffness of the 'spring'.
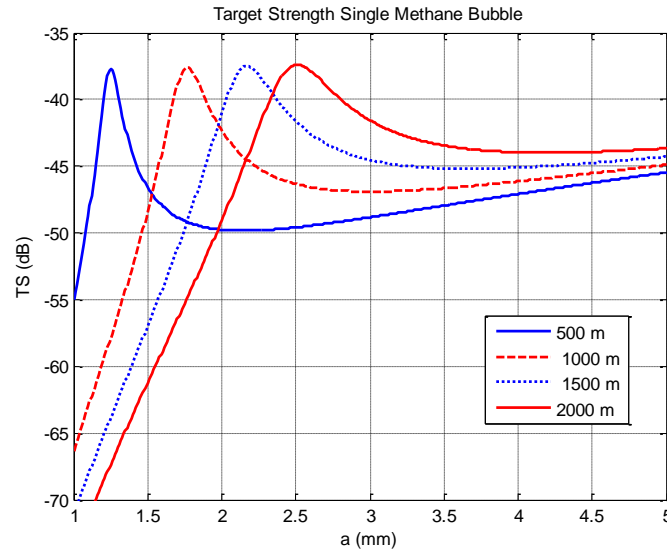
Figure 7: Target strength (TS) of a methane bubble showing resonance peak for four water depths.
TS is calculated based on the Clay and Medwin model [Clay and Medwin, 1977]

For a given water depth, a bubble larger than the respective resonant bubble size at that depth is still a strong acoustic scatterer; stronger than a bubble smaller than the respective resonant bubble size. A bubble is always a stronger acoustic target than a rigid sphere of equivalent size. This is because the acoustic cross-section of a bubble is several factors larger than the geometric cross-section (1000 times greater at resonance).

Pillsbury 2015

A resonating bubble dominates the acoustic response from a gas seep making observations of

other bubbles difficult. When using only one frequency, a strong acoustic target strength leads to

two conclusions: there are a large number of bubbles being insonfied away from resonance; or

there are much fewer bubbles being insonfied at resonance. This ambiguity can lead to

discrepancies in the quantification of a gas seep bubble size source distribution [Weber et al

2014]. However, using the trends of the target strength profile can lead to clarity of the bubble

size distribution by fitting different models of bubble size distribution dissolution and analyzing

the goodness of fit.
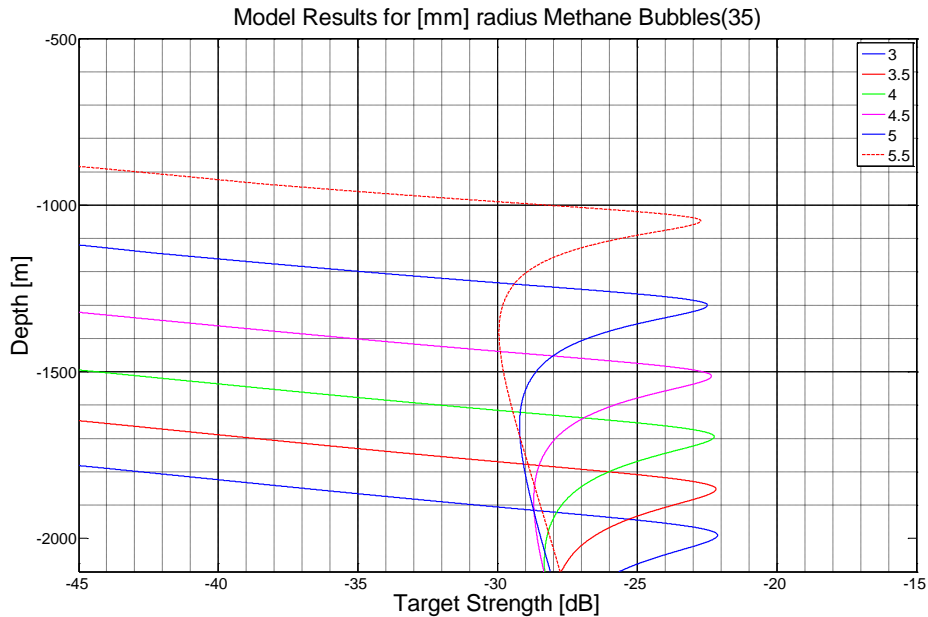
Figure 8: Theoretical target strength trends for different mm radius bubbles released at 2100 meters water depth
showing corresponding resonance peak

Figure 8 shows the output of the bubble dissolution model which has been translated to TS using

equations 14 and 15. The six bubble sizes shown demonstrate the difference in the dissolution

depth and the resonance peaks respective to certain model bubble sizes and depths.

23

3   ACOUSTIC OBSERVATIONS OF GAS BUBBLES

One of the ways we observe bubbles rising through the water column is using acoustic sensors. When an acoustic transducer sends a pulse of sound into the ocean, the echo is recorded by the transducer and is the measure, in terms of echo strength and time, of the echo arrival of targets in the ocean. Examples of targets include marine organisms, the seafloor, and gas bubbles [Figure 9].
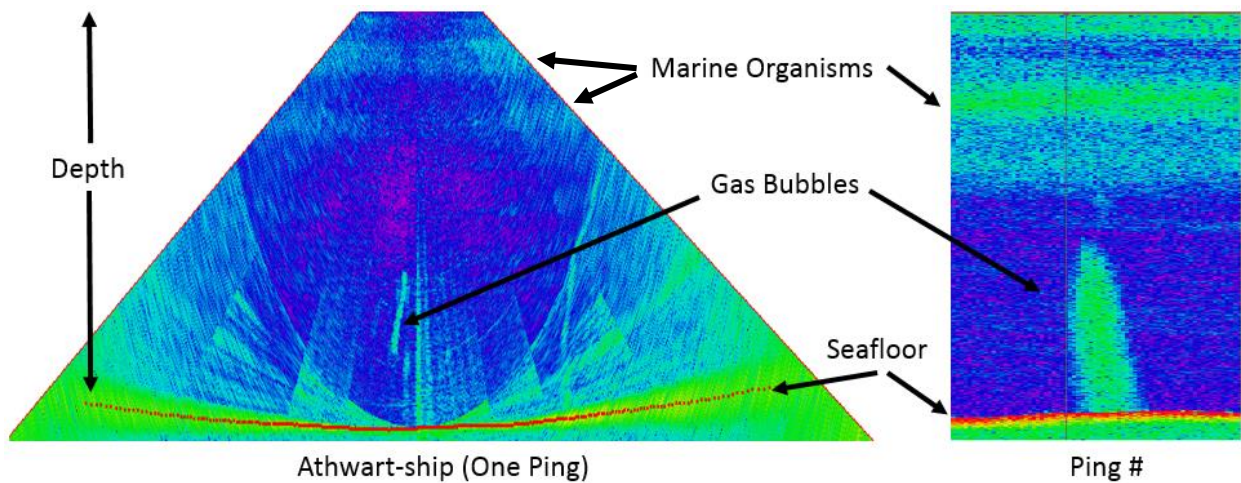
Figure 9: Echogram showing a methane seep rising through the water column in the 18 kHz EK60 (Right). An EM302 ping showing the full water column acoustic response and a seep rising through the water column (Left) Both show a seep rising from the seafloor at ~2100 meters water depth

There are several studies of methane gas seeps and bubble-mediated air-sea gas transfer using acoustic bubble observations. In-situ measurements of surface wave driven gas bubbles using acoustic backscatter were evaluated by Medwin et al (1970) who used a broadband echo-sounder to study the gas bubbles in shallow coastal waters. Medwin et al (1970) used the bubble resonance peaks and the rise velocity to determine bubble size and estimated the number of bubbles based on the acoustic backscatter; demonstrating that acoustic measurements could constrain gas bubble in size and number. Merewether et al (1985) observed deep ocean gas

Pillsbury 2015

bubbles and hypothesized that some film or layer protected them based on observations of bubbles surviving longer than expected. Merewether et al (1985) evaluated the two-phase methane based on the compressibility and reflectivity of the different size bubbles and their different coatings and calculated the target strength of a bubble whether covered with a hydrate skin or not; but did not look at the effect of a hydrate coating on the bubble-ocean gas transfer. The bubble-ocean gas transfer process was looked at in detail by Rheder et al (2002) who used an ROV to study naturally occurring bubbles in a deep ocean environment and discussed the onset of a hydrate coating that inhibited bubble dissolution. Greinert et al (2004) looked at the methane bubble gas flux from a seep using the resonant frequencies including higher acoustic frequencies and the bubble's damping coefficient. The flux results determined by Greinert estimated that 50% of the methane gas in a seep is transported by the largest 7% of the methane bubbles, with diameters greater than 7 mm. An attempt to determine the flux of methane gas in the Gulf of Mexico over a 6000 km^2 area [Weber et al 2014] used quantitative estimates of the bubble size source distribution and the gas flux rate as observed by ROV's and compared these results to the acoustic response. Weber et al (2014) estimated the total flux of methane from the 6000 km^2 area "to be between 0.0013 and 0.16 Tg/yr, or between 0.003 and 0.3% of the current estimates for global seabed methane seepage rates", [Weber et al 2014]. As examined by Jerram et al (2014), flux estimates for seeps vary spatially and temporally, limiting the repeatability of results and deterministic quantification of a free-gas seep. Jerram et al's (2014) study showed how estimates of seep flux can change temporally on scales as short as an hour and how gas flux can change spatially meaning that seeps can 'turn off' and new ones can appear where there were none previously. All of these studies set the foundation for an in-depth look at the bubble-ocean

Pillsbury 2015

gas transfer process and modeling of bubble dissolution calibrated with acoustic measurements, as well as possible conclusions about the fate of methane gas from a marine methane seep.

3.1 18 kHz Ek60

The EK60 is an 18 kHz split-aperture echo-sounder (SBES), which for the experiment described here was set to use a 4 millisecond pulse [Jerram 2014]. The nature of a split-aperture echo-sounder is the transducer face is split into sections, and the comparison of backscatter from each section enables the ability to calculate the electrical angles (athwart-ship and along-ship) to a target, allowing for the ability to locate the target in the acoustic beam [Burdic, 1991]. This was useful in two ways: estimating the location of the seep in the acoustic beam to determine if the top of the seep was 'cut off' by the narrow beam of the transducer (if the acoustic data captured the complete bubble dissolution) [Figure 10]; and for calibrating the target strength estimates.
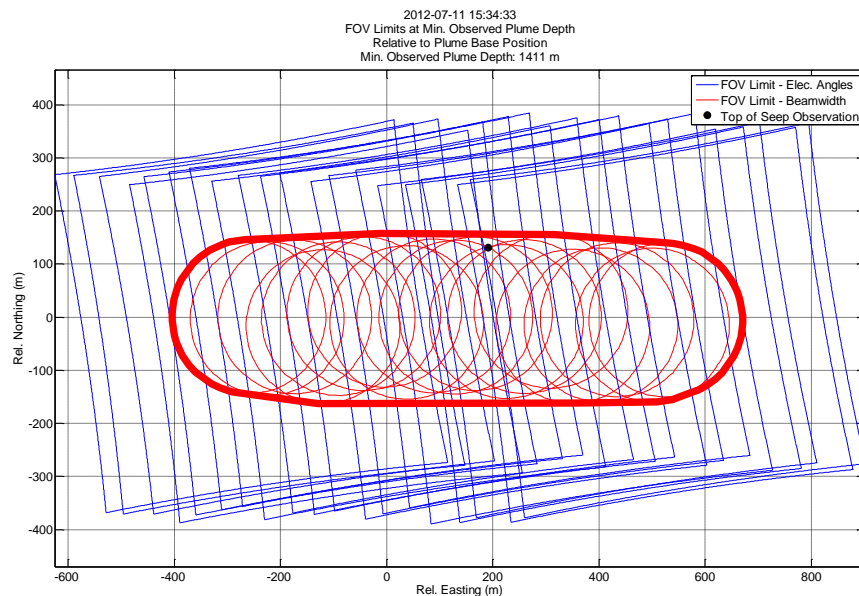
Figure 10: Shows the black dot as the top of a seep, and how it was captured in the transducers field of view. Easting and Northing are based on the ship position and direction. This enabled the conclusion that the entire seep was captured in the echogram of the EK60

The ability to locate targets in the beam also enables a TS correction for targets located in the extremities of the acoustic beam, where the TS is biased weaker than if the target was in the center of the beam. Therefore a beam pattern of angular target strength offsets was created using a calibration sphere with a known acoustic target strength which was swung throughout the acoustic beam as acoustic measurements was collected. From the electrical angles and the TS measurement of the sphere, a relative TS beam pattern was interpolated and used for calibrating the system [Figure 11]. The beam pattern corrected for the parts of the seep that were not captured on the MRA or 'main response axis' of the EK60 transducer by using the respective electrical angles recorded by the transducer, and adding the target strength offset of the calibration beam pattern at those respective angles. Using this method the true target strength for all objects in the acoustic beam was calculated.
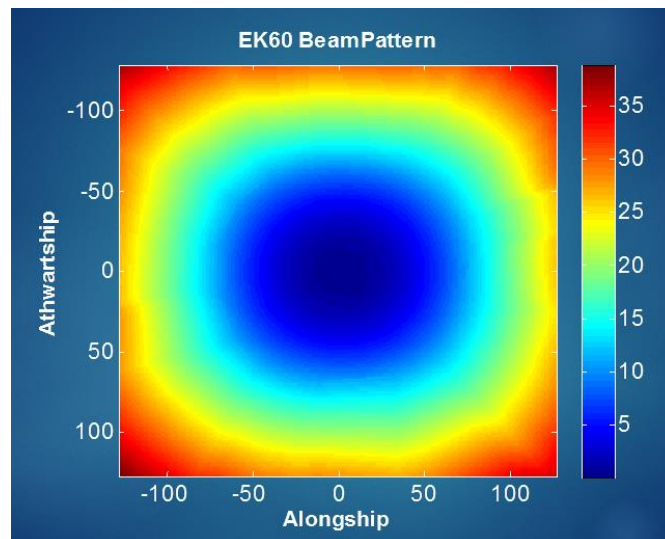
Figure 11: 18KHz EK60 calibration beam pattern. Color bar is target strength offset in dB.

As shown in Figure 12, the edges of the gas plumes often appear 'weak', even though the seep should be mostly uniform in a horizontal section. The seep does not appear uniform because as the ship passes over the seep, demonstrated by the angles in the along ship direction, the seep is

at the limits of the transducers beam as the ship approaches and leaves the seep; this accounts for the loss in target strength for a target at the extremities of the acoustic beam (and makes the seep edges appear weak). After accounting for the beam pattern, the seeps appear more uniform.
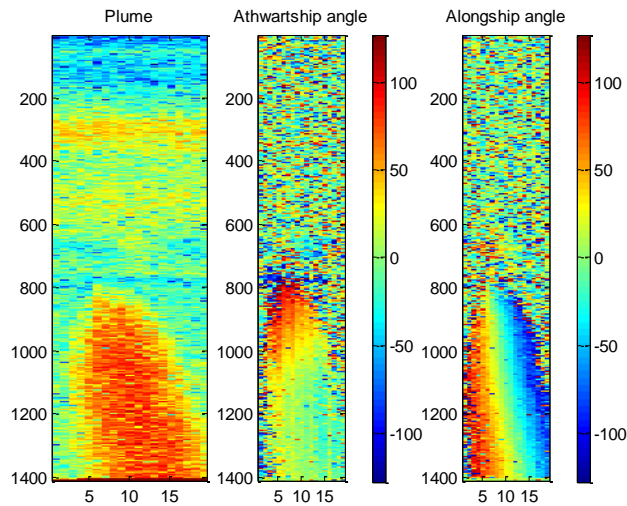
Figure 12: Y-axis is sample # and x-axis is ping #. SBES 18 kHz EK60 showing a methane seep and its corresponding along-ship and athwart-ship electrical angles. The angles help determine if the top of the seep was cut off by the view of the narrow acoustic beam, and for reference when calibrating the backscatter using the beam pattern

Figure 13 shows two horizontal transects of TS for the seep shown in Figure 12, both before and after the TS corrections have been applied. The corrected TS is more uniform for each ping than the original data. This is the expected result of applying the relative TS measurements based on the calibration beam pattern.

The transects show that for the samples 960 and 1230, at the respective electrical angles from Figure 12, the TS corrections demonstrate the ability to correct the seep TS. For sample 960 [Figure 13] the electrical angle is large for all pings [Figure 12], leading to a large correction for all pings; and for sample 1230 only the edges of the seep are corrected based on the respective electrical angles from Figure 12.

28

Pillsbury 2015
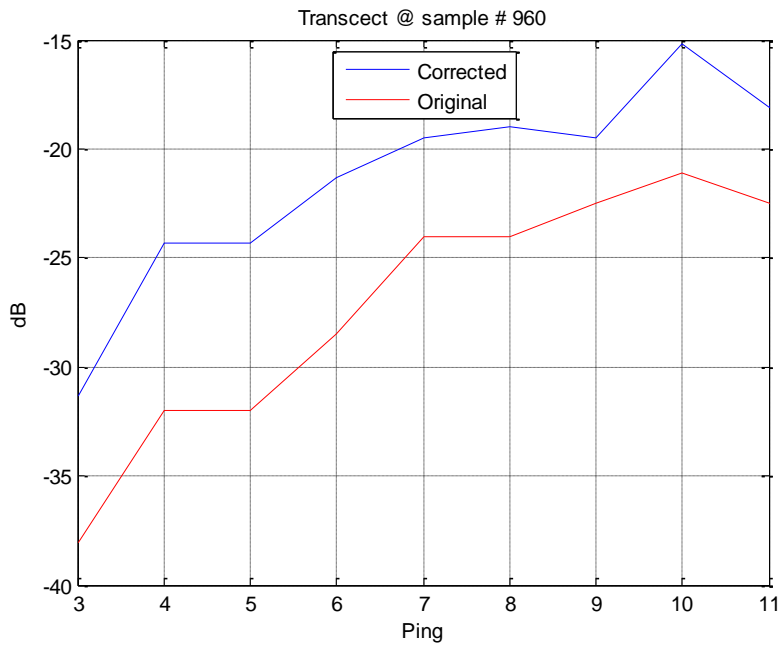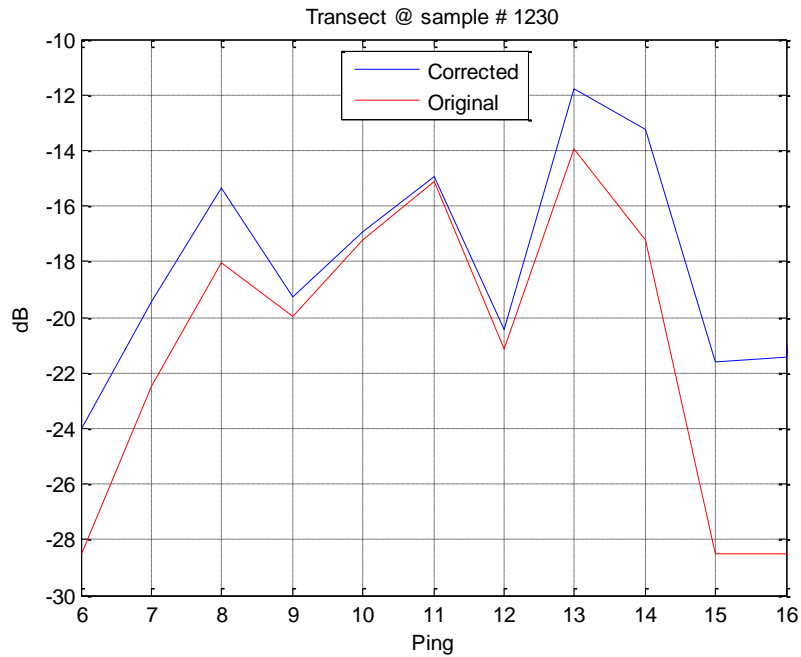
Figure 13: Two horizontal transects of the TS of the seep shown in Figure 12, both before and after the TS corrections have been applied. (Top) shows where just the edges of the seep need to be fixed (for along-ship angle). (Bottom) shows where the seep was corrected for all pings (based on the athwart-ship angle)

The EK60's calibrated TS measurements were used for processing the seeps and

deterministically quantifying the acoustic data.

29

Pillsbury 2015

3.2 Processing of Acoustic Backscatter

After determining that the observed seep in the EK60 data was indeed a discrete target and completely captured by the EK60's acoustic beam, analysis of the amplitude return from the bubbles was started using the process created by Jerram et al (2014). Using Jerram et al's (2014) *seep hunter* code, the seep and 30 surrounding pings were selected (in Matlab) and saved as 'plume plus noise', and the pings surrounding that selection where no seep was present was saved as 'noise'. The selection of noise surrounding the seep is done to evaluate the amount of inherent noise included in the 'plume plus noise' selection. To estimate true target strength values (which are needed to compare to bubble evolution models), the background noise of the ocean must be subtracted from the seep to evaluate the true acoustic response from just the bubbles. The echogram in Figure 14 is in Sp [dB], which is TS uncorrected for the beam pattern.
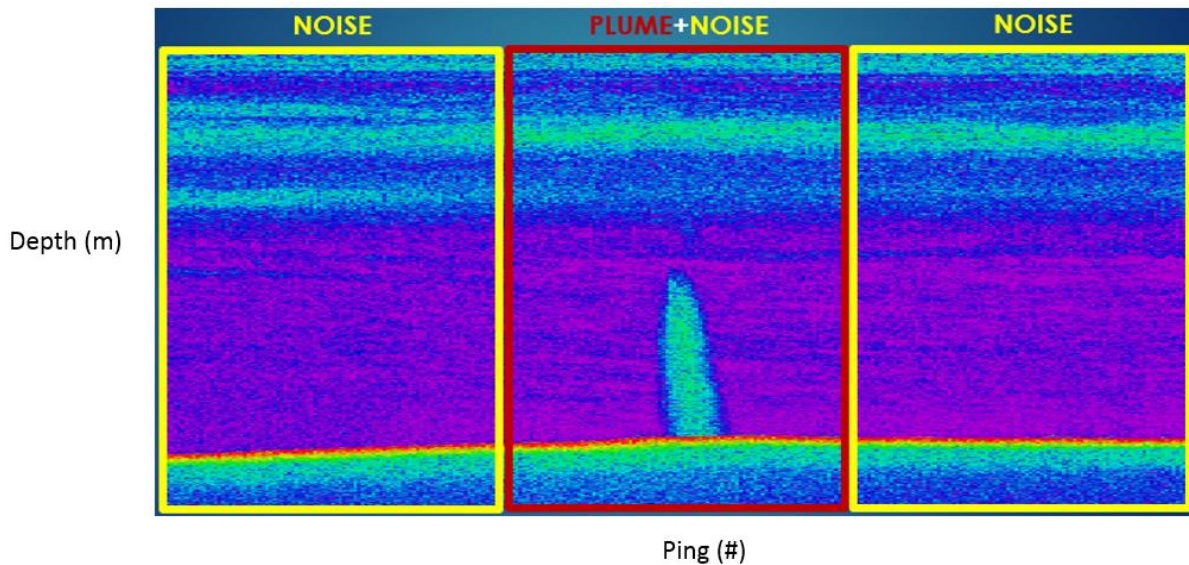
Figure 14: Echogram showing selection of seep and noise and only noise. red/green colors are strong acoustic targets and purple/blue are weak acoustic scatterers.

Pillsbury 2015

To accomplish this task of de-coupling the plume from the inherent background noise, Jerram et al (2014) averaged the noise into one profile and created a Sp profile as if the noise in the ocean were targets, where N is the total number of pings in the noise subset of the echogram

$$Intensity_{noise\ averaged}(z) = ((\frac{1}{N})\sum_{i=1}^{N} 10^{Sp_i(z)/10}) \quad , \qquad (16)$$

and z is depth,

$$Sp_{Noise}(z) = 10log_{10}(Intensity_{noise\ averaged}(z)) \quad . \qquad (17)$$

The Sp noise profile shows the trends in background noise in the echogram [Figure 15]. The increases in noise at ~ (800, 500 and 100 meters) is due to the biological scattering layers. The seafloor reverberation at ~2100 meters gives a loud acoustic response increasing the noise to greater than 0dB. The window of opportunity to observe seeps is where the noise is lowest (1000-2100 meters).
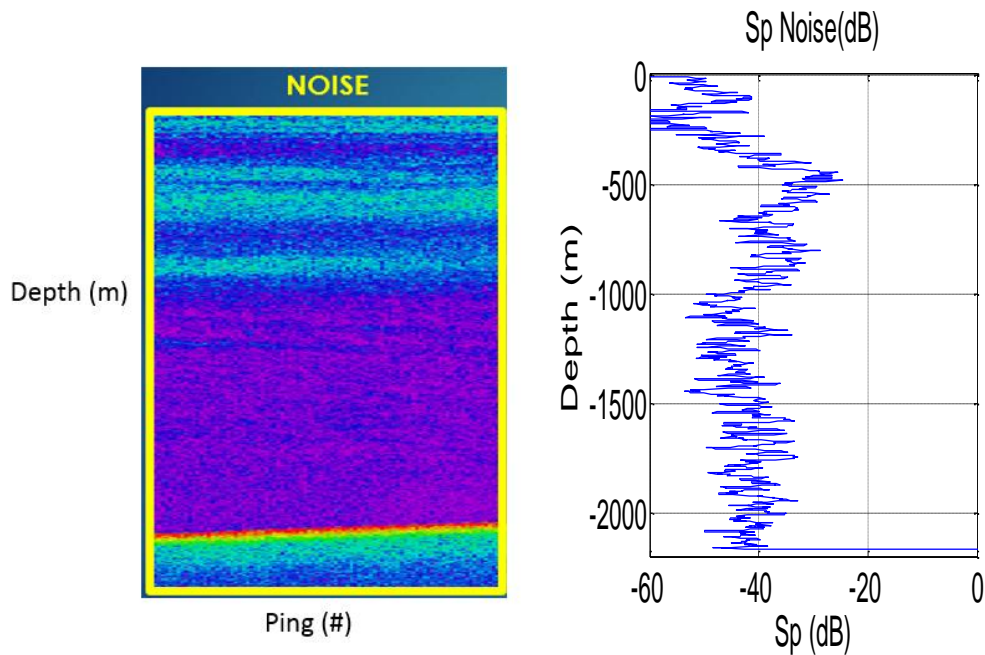
Figure 15: Shows the noise average profile. The sharp increase in dB at ~2100 meters is the response from the seafloor. The window of opportunity to observe seeps is where the noise is lowest (1000-2100 meters)

31

Pillsbury 2015

After calculating the background noise profile, the subset of 'plume plus noise' was threshold filtered. This filter eliminated weak targets (below 40dB) and strong targets (above 0dB ~seafloor reverb). After the mask filter was applied, the data was filtered again using a SNR (signal to noise ratio) of 10dB. Adding the SNR of 10dB (in the intensity domain) to Equation 16 created an intensity threshold

$$Intensity_{Threshold} = Intensity_{noise\ averaged} * 10^{\frac{10}{10}} \quad . \qquad (18)$$

The SNR filter only passed targets that were above the intensity threshold; eliminating targets in the data set that were less than 10dB above the background noise. The targets that survive both filters are then corrected for the beam pattern using angle dependent corrections based on the SBES calibration and then georeferenced for vessel position, vessel attitude, orientation of SBES transducer, and refraction of acoustic ray path. Figure 16 shows the output of Jerram et al (2014) filtering process for the seep echogram shown in Figure 14.
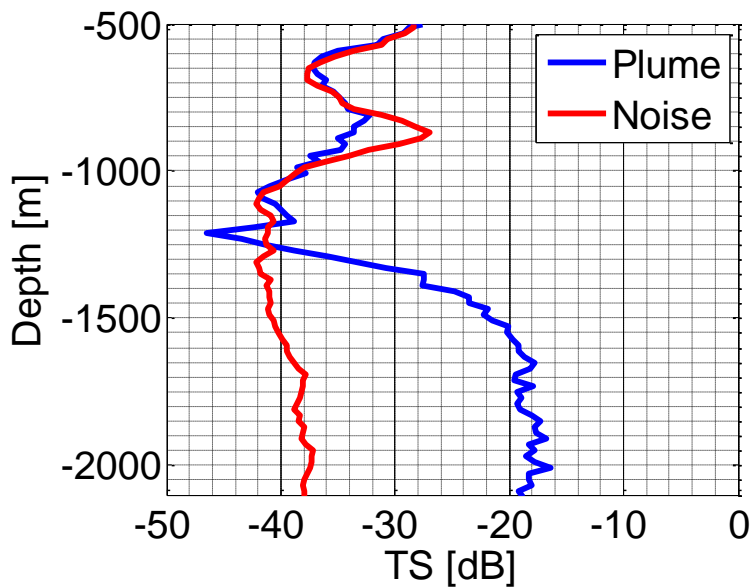
Figure 16: Strong seep, uncorrelated profiles with a large SNR (~ 20dB)

Pillsbury 2015

For strong seep targets (with acoustic returns from the seep much greater than 10dB above the background noise) this process worked as can be seen by the uncorrelated noise and plume profiles in Figure 16. From the plume profile, seep metrics that describe the trends observed in the acoustic data can be analyzed; for instance the dissolution depth, lack of resonant bubbles, and slope of dissolution and decay can all be analyzed for Figure 16. All of these metrics will be used in comparing acoustic trends to models of bubble dissolution by visually matching the trends seen in the empirical data to trends of bubble dissolution to estimate bubble size. Figure 16 shows a weak SNR seep and the output of the filtering process. The same metrics described above are used to determine the trends seen in the acoustic data for Figure 17. However, over a limited extent of the seeps true shape, this noise filtering process correlated the noise and the seep profile. This noise-following behavior has been observed in other work (e.g. Weber et al 2014). Unfortunately, the crucial seep metrics lie in the portion of the acoustic profile that seems to follow the noise floor. This noise following behavior is explained in Figure 18.
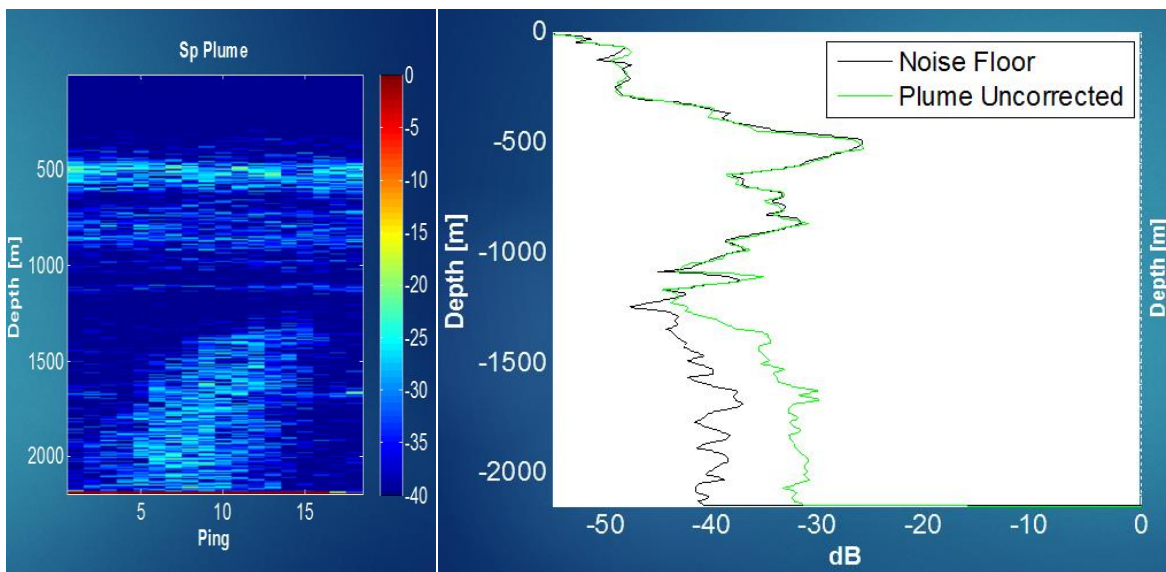
Figure 17: weak SNR seep showing correlated portions of the noise and plume profiles

33

Figure 18 shows examples of what could be the resulting Sp plume distribution for a strong SNR seep [left Figure 18] and a weak SNR seep [right Figure 18] using the SNR threshold filter. For a strong seep the mean of the resulting plume distribution is very similar to the actual plume distribution mean. For the weak seep the average of the resulting plume distribution shows significant error estimating the actual plume distribution mean. The resulting plume distribution average does not appear to estimate the correct plume average based upon the original plume distribution. This is due to the SNR thresholding process. The threshold eliminates weak seep targets and contributes strong noise targets to the estimation of the average plume profile (based upon 10dB threshold). Even though the weak seep plume profiles do not follow the exact threshold of 10dB, the filtering process strongly correlates the seep profile to the background noise profile.
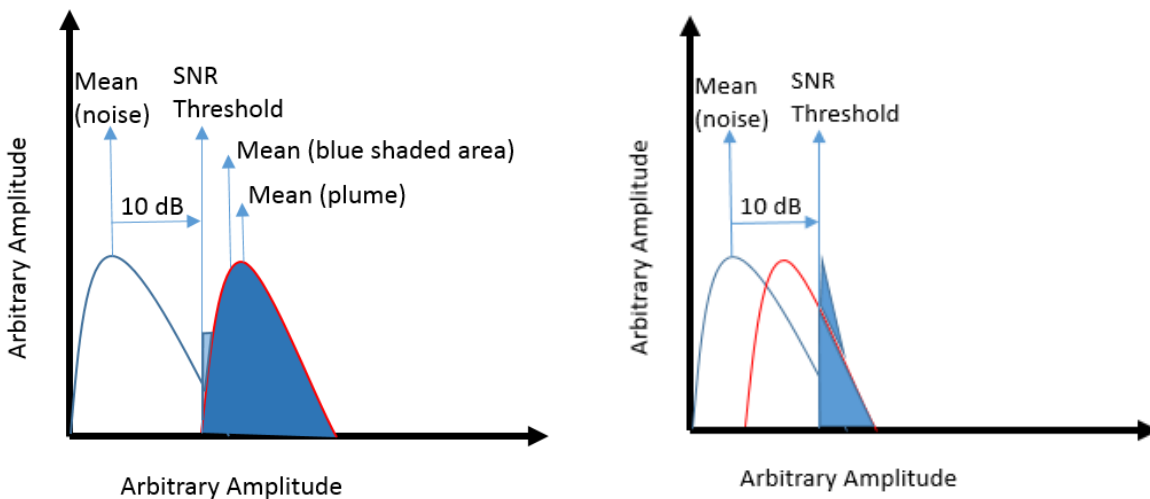
Figure 18: Shows Rayleigh distributions of plume and noise (pressure amplitudes), and the SNR threshold effect on plume average. (not to scale)
(Left) shows an example of a SNR threshold filter for a high SNR seep. The average of the blue shaded area is very similar to the average of the plume distribution.
(Right) as the SNR decrease, the error in the SNR threshold filter increases, leading to a very different average for the plume than estimated by the blue shaded area

Pillsbury 2015

The solution to this error of SNR filtering is found by recognizing that the area under the

resulting plume distribution does not accurately represent the distribution of plume [Figure 18].

The solution relies on estimating the parameters of the noise distribution, with an inherent

assumption that the noise is stationary, and using these estimated parameters to decouple the

plume from the noise. This new filter is based upon the assumptions that both the seep pressure

amplitudes and the noise pressure amplitudes are Rayleigh-distributed random variables. For the

plume, this assumption is examined by analyzing a very high SNR plume. This is because the

noise in the selected plume was considered negligible and would not affect the plume

distribution analysis.

Using the KS-test in Matlab the amplitudes of the noise and the plume were shown to be

Rayleigh distributed random variables. Showing that the pressure amplitudes for both the seep

and noise at the working frequency of 18 kHz is Rayleigh distributed allows for a new filtering

process to replace the SNR filter. A Rayleigh sum distribution model was created, using the fact

that two summed Rayleigh distributions equal a Nakagami distribution [Beaulieu 1990, Hu et al

2005].
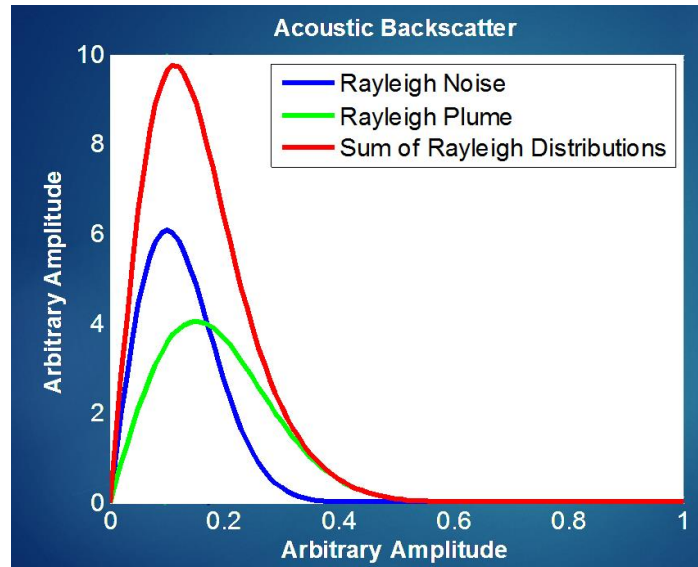
Figure 19: Shown are distributions of plume, noise, and sum of the distributions (plume plus noise) which is Nakagami distributed

Once the Rayleigh distribution parameter for the noise was calculated, the remaining Rayleigh distribution of plume (the true plume with no inherent background noise) could be evaluated. By creating a processing algorithm in Matlab, the distribution of Rayleigh distributed 'plume' was evaluated by iteratively guessing at the 'plume' Rayleigh parameter. Each plume parameter guess was added to the known Rayleigh distribution of background noise to create an estimated Nakagami distribution of "seep plus noise". This newly created Nakagmi distribution was compared to the observed Nakagami distribution from the 'plume plus noise' subset [Figure 14]. The comparison of distributions was evaluated to determine if the Nakagami distributions were equivalent. If they were equivalent, than the 'plume' Rayleigh parameter for the seep was determined to be that of the guessed Rayleigh parameter.

A Rayleigh parameter was created for each ping in binned values of 20 depth samples (for robust, accurate processing).The process for evaluating and comparing the two Nakagami

36

distributions involved the Kolmogorov-Smirnov (KS2) test. The KS2 test determined with 95% probability whether two independent samples come from the same distribution. This processing was done over a range of possible seep parameters and the KS test examined the best match between the guessed and observed distributions. This led to a 'true plume' target strength estimate using the calculated Rayleigh parameters. The output of the Rayleigh sum distribution algorithm is shown below in Figure 20.
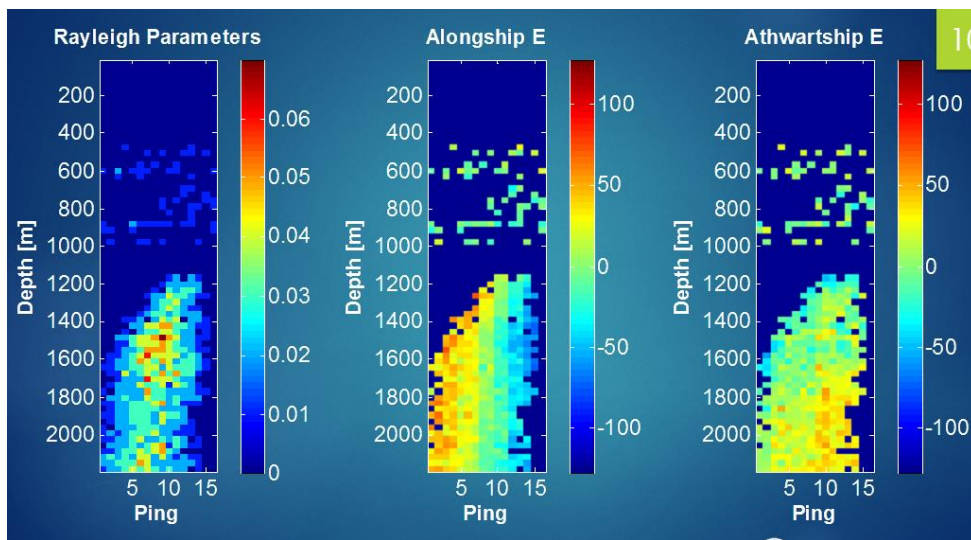
Figure 20: The binned Rayleigh parameters, and the respectively binned along-ship and athwart-ship angles (for calibration purpose). The noise is not completely coherent (as can be shown by the weak targets surviving high up in the water column (horizontal trend)

From the Rayleigh parameters, which describe the acoustic return from the plume bubbles, the target strength was calculated. Figure 21 shows the uncorrected TS (Sp) calculated from the Rayleigh parameters from Figure 20, as well as the TS corrections based on the electrical angles from Figure 20, and the final corrected TS.

Pillsbury 2015
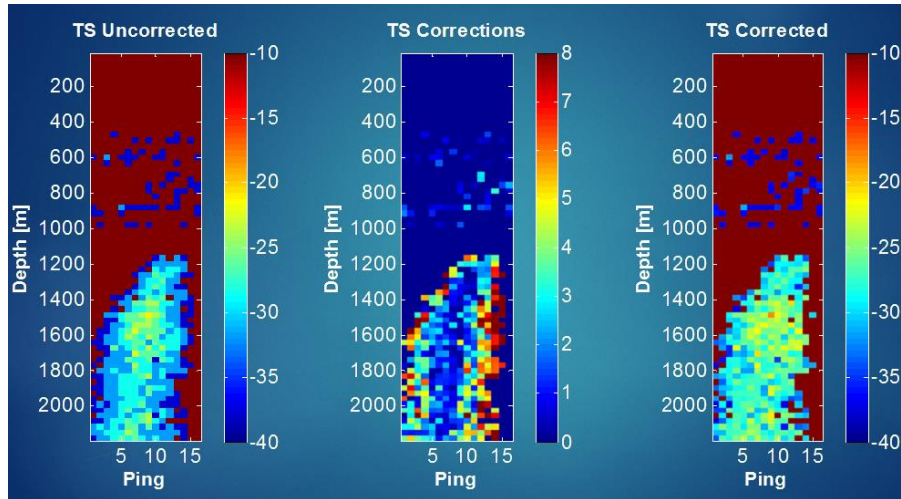
Figure 21: Shows the TS of a seep calculated from the Rayleigh parameters and the resulting TS corrections, and the corrected TS seep (right) showing a more uniform seep, as expected.

After the TS corrections are applied, the seep appears more uniform in the horizontal. Figure 22 shows the output TS profile of Figure 21, and how it compares with the previous estimate of the plume TS profile. The new plume profiles in a seep with large SNR also led to a more accurate representation of the seep metrics.
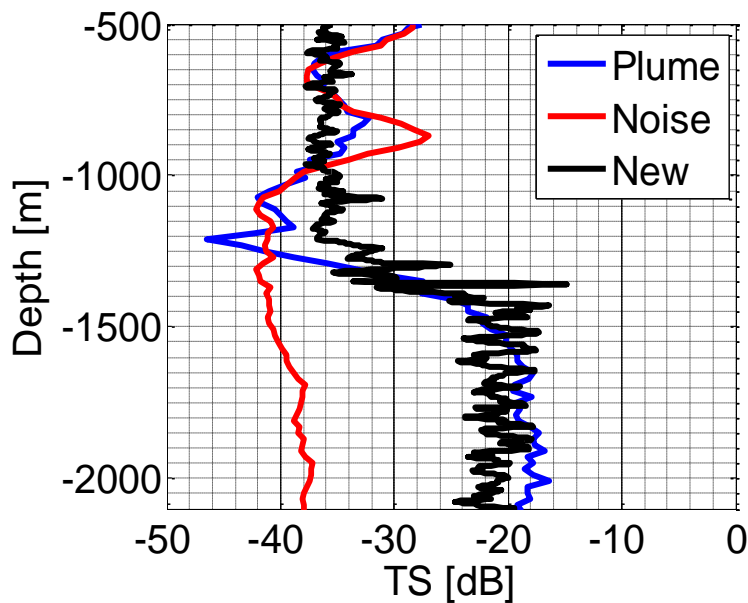
Figure 22: Strong seep showing the TS profile from the new Rayleigh distribution filter compared to the previous TS profile from the SNR filter

38

Pillsbury 2015

Figure 22 shows the slope of decay between the new and old plume profiles was significantly affected by the new filtering process. This would affect the result of the comparison to models of methane gas bubble dissolution. An example of a weak SNR seep is shown in Figure 23. The new filtering method using Rayleigh distribution parameters instead of the SNR threshold appears advantageous when comparing seep metrics to models of bubble dissolution.
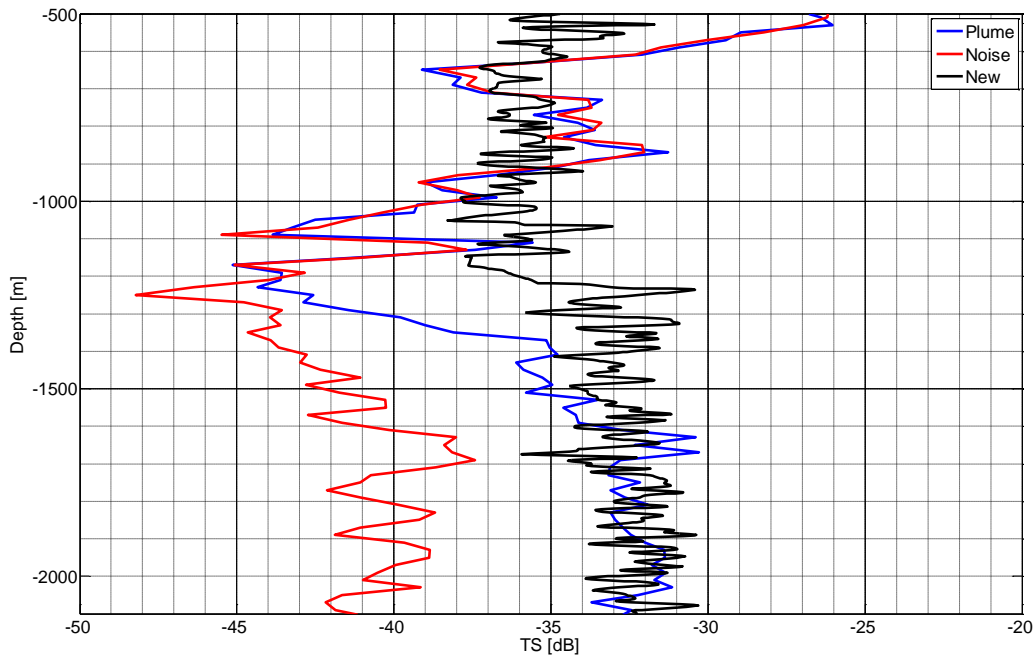
Figure 23: weak SNR seep showing a corrected TS profile (same seep from Figure 17)

From this new TS profile, the trends of the profile were compared to single bubble model runs. The trends that were observed were the resonance peak(s), slope(s), and height of decay or where the profile disappears into the background noise. The trends were then compared to different size bubble models to determine which bubble size was dominant for each seep, or if a particular bubble size source distribution would account for the observed TS profile.

39

Pillsbury 2015

4 COMPARING MODEL AND ACOUSTIC DATA

4.1 Acoustic Gas Seep Observations

Acoustic data was collected along the continental shelf of the East Coast of the United States over a span of two years (2012, 2013); five cruises in 2012 (1201, 1204, 1205L1, 1205L2, 1206), and two cruises in 2013 (1301 and 1302) [Skarke et al, 2014]. Figure 24 shows the majority of seep observations occurred along the continental shelf at depths ranging from 1500 to 200 meters, with the inclusion of seep 1205L1 @~2200 meters. The shallow seep observations, less than 100 meters water depth, are estimated to be the primary sources of oceanic methane to the atmosphere [McGinnis et al 2006].
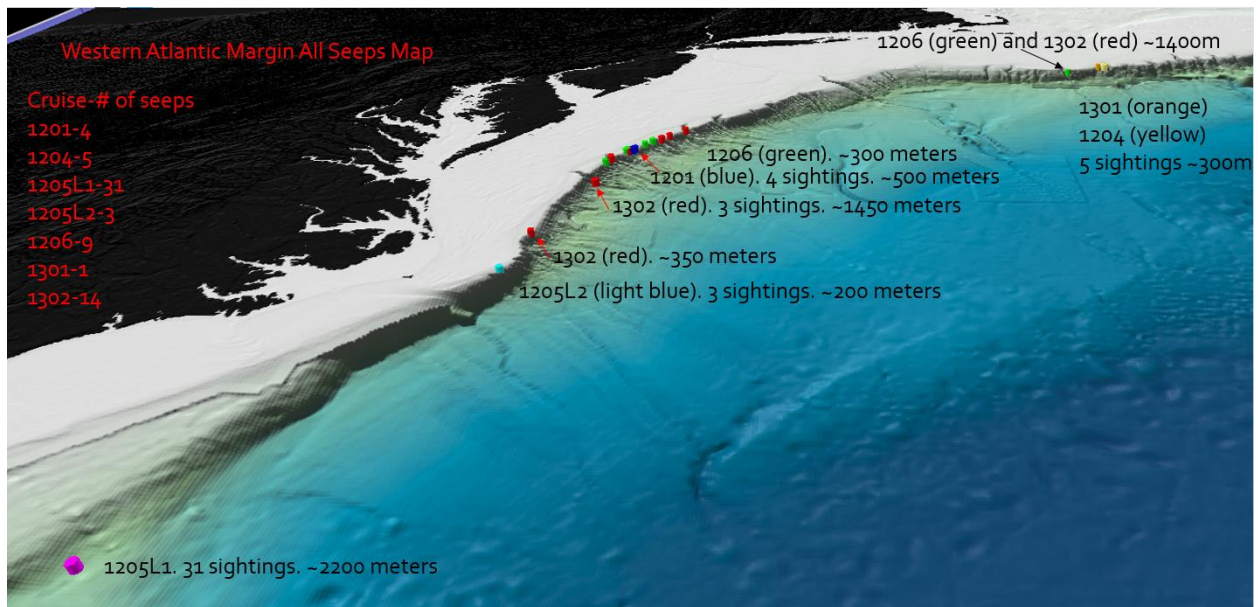
Figure 24: Map of all seeps observed along USAM

Before the cruises shown in Figure 24 (not including 1205L1), there were only three known

seeps observed on the Western Atlantic US Margin. Now that there are hundreds of seep

observations, the origin of the methane and the stability of the hydrate in the region are

significant. The extent of the acoustic survey covered the entire US east coast with 57% of the

seep observations occurring between Cape Hatteras and Hudson Canyon [Skarke et al, 2014].

The NOAA E/V Okeanos Explorer identified over 700 observations of bubble plumes in the

EM302 backscatter (due to its wide field of view and high resolution backscatter) during the

2012 and 2013 seasons between Georges Bank and Blake Ridge. Skarke et al (2013) compiled a

list of those observations in an excel spreadsheet including: latitude, longitude, cruise #, depth,

line, date and time. This information was used to find possible seeps in the EK60 echograms

(which was done visually using FMMidwater, a QPS Fledermaus product). If the seep

observations were captured in the EK60 in its full form (base to dissolution), than the echogram

was saved for further processing. The emphasis on capturing the 'full form' of the seep is to fully

capture the bubble evolution, which elucidates the comparison to the bubble dissolution models.

Comparisons of the saved echograms (73 in total ~ index number) rise height seen in the EM302

and EK60 are compared to distinguish variability in the observations between the two echo-

sounders [Figure 25]. For the majority of the seep observations the dissolution depth agree

between the echo sounders. Figure 25 also shows that shallow water seeps appear to make it

much closer to the ocean surface than deep water seeps which agree with McGinnis et al (2006).

Pillsbury 2015
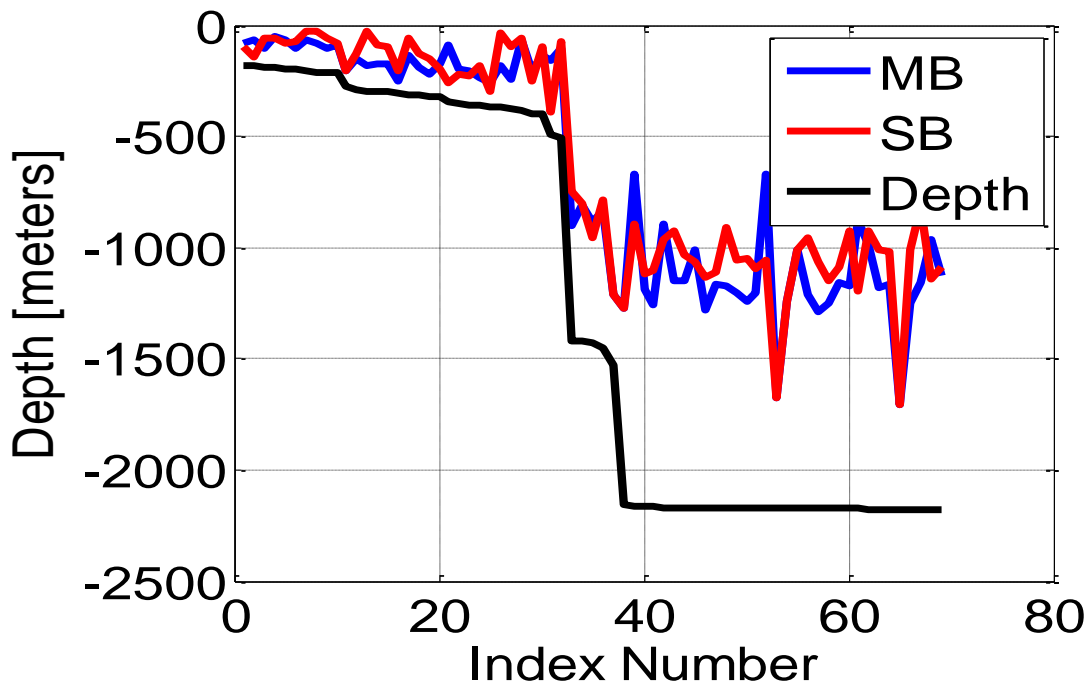
Figure 25: Comparison of the rise heights seen in both the EK60 and EM302 transducers, compared visually in a Fledermaus tool FMMidwater. Index numbers 45 and above refer to seep 1205L1

There were several sightings of the 1205L1 seep with great resolution, including a few observations with large SNR and complete plume observations. In Figure 26, it appears that one can observe the bubbles dissolving (or at least becoming acoustically unobservable). If the bubbles were to dissolve at the depth of acoustic disappearance, the methane would not reach the atmosphere, but could contribute to ocean acidification and local oxygen depletion.
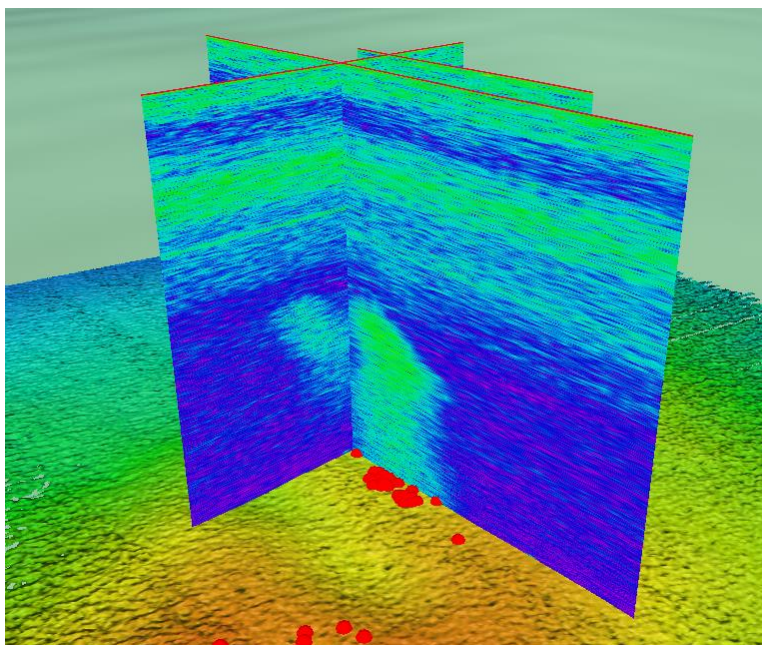
Figure 26: EK60 Echo-grams over-laid to show repeat passes over the same area, leading to investigations of temporal evolution

The numerous EK60 measurements made of 1205L1 lead to an interesting comparison to the bubble dissolution model, and could help elucidate the distinction between a large number of non-resonant bubbles and a smaller number of resonating bubbles. Using the seep observations that appear similar in amplitude evolution and SNR, the methane flux estimates can be compared.

4.2 Environmental Parameters used in the model

CTD (conductivity-temperature-depth) casts collected near in time to the acoustic observations where possible, and from the WOD [World Ocean Database, 2015] where not, were used to capture water-column environmental data [Figure 27]. This environmental data was used to

43

calculate the local upper limit of the gas hydrate stability zone, and to input in-situ parameters into the bubble dissolution model for accurate processing.
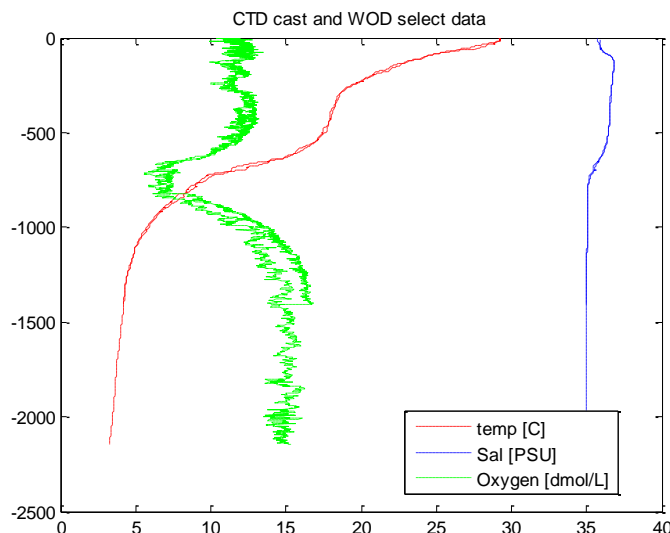
Figure 27: CTD data from deep water site and WOD aqueous oxygen concentration

Of significance was the aqueous concentration of methane which was in the micromole range throughout the water column, several orders of magnitude lower than found in the anoxic sediments [Reeburgh, 2007]. Brewer et al (1978) showed that surface ocean waters are generally supersaturated in CH4 in relation to the atmospheric concentration, but the dissolved CH4 concentration shows a rapid depletion with water depth caused by methane-oxidizing bacteria. The dissolved methane concentrations local to a seep, or local to sediment diffusing dissolved methane, was difficult to quantify due to the potentially large gradient of decay for dissolved methane as distance increases from the source [Reeburgh, 2007]. A study [Mau et al, 2007] on dissolved methane concentrations local to a seep off the coast of southern California showed dissolved concentrations of methane ranging from 1 to 10 micromoles per liter, increasing with

44

decreasing water depth. Mau et al (2007) found that the highest concentration of dissolved methane near an ebbulating methane seep was 20 micromoles per liter, several orders of magnitude less than saturation values. Similarly, a study of the sedimentary methane concentration of Blake Ridge showed sediment concentrations upwards of 100 micromoles per liter in a limited amount of pore water samples [Paull and Ussler, 2004], with pore samples showing an average of 1.5 micromoles per liter. This average is well below the concentration values that would observably impact the methane dissolution models described in Chapter 2 (see Figure 5).

Another significant dissolved gas in the study of dissolving methane gas bubbles was nitrogen. Nitrogen is abundant in the ocean, leading to relatively constant dissolved concentrations throughout the major ocean basins. Figure 1.7 B of [Gruber, (2008)] showed the dissolved concentration of Nitrogen, and all profiles appear to distinguish 1 micromole as the maximum nominal dissolved nitrogen concentration.

4.3 Data/model comparisons

Trends in the acoustic TS profile can be evaluated to determine possible bubble sizes by comparison to the trends of bubble dissolution. Comparisons of the slope and resonance height of the acoustic data to the methane bubble dissolution models help to constrain the acoustic data to certain bubble sizes. When the acoustic slope and resonance match a respective model, the assumption can be made that the dominant acoustic bubble size of the methane seep is of that

45

model bubble size. The resonance peak is specific to a bubble size and water depth, and the increase in target strength of the resonance peak is a method of determining the median bubble size, bubble size evolution, the depth of bubble dissolution, and the fate of the methane gas in the bubble. It is important to note that this comparison only tests the consistency between the model and data; with only a single acoustic frequency, ambiguity remains in the true bubble-size distribution.

The focus on model comparisons to empirical data collected from the 1205L1 seep site is for several reasons: several repeat observations of the full acoustic profile with great SNR allow for more accurate model comparisons; 1205L1 is well within the hydrate stability zone leading to analysis of hydrate dissolution; and the seep was captured in several pings decreasing the error in the TS profile calculations.

Since the model comparisons for 1205L1 are constrained to bubble sizes released at 2100 meters water depth, model families were created in increments of 0.1 mm from 2mm radius to 5.5mm radius. Bubbles smaller than 2mm radius would not resonate at this depth and would be hidden in the acoustic signature of the larger bubbles; therefore, bubbles under 2mm radius @2100 meters water depth are largely acoustically invisible when larger bubbles are present. The modeled dissolving bubble radius as a function of depth was translated to acoustic target strength, which was then compared to the EK60 acoustic data.

46

An example of the empirical data from site 1205L1 is shown below [Figure 28] and is compared to TS models of bubble dissolution. The empirical data was constrained to certain bubble size models by visually analyzing the goodness-of-fit.

Figure 28: An example of the empirical data from site 1205L1 compared the TS models of bubble dissolution. From this evaluation the empirical data is constrained to a bubble size ~5mm in radius which compares well with the ROV observations collected by Van Dover et al (2003)

Figure 28 shows that the empirical acoustic data was constrained to a 5mm radius bubble by visual comparison to different bubble size TS models. This 5mm radius bubble compares well with the ROV observations of a 1cm diameter bubble from Blake Ridge [Van Dover et al, 2003], although there is a decade between these two measurements.

47

Pillsbury 2015
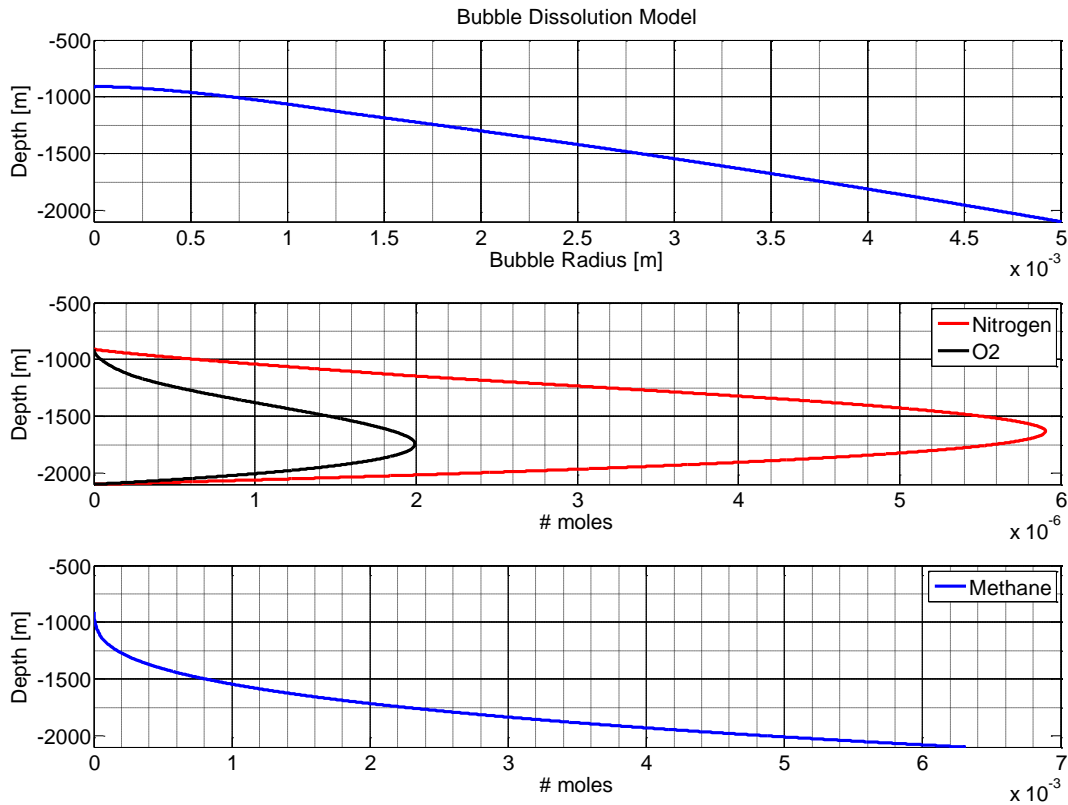
Figure 29: The outputs of the bubble dissolution model for a 5mm radius bubble released at 2100 meters water depth. These outputs include the degassing of methane, the transfer of nitrogen and oxygen into and out of the bubble as it ascends through the water column, and the dissolution of the bubble leading to a bubble size depth-dependent profile. From the model one can estimate the dissolution depth of the bubble to be ~900 meters

Figure 29 shows the outputs of the bubble dissolution model for a 5mm radius bubble released at

2100 meters water depth. These outputs include the degassing of methane, the transfer of

nitrogen and oxygen into and out of the bubble as it ascends through the water column, and the

dissolution of the bubble leading to a bubble size depth-dependent profile. From the model one

can estimate the dissolution depth of the bubble to be ~900 meters water depth. The vast

majority of the methane transfer (~85%) occurs in the first 500m of the bubble rise, between
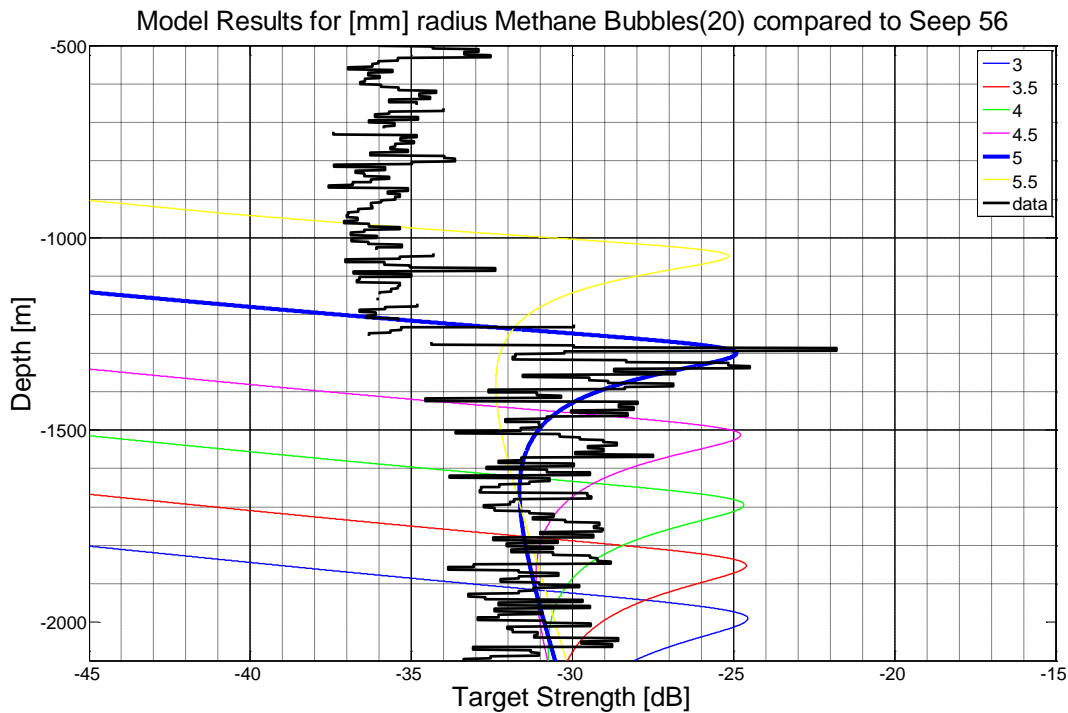
2100m and 1600m water depth.

Pillsbury 2015
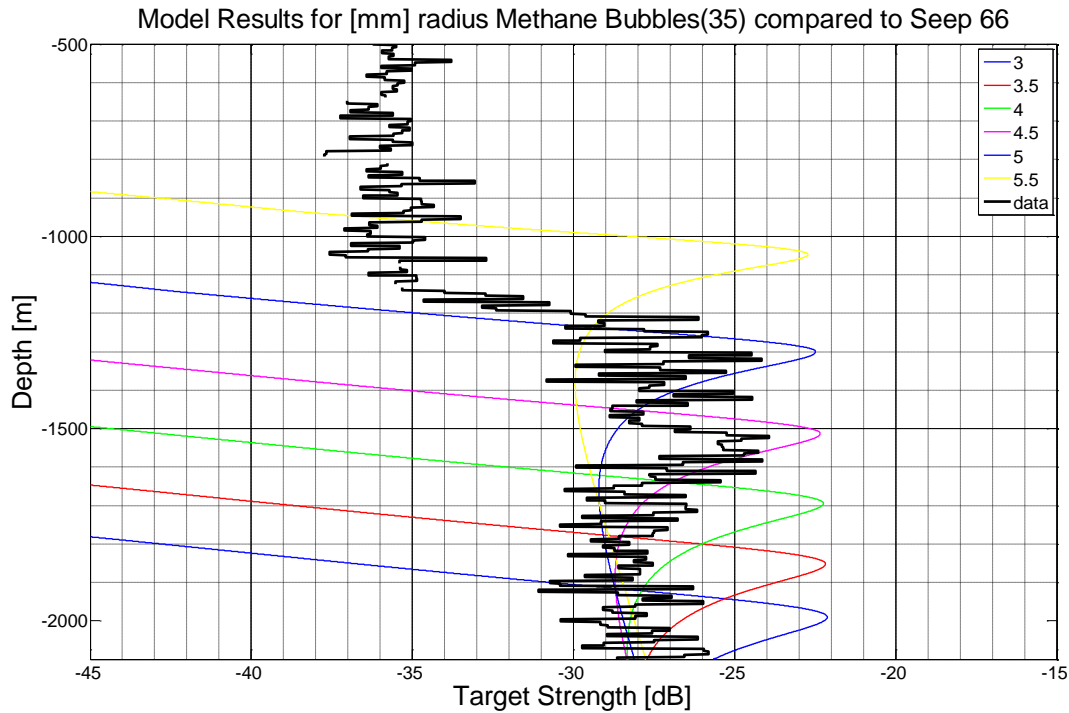
Figure 30: An example of the empirical data from site 1205L1 compared the TS models of single bubbles. From this evaluation the empirical data appears not to be constrained to a single bubble size.

An example from the empirical acoustic data showing a methane seep TS profile that does not appear to follow the trends of a single bubble size TS model are shown above [Figure 30]. The resonance peak in Figure 30 appears to be stretched vertically (1300-1600m) compared to a trend of a single bubble size (e.g. 1250-1350m in Figure 28). Therefore, the conclusion was to fit a uniform distribution of bubble sizes to try and account for this stretched resonance peak. To estimate the bubble size source distribution, a large bubble size TS model that would account for the slope of decay in the empirical data was estimated to be of ~5.2 mm radius. Then, smaller bubble sizes were iteratively added until the resonance peak of the estimated bubble distribution appeared to fit the resonance peak of the empirical data. The TS model for the source distribution that appeared to fit the empirical data [Figure 30] is shown below in Figure 31. The source

49

distribution that appeared to fit the acoustic data from Figures 30 and 31 was a uniform

distribution of bubbles ranging from 4.4-5.2 mm radius. To account for the empirical TS model

there are 4 of each bubble size (in increments of 0.1 mm) per unit meter water depth.
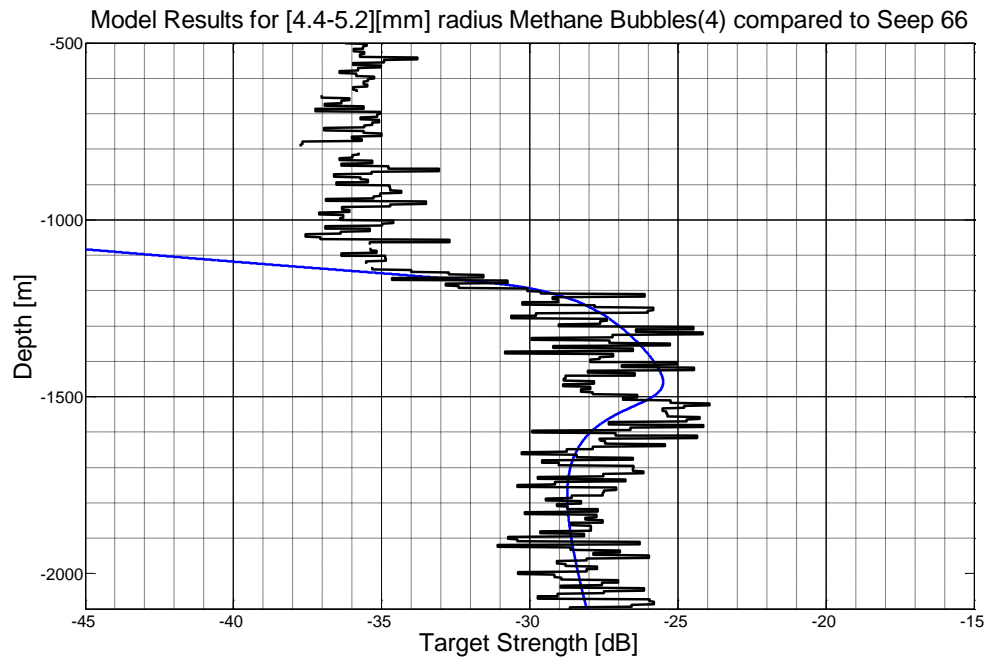
Figure 31: The source distribution that appeared to fit the acoustic data from Figure 30 was a uniform distribution of bubbles ranging from 4.4-5.2 mm radius. To account for the exact empirical TS model there are 4 of each bubble size (in increments of 0.1 mm) per unit meter water depth.

Another example of a source distribution fitting an empirical observation of the 1205L1 seep site

is shown in Figure 32, which has a similar distribution as Figure 31, but with the inclusion of a

fewer number of smaller bubbles that increases the base TS of the model to account for the

increase seen in the empirical TS profile base.

Pillsbury 2015

Model Results for range [2.5(1)[4.3-5.4](2)][mm] radius Methane Bubbles
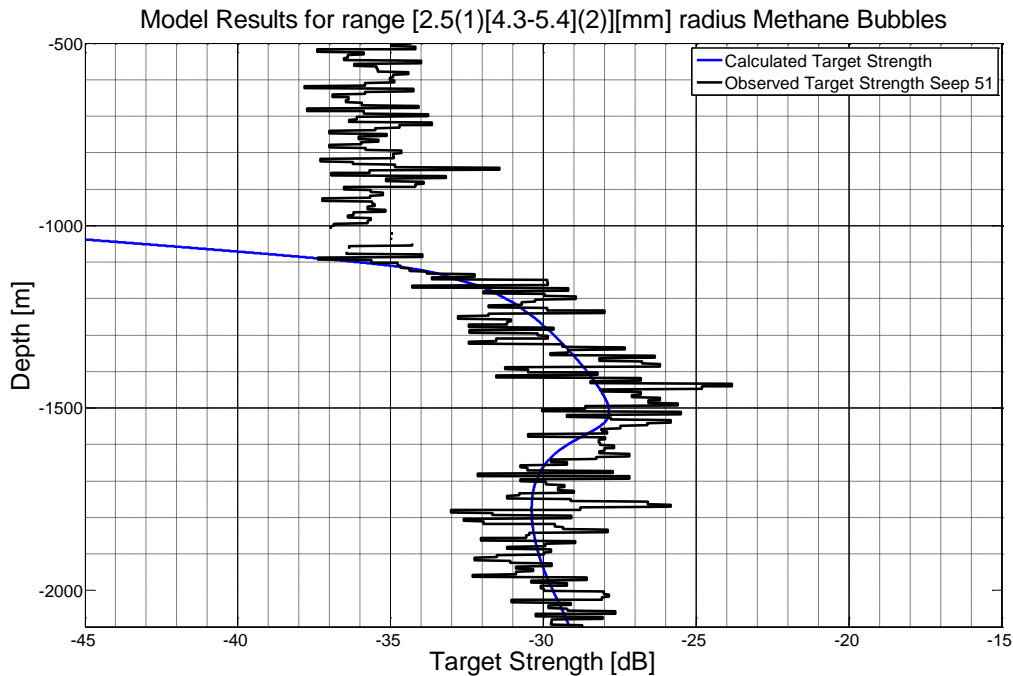
Figure 32: Another example of a source distribution fitting the empirical observation of the 1205L1 seep site is shown in Figure 32, which has a similar distribution as Figure 31, but with the inclusion of a fewer number of smaller bubbles that increases the base TS of the model to account for the increase seen in the empirical TS profile base

If the estimations of the bubble size source distributions from Figures 31 and 32 are correct, then evaluations of the largest bubble size present will determine the fate of the methane gas from the gas plume. For figures 31 and 32 the largest bubble size evaluated by the TS model is a 5.4 mm radius bubble. Figure 33 shows the dissolution model for a 5.4 mm radius bubble released at 2100 meters water depth. From the output of the model one can estimate that the bubble would dissolve at ~750 meters water depth. If the bubble truly dissolves at ~750 meters water depth than it is likely to oxidize its methane to CO_2 and would not contribute directly to atmospheric methane contributions.

Pillsbury 2015
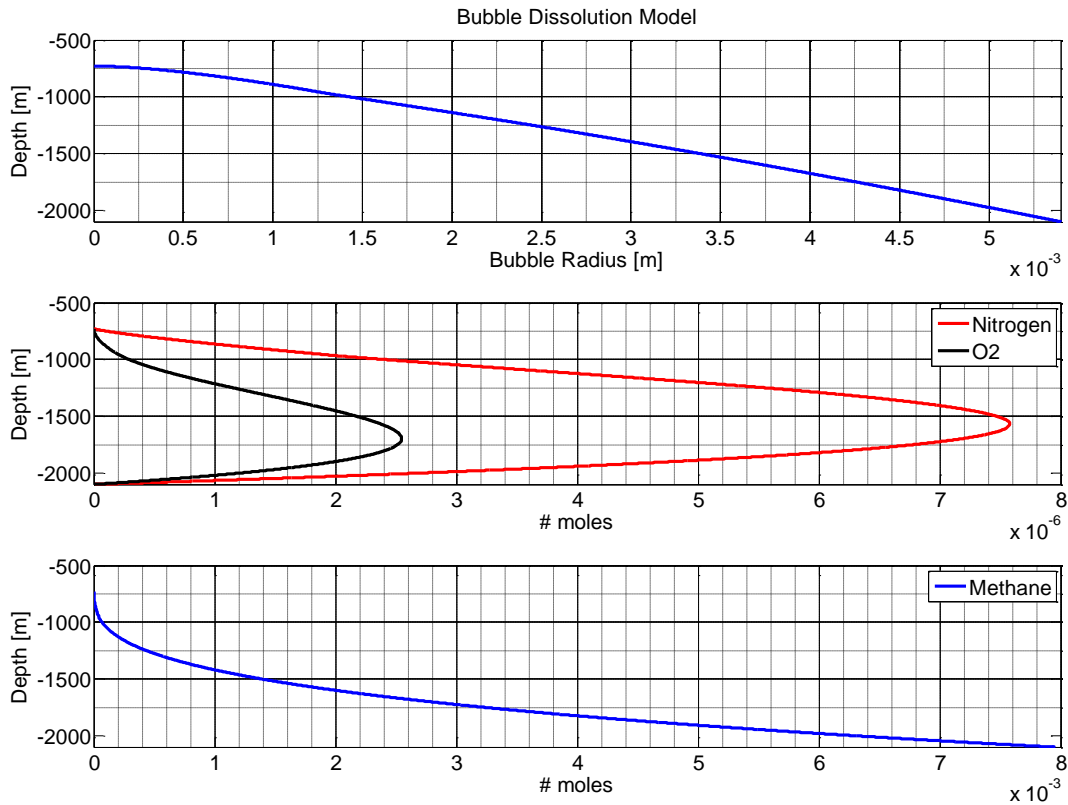
Figure 33: The dissolution model for a 5.4 mm radius bubble released at 2100 meters water depth. From the output of the model one can estimate that the bubble would dissolve at ~750 meters water depth.

4.4 Flux Estimates and Acoustic Variability of Deep Seep Site (2100m)

Figure 34 shows a few observations of the 1205L1 site empirical acoustic data. There are

multiple acoustic observations that appear to follow the single bubble size TS model trends

[Figure 34A], as well as multiple observations that appear to follow the bubble size TS trends

created by a distribution of bubble sizes [Figure 34B]. Perhaps the green line representing seep

#51 [Figure 34B] does not follow the TS trends as well as seep #66 [Figure 34B], but this could

be easily explained by a slight variance in the source distribution. Figure 34C shows a few

empirical observations of the seep that do not appear to follow the trends of a single bubble

Pillsbury 2015

model or a distribution of bubble sizes. While there appears to a be a decay in the empirical TS profile corresponding to the decay of a modeled 5mm radius bubble, there are no resonance effects of a 5mm radius bubble (like the ones seen in Figure 34A).
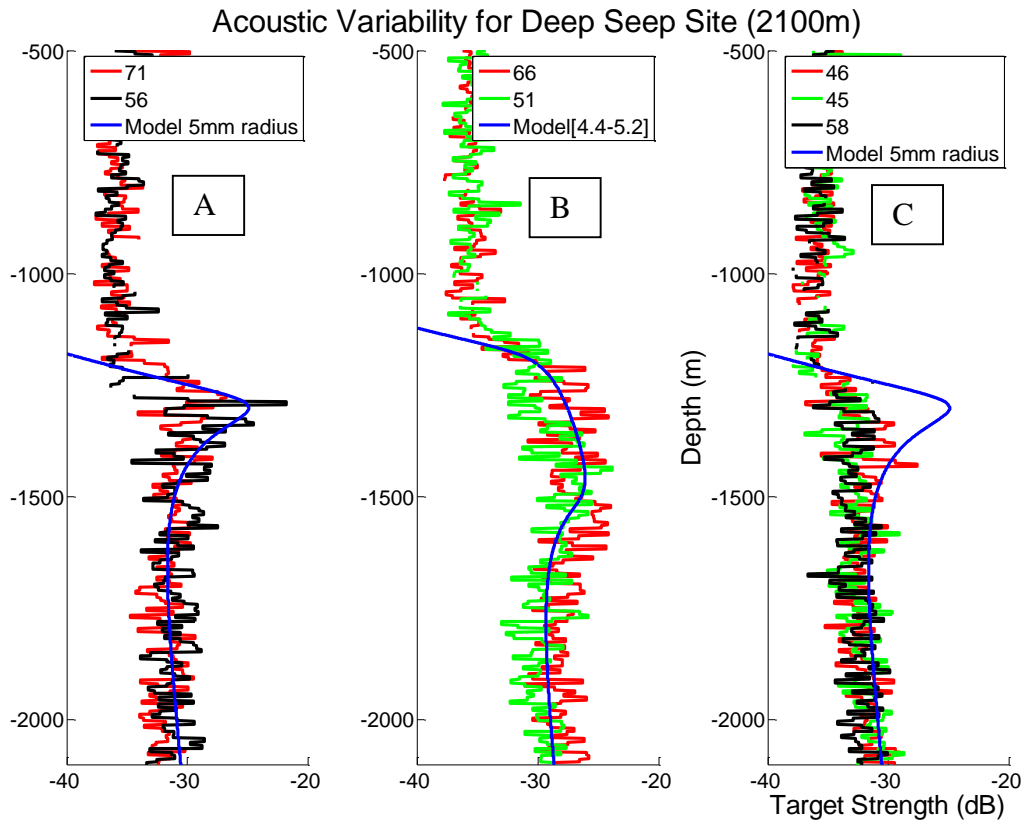
Figure 34: Shows a few observations of the 1205L1 site empirical acoustic data. There are a couple that appear to follow the single bubble size TS model trends [A], as well as a couple that appear to follow the bubble size TS trends created by a distribution of bubble sizes [B]. Subplot C shows a few empirical observations of the seep that do not appear to follow the trends of a single bubble model or a distribution of bubble sizes.

Unfortunately, for weak seep observations like the ones shown in Figure 34C, estimates of bubble size source distributions are difficult using acoustic data constrained to one frequency. Using multiple frequencies could possibly elucidate the process of estimating bubble sizes.

Pillsbury 2015

For the acoustic observations in Figure 34 [Subplots A and B] where the empirical data is possibly constrained to bubble sizes, the flux from the dissolving methane bubbles was calculated [Figure 35]. The flux from the distributions of bubbles is larger and also transports methane higher in the water column due to the larger bubble sizes (above 5mm radius) transporting more methane for longer than a 5mm radius bubble would. The sharp transition seen in the 5mm radius flux is from the bubble dissolving, when it reaches less than 2.5 mm in radius the surface tension of the bubble leads to a larger internal pressure and a larger flux of methane out of the bubble. The sharp transition is not seen in the distribution of bubbles because each different size in the distribution reaches the 2.5 mm radius limit at a different depth, leading to a smoother transition.
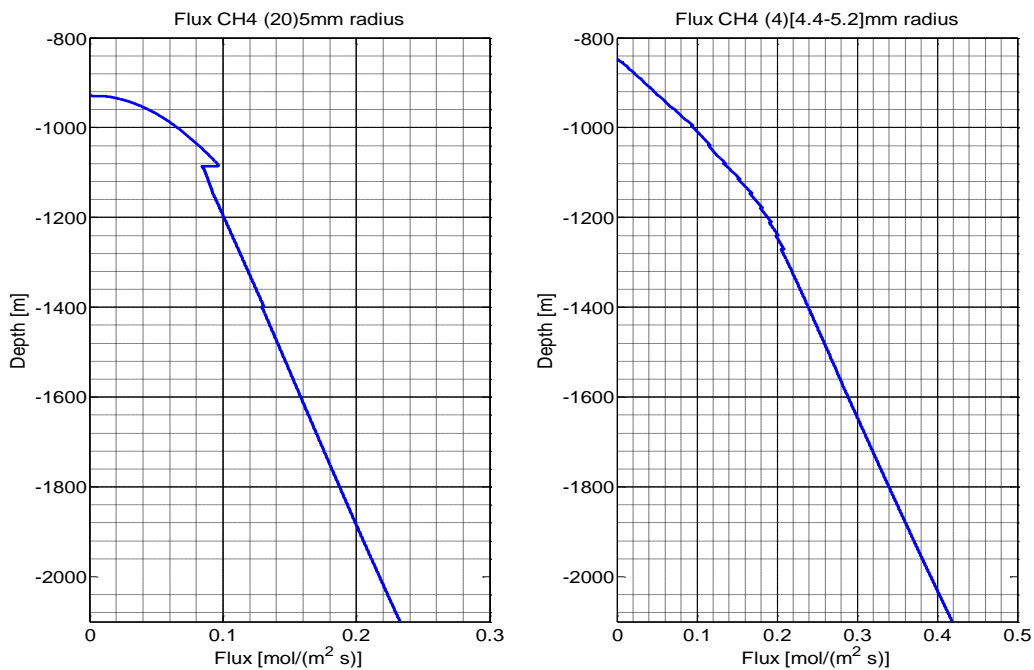
Figure 35: For the acoustic observations in Figure 34[A and B] where the empirical data is possible constrained to bubble sizes, the flux from the dissolving methane bubbles was calculated. The sharp transition seen in the 5mm radius flux is from the bubble dissolving under 2.5 mm in radius where the surface tension of the bubble leads to a larger internal pressure and a larger flux of methane out of the bubble.

Pillsbury 2015

4.5 Gas Transfer Velocity Comparisons

Until the gas transfer rate is constrained, there is no unique result for estimating the bubble size

from the empirical acoustic data. Larger bubbles with 100% of the K value and smaller bubbles

with a reduced K value can be made to fit the same empirical acoustic trends. This is shown in

Figure 36 where a 3.4 mm radius bubble with 50% of the 'dirty' K value (green line) is

compared to the estimated source distribution from Figure 31 which was estimated using the

original 'dirty' K value (blue line).
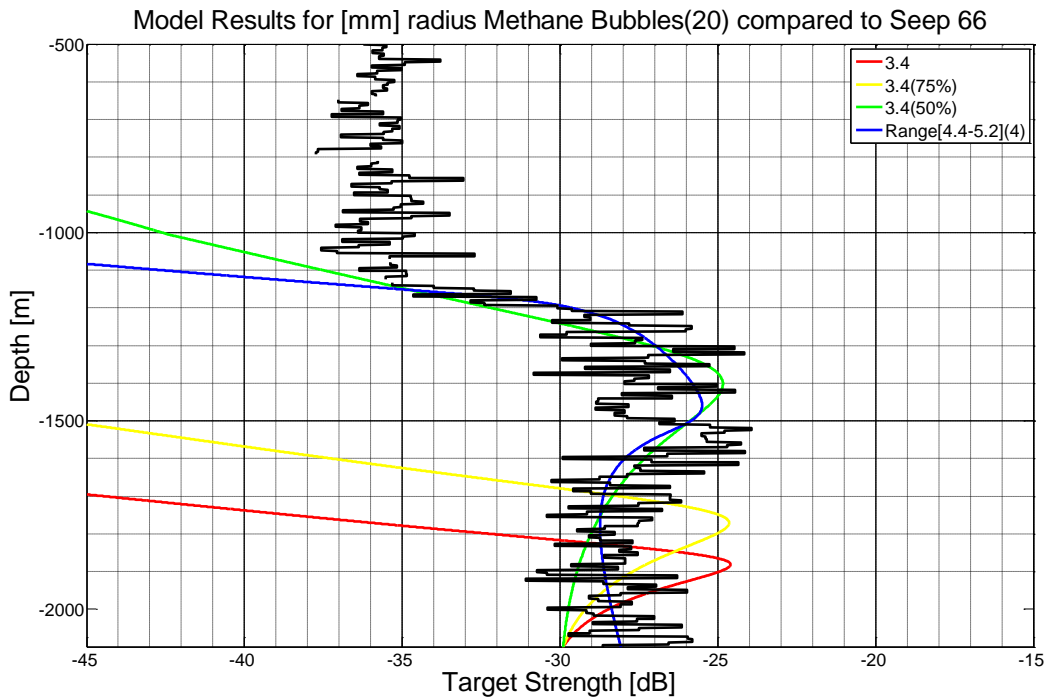
Figure 36: Larger bubbles with 100% of the K value and smaller bubbles with a reduced K value can be made to fit the same empirical acoustic trends. This is shown above where a 3.4 mm radius bubble with 50% of the 'dirty' K value (green line) is compared to the estimated source distribution from Figure 31 which was estimated using the original 'dirty' K value (blue line).

Since two very different bubble sizes can account for the same empirical acoustic trends,

comparisons of the methane flux caused by the different bubble sizes was evaluated [Figure 37].
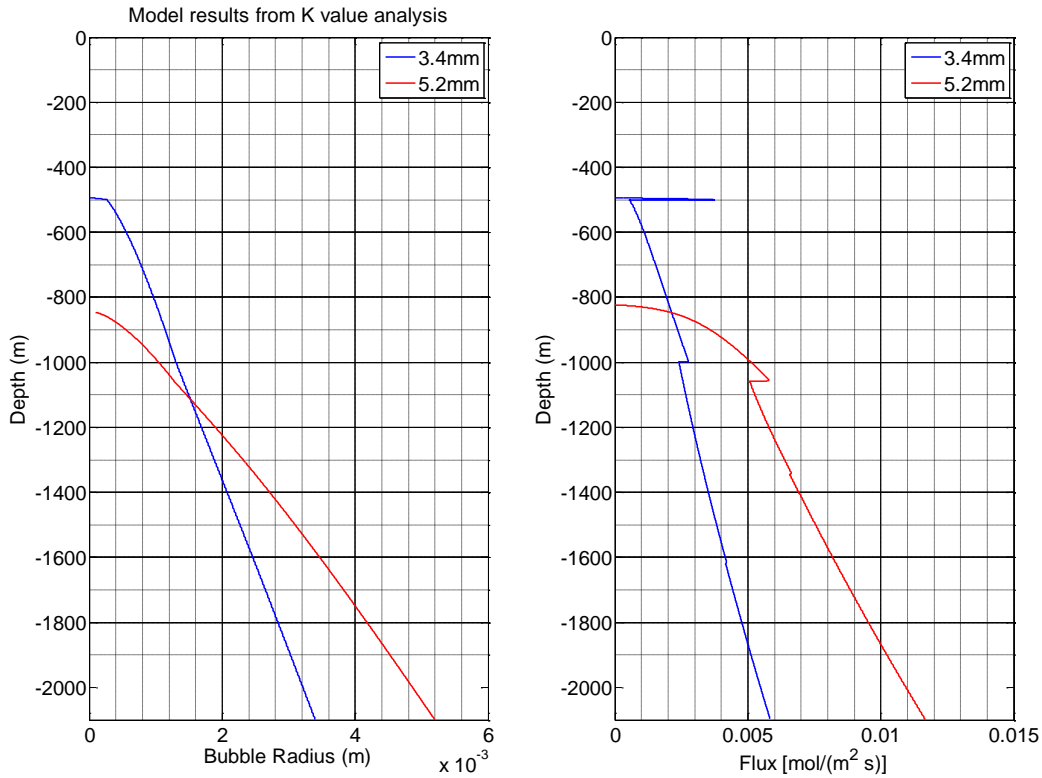
Pillsbury 2015

Figure 37: shows the model dissolution and the model methane flux for a 3.4 mm radius bubble at 50% of the K value and a 5.2 mm radius bubble at 100% of the 'dirty' K value. The 3.4 mm radius bubble with the reduced gas transfer velocity transports methane higher in the water column

Figure 37 shows the model dissolution and the model methane flux for a 3.4 mm radius bubble at 50% of the K value and a 5.2 mm radius bubble at 100% of the 'dirty' K value. The 3.4 mm radius bubble with the reduced gas transfer velocity transports methane higher in the water column. This could be significant to methane flux to the atmosphere if the thermocline, which controls the upper limit of the GHSZ, was closer to the ocean surface (like in the Artic). The spike in the methane flux of the 3.4 mm radius bubble (~500 meters water depth) is caused by the dissolution of the hydrate coatings (at the upper limit of the GHSZ) where the K value switches from the 'dirty' value to the 'clean' value which leads to a quick expulsion of methane and a rapid dissolution of the bubble.

Pillsbury 2015

5 CONCLUSION

The empirical trends observable in EK60 acoustic data of gas seeps were extracted from the background noise using a more efficient, accurate method. This approach which uses the KS test to iteratively solve for the unknown distribution of plume targets, along with calibrating for the acoustic beam pattern, helped to determine a true depth-dependent target strength profile for a gas seep. In order to compare the true target strength to models of bubble evolution, the acoustic observation of the seep must capture its full evolution; i.e., when the top of the seep disappears in the acoustic echogram, the electrical angles can determine whether the top of the seep disappeared because the bubbles disappeared (presumably dissolved) or because the top of the seep went out of the acoustic beam and was 'cut off', (which leads to difficulties predicting bubble size evolution). Another important aspect of acoustic data collection is to use the fastest ping rate possible to collect the highest resolution acoustic data. With higher resolution, more accurate acoustic processing and more accurate comparisons to bubble dissolution models can be achieved. Gas bubbles are excellent acoustic scatterers but by using a single frequency acoustic pulse one cannot determine what kind of gas is in the bubble, nor the bubble size without using broadband acoustics or at least multiple frequency transducers.

The acoustic trends observed were the deepest (initial) bubble target strength, bubble resonance peaks, target strength profile slope(s), and the slope of decay from the point of inclusion. The point of inclusion is the shallowest resonance peak, which is evaluated as the final bubble target strength indicator before the target strength decays to below the background noise. The point of inclusion does not have to be a resonance peak, but the inclusion point is still the shallowest

Pillsbury 2015

target strength indication of a bubble's presence. Using all of these observable features, bubble dissolution models were compared to the acoustic data to determine possible bubble sizes and bubble size source distributions, as well as the fate of the methane being transported in the seep.

Constraining the parameters that affect bubble dissolution is also of importance. The parameters that affect the bubble dissolution the most, and therefore the transport of methane the most, are the local aqueous methane concentrations and the gas transfer velocity. If the water column local to a seep becomes highly concentrated with aqueous methane, the methane bubbles survive much longer in the water column leading to the transport of methane gas much higher in the water column. The gas transfer velocity through an inhibited bubble wall (coated with a surfactant, oil, hydrate, or some combination thereof) significantly affects the bubble dissolution. Therefore, the bubble model created in this study examined the gas transfer rate for slower gas transfer velocities than previously evaluated. This decrease could be caused by an oil coating, hydrate coating or some combination thereof, which has been observed inhibiting the dissolution of a bubble and has led to bubble surviving much longer in the water column than previously estimated. If the gas transfer velocity of a bubble is inhibited by 50%, the average sized bubble in this study would deviate from ~5mm radius to smaller bubbles on the order of ~3mm radius. Although a 5.4 mm radius bubble is very large and is at the upper limit of previously observed bubble sizes in the ocean [e.g. Weber et al, 2014] it is possible that the model is correct. Laboratory studies of the gas transfer velocity through different bubble coatings would be very beneficial in predicting methane transport in a gas seep. Once the important parameters affecting the transport of methane have been constrained, they can be input in a bubble dissolution model to attempt more accurate predictions of methane seep bubble dissolution.

Pillsbury 2015

The initial results of the model in this study, in accordance with the acoustic data collected for comparison, determine that the methane gas released from a site of 2000 meters would dissolve in the water column and oxidize to CO_2. This is a significant finding because it demonstrated that a deep methane plume is not necessarily a direct method of transport for methane to the atmosphere, but would result in a flux of methane to the water column which would then be oxidized. This oxidation process consumes large quantities of oxygen, potentially leading to an increase in anoxic regions of the oceans. The CO_2 produced also leads to ocean acidification which is detrimental to biology in the ocean, especially the creatures that create calcium carbonate shells or skeletons. The model results agree with other studies which have determined that only methane bubbles released in less than 100 meters of water would have a direct methane input to the atmosphere [USGS, 2015] [McGinnis et al, 2006].

Pillsbury 2015

6   REFERENCES

[1]   Ambrose, Douglas, and Constantine Tsonopoulos. "Vapor-liquid critical properties of elements and compounds. 2. Normal alkanes." *Journal of Chemical and Engineering Data* 40.3 (1995): 531-546.

[2]   Aoyama, C.; Matsumoto, R.; Hiruta, A.; Ishizaki, O.; Machiyama, H.; Numanami, H.; Hiromatsu, M.; Snyder, G., Acoustical surveys of Methane plumes using the quantitative echo sounder in Japan Sea, *Underwater Technology and Workshop on Scientific Use of Submarine Cables and Related Technologies, 2007. Symposium on* , vol., no., pp.249,255, 17-20 April 2007 doi: 10.1109/UT.2007.370804

[3]   Beaulieu, Norman C. "An infinite series for the computation of the complementary probability distribution function of a sum of independent random variables and its application to the sum of Rayleigh random variables."*Communications, IEEE Transactions on* 38.9 (1990): 1463-1474.

[4]   Brothers, D. S., Uri, S., Andrews, B. D., & Chaytor, J. D. (2013). Geomorphic characterization of the US Atlantic continental margin. *Marine Geology*, *338*, 46-63.

[5]   Burdic, William S., and James F. Bartram. "Underwater Acoustic System Analysis by William S. Burdic." *The Journal of the Acoustical Society of America* 76.3 (1984): 996-996.

[6]   Cicerone, Ralph J., and Ronald S. Oremland. "Biogeochemical aspects of atmospheric methane." *Global biogeochemical cycles* 2.4 (1988): 299-327.

[7]   Ehhalt, Dieter H. "Methane in the atmosphere." *Journal of the Air Pollution Control Association* 17.8 (1967): 518-519.

[8]   Epstein, C.E.P., and M. S. Plesset. "On the Stability of Gas Bubbles in Liquid-Gas Solutions." *The Journal of Chemical Physics* 18.11 (1950): 1505-1509.

[9]   Gentz, T., Damm, E., von Deimling, J. S., Mau, S., McGinnis, D. F., & Schlüter, M. (2014). A water column study of methane around gas flares located at the West Spitsbergen continental margin. *Continental Shelf Research*, *72*, 107-118.

[10]   Greinart, G., Nutzel, B., Hydroacoustic experiments to establish a method for the determination of methane bubble fluxes at cold seeps. *Marine Geophysics Research Inst*. (2004) 24:75-85

[11]   Greinert, J. and McGinnis, D.F. (2009): Single Bubble Dissolution Model: The Graphical User Interface SiBu-GUI. Environmental Modelling & Software, doi:10.1016/j.envsoft.2008.12.011.

Pillsbury 2015

[12] Gruber, Nicolas. "The marine nitrogen cycle: overview and challenges."*Nitrogen in the marine environment* (2008): 1-50.

[13] Heeschen, K., Trehu, A., Collier, R., et al, Distribution and height of methane bubble plumes on the Cascadia Margin characterized by acoustic imaging, *Geophys. Res. Lett., 30(15),* 1643,

[14] Hornbach, Matthew J., et al. "Three-dimensional seismic imaging of the Blake Ridge methane hydrate province: Evidence for large, concentrated zones of gas hydrate and morphologically driven advection." *Journal of Geophysical Research: Solid Earth (1978–2012)* 113.B7 (2008).

[15] Hu, Jeremiah, and Norman C. Beaulieu. "Accurate simple closed-form approximations to Rayleigh sum distributions and densities." *Communications Letters, IEEE* 9.2 (2005): 109-111.

[16] Intergovernmental Panel on Climate Change (1996), *Climate change 1995: The Science of Climate Change,* 572 pp. Cambridge University Press, New York

[17] Ja¨hne, B., K. O. Mu¨nnich, R. Bo¨singer, A. Dutzi, W. Huber, and P. Libner (1987), On the parameters influencing air-water gas exchange, *J. Geophys. Res*., 92, 1937 – 1949

[18] Jerram, Kevin, Thomas C. Weber, and Jonathan Beaudoin. "Split-beam echo sounder observations of natural methane seep variability in the northern Gulf of Mexico." *Geochemistry, Geophysics, Geosystems* 16.3 (2015): 736-750.

[19] Johnson, Paul, Una Miller, Marie Salmi, Evan Solomon. "Analysis of bubble plume distributions to evaluate methane hydrate decomposition on the continental slope.." *Geochemistry, Geophysiscs, Geosystems. (2015)*

[20] Kobolev, Yu. A., Ostrovsky, L. A., Nonlinear Acoustic Phenomena due to Bubble Drift in a Gas-Liquid Mixture, *J. Acoustic Soc. Am. 85(2), Feb 1989*

[21] Leifer, Ira, and Ranjan Kumar Patro. "The bubble mechanism for methane transport from the shallow sea bed to the surface: A review and sensitivity study." *Continental Shelf Research* 22.16 (2002): 2409-2428.

[22] Leighton, T. G., S. D. Meers, and P. R. White. "Propagation through nonlinear time-dependent bubble clouds and the estimation of bubble populations from measured acoustic characteristics." *Proceedings of the Royal Society of London A: Mathematical, Physical and Engineering Sciences*. Vol. 460. No. 2049. The Royal Society, 2004.

[23] Maini, Brij B., and P. R. Bishnoi. "Experimental investigation of hydrate formation behaviour of a natural gas bubble in a simulated deep sea environment." *Chemical Engineering Science* 36.1 (1981): 183-189.

61

[24] Mau, S., Valentine, D. L., Clark, J. F., Reed, J., Camilli, R., & Washburn, L. (2007). Dissolved methane distributions and air-sea flux in the plume of a massive seep field, Coal Oil Point, California. *Geophysical Research Letters*, *34*(22).

[25] McGinnis, D. F., Greinert, J., Artemov, Y., Beaubien, S. E., & Wüest, A. N. D. A. (2006). Fate of rising methane bubbles in stratified waters: How much methane reaches the atmosphere?. *Journal of Geophysical Research: Oceans (1978–2012)*, *111*(C9).

[26] Medwin, H. Counting bubbles acoustically: a review. *Ultrasonics: January 1977*

[27] Merewether, R., M. S. Olsson, and P. Lonsdale, Acoustically detected hydrocarbon plumes rising from 2-km depths in Guayamas Basin, Gulf of California, *J. Geophys. Res. Lett.,* 18, 432-434, 1985

[28]   - Orbey, Hasan, and Stanley I. Sandler. *Modeling vapor-liquid equilibria: cubic equations of state and their mixing rules*. Vol. 1. Cambridge University Press, 1998.

[29] Paull, C. K., & Ussler III, w. "No evidence for enhanced gas flux from the blake ridge depression." (2014)

[30] Reeburgh, Williams S. "Oceanic Methane Biogeochemistry." *Chem. Rev*.107 (2007): 486-513. University of California. Web. 4 Nov. 2015.

[31] Rehder, G., Brewer, P. W., Peltzer, E. T., & Friederich, G. (2002). Enhanced lifetime of methane bubble streams within the deep ocean. *Geophysical research letters*, *29*(15), 21-1.

[32] Rettich, T. R., Handa, Y. P., Battino, R., & Wilhelm, E. (1981). Solubility of gases in liquids. 13. High-precision determination of Henry's constants for methane and ethane in liquid water at 275 to 328 K. *The Journal of Physical Chemistry*, *85*(22), 3230-3237.

[33] Schlee, John Stevens. *A comparison of two Atlantic-type continental margins*. No. 1167. US Govt. Print. Off.,, 1980.

[34] Schoell, M., 1983, Genetic characterization of natural gases: *AAPG Bulletin, v. 67*, p. 2225-2238.

[35] Solomon, E. A., Kastner, M., MacDonald, I. R., & Leifer, I. (2009). Considerable methane fluxes to the atmosphere from hydrocarbon seeps in the Gulf of Mexico. *Nature Geoscience*, *2*(8), 561-565.

[36] Sullivan-Silva, K. B. *Underwater Acoustic Scattering from Spherical Particulates and Bubbles*. No. NUSC-TR-6772. NAVAL UNDERWATER SYSTEMS CENTER NEWPORT RI, 1989.

[37] Skarke, A., Ruppel, C., Kodis, M., Brothers, D., & Lobecker, E. (2014). Widespread methane leakage from the sea floor on the northern US Atlantic margin. *Nature Geoscience*.

Pillsbury 2015

[38] "U.S. Geological Survey Gas Hydrates Project." *The , Primer*. 2014. Web. 05 Oct. 2015.

[39] USNA. "Target Strength." *Fisheries Acoustics* (2005): 217-61. United States Naval Academy. Web. 7 Oct. 2015.

[40] Van Dover, C. L., Aharon, P., Bernhard, J. M., Caylor, E., Doerries, M., Flickinger, W., ... & Vrijenhoek, R. (2003). Blake Ridge methane seeps: characterization of a soft-sediment, chemosynthetically based ecosystem. *Deep Sea Research Part I: Oceanographic Research Papers*, *50*(2), 281-300.

[41] Vagle, Svein, and Farmer, David M. "The measurement of bubble-size distributions by acoustical backscatter." *Journal of Atmospheric and Oceanic Technology* 9.5 (1992): 630-644.

[42] Vagle, S., Farmer, D. M., Booth, A. D. A free flooding acoustical resonator for measurement of bubble size distributions. *J. Atmos. And Oceanic Technol. 15: 1132-1146*

[43] Weber, T. C., Lyons, A. P., & Bradley, D. L. (2005). An estimate of the gas transfer rate from oceanic bubbles derived from multibeam sonar observations of a ship wake. *Journal of Geophysical Research: Oceans (1978–2012)*,*110*(C4).

[44] Weber, T. C., Mayer, L., Jerram, K., Beaudoin, J., Rzhanov, Y., & Lovalvo, D. (2014). Acoustic estimates of methane gas flux from the seabed in a 6000 km2 region in the Northern Gulf of Mexico. *Geochemistry, Geophysics, Geosystems*, *15*(5), 1911-1925.

[45] "World Ocean Database." *World Ocean Database*. NOAA, 9 Apr. 2015. Web. 16 Nov. 2015.

[46] Wüest, Alfred, Norman H. Brooks, and Dieter M. Imboden. "Bubble plume modeling for lake restoration." *Water Resour. Res* 28.12 (1992): 3235-3250.

[47] Yamamoto, A., Y. Yamanaka, and E. Tajika. "Modeling of methane bubbles released from large sea-floor area: Condition required for methane emission to the atmosphere." *Earth and Planetary Science Letters* 284.3 (2009): 590-598.

Pillsbury 2015

7   APPENDICES

7.1 Parameter Units and Notation

Notation	Parameter Description	Units
a or r	Bubble radius	Meters
g	Gravitation constant	$Meters^2/second^2$
P	Pressure	Pascal
V	Volume	$Meters^3$
R	Gas constant	Joule/(mol Kelvin)
T	Temperature	Kelvin
N	Number of moles	Moles
Z	Depth	Meters

7.2 Pillsbury Bubble Dissolution Matlab Code

First Code:

```
%% Pillsbury/Weber Bubble Dissolution Model
clc
clear all
close all
%% Model Code
% 3 Major codes
%   Pillsbury_Dissolution_Model
%   MethaneBubble
%   radii_rateofchange2

% All other codes used within 3 major codes
%Henrys Law
%INTbubPRESSURE
%MCGINNIS_Kbub
%MCGINNIS_Vbub
%Mu
%PengRobinson
%SW_Density
%SW_KViscosity
%SW_viscosity
%TArgetStrength
```

64

Pillsbury 2015

```matlab
%Tau
%bubble_paramters
%diffusionConstants

%% choose initial conditions
T = 6.5;          % temperature of water in degC - assumed constant with depth
S = 34.5;         % salinity in psu  - assumed constant with depth
y = 2100;         % bubble release depth in m
aa = 5.4e-3;      % bubble radius in mm

%% Run Bubble Dissolution Model
[t,a,y,N_CH4,N_CO2,N_O2,N_N2,N_Total,dN_dt_O2,dN_dt_N2,dN_dt_CH4,dN_dt_CO2,fl
ux_CH4,flux_Gas] = MethaneBubble( aa(1),y(1),T(1),S(1) );

%% Translate model radius to TS

N =35; % number of theoretical bubbles

for ii = 1:length(a)
[sigma_bs(ii) ] = TargetStrength( y(ii),a(ii)*1000,1,T,S );%
TS(ii) = 10*log10(sigma_bs(ii)*N);
end

%% Figures

xmax_a = max(a);
xmax_N = max(N_N2);
ymin_a = max(y)*-1;

figure,
plot(a,0-y(1:length(N_Total)),'linewidth',3)
xlim([0 xmax_a])
ylim([ymin_a 0])
title('Bubble Dissolution Model','fontsize',20)
ylabel('Depth [m]','fontsize',20)
xlabel('Bubble Radius [m]','fontsize',20)

figure,
subplot(311)
plot(N_CH4./N_Total,0-y(1:length(N_Total)),'linewidth',3)
hold on
plot(N_N2./N_Total,0-y(1:length(N_Total)),'r','linewidth',3)
plot(N_CO2./N_Total,0-y(1:length(N_Total)),'g')
plot(N_O2./N_Total,0-y(1:length(N_Total)),'k')
axis([0 1 ymin_a 0])
title('Bubble Dissolution Model','fontsize',20)
ylabel('Depth [m]','fontsize',20)
xlabel('Bubble Gas Fraction [m]','fontsize',20)
legend([],'Methane','Nitrogen','O2')
set(gca,'fontsize',20)
grid minor

subplot(312)
plot(N_N2,0-y,'r','linewidth',3)
```

65

Pillsbury 2015

```matlab
hold on
plot(N_O2,0-y,'k','linewidth',3)
xlim([0 xmax_N])
ylim([ymin_a 0])
ylabel('Depth [m]','fontsize',20)
xlabel('# moles','fontsize',20)
legend([],'Nitrogen','O2')
set(gca,'fontsize',20)
grid minor

subplot(313)
plot(N_CH4,0-y,'linewidth',3)
legend([],'Methane')
ylabel('Depth [m]','fontsize',20)
xlabel('# moles','fontsize',20)
set(gca,'fontsize',20)
grid minor
ylim([ymin_a 0])

%% Then save output to create model families

% save('Xmm_Ym.mat','y','a','t','sigma_bs','flux_CH4')
```

Second Code:

```matlab
function [
t,a,y,N_CH4,N_CO2,N_O2,N_N2,N_Total,dN_dt_O2,dN_dt_N2,dN_dt_CH4,dN_dt_CO2,flu
x_CH4,flux_Gas ] = MethaneBubble( a,y,T,S )

%%%%%%%%%%%%%%%%%%%%%%%%%%%%%%%%%%%%%%%%%%%%%%%%%%%%%%%%%%%%%%%%%%%%%%%%%
%        environmental parameters
%%%%%%%%%%%%%%%%%%%%%%%%%%%%%%%%%%%%%%%%%%%%%%%%%%%%%%%%%%%%%%%%%%%%%%%%%


R = 8.31;            % universal gas law constant J/(mol K)
Tk = T + 273.15;        % temperature in degrees Kelvin
Pa = 1.01325e5;         % atmospheric pressure
g = 9.81;            % gravitational constant

X_O2 = 0;            % initial molar fraction of oxygen
X_N2 = 0;            % initial molar fraction of nitrogen
X_CO2 = 0;               % initial molar fraction of C02
X_CH4 = 1;               % initial molar fraction of methane

tau = 1e-3 * (30 - (Tk - 273.15) * 0.1445);   %METHANE
```

66

Pillsbury 2015

```matlab
%%%% internal bubble pressure %%%%
[ Pb,rho_seawater ] = INTbubPRESSURE( y,T,S,a,tau );%   [Pa]



% partial pressures [Pa]
Pb_O2 = X_O2*Pb;
Pb_N2 = X_N2*Pb;
Pb_CH4 = X_CH4*Pb;
Pb_CO2 = X_CO2*Pb;


Ph = 1.01325e5*(1+0.1*(y));       % hydrostatic pressure (see White, Fluid
Mechanics)
%  [ N_CH4,N_CO2,N_N2,N_O2 ] = MCGINNIS_VANDERWAALS(
R,Tk,a,Ph,X_CH4,X_CO2,X_N2,X_CO2 );
%% %%%% molar quantities %%%%%%
%%%%%%%%%%%%%% Methane %%%%%%%%%%%%%%%%%%%%%%%%%
Tc = 191.15; %kelvin critical temperature
%
Pc = 4641000; %Pa critical pressure
%
MW = 16.043; %molecular weight
%
Liquido = 0;
%
w = 0.0115; %accentric factor
%
[Z_CH4] = PengRobinson(Tk,Pb_CH4,Tc,Pc,w,MW,Liquido);                     %
N_CH4 = Pb_CH4*4/3*pi*a^3/R/Tk/Z_CH4;
%
% keyboard
% [ N_CH4 ] = VanderWaals( Ph/1000, a, Tk );


%%%%%%%%%%%%%%%%%%%%%%%%%%%%%%%%%%%%%%%%%%%%%%%%%%%


%%%%%%%%%%%%%%% Oxygen %%%%%%%%%%%%%%%%%%%%%%%%%%%%
Tc = 273.15-118.6; %kelvin critical temperature
%
Pc = 5050000; %Pa critical pressure
%
MW = 16; %molecular weight
%
Liquido = 0;
%
w = 0.021; %accentric factor
%
[Z_O2] = PengRobinson(Tk,Ph,Tc,Pc,w,MW,Liquido);
%
N_O2 = Pb_O2*4/3*pi.*a.^3/R/Tk/Z_O2;
%
%%%%%%%%%%%%%%%%%%%%%%%%%%%%%%%%%%%%%%%%%%%%%%%%%%%


%%%%%%%%%%%%%% Nitrogen %%%%%%%%%%%%%%%%%%%%%%%%%%
Tc = 273.15-146.9; %kelvin critical temperature
%
```

Pillsbury 2015

```matlab
Pc = 3390000; %Pa critical pressure
%
MW = 28.0134; %molecular weight
%
Liquido = 0;
%
w = 0.038; %accentric factor
%
[Z_N2] = PengRobinson(Tk,Ph,Tc,Pc,w,MW,Liquido);
%
N_N2 = Pb_N2*4/3*pi.*a.^3/R/Tk/Z_N2;   %mols
%
%%%%%%%%%%%%%%%%%%%%%%%%%%%%%%%%%%%%%%%%%%%%%%%%%%

%%%%%%%%%%%%%%%%%%% Carbon Dioxide %%%%%%%%%%%%%
Tc = 273.15+31.04; %kelvin critical temperature
%
Pc =7380000; %Pa critical pressure
%
MW = 44.01; %molecular weight
%
Liquido = 0;
%
w = 0.225; %accentric factor
%
[Z_CO2] = PengRobinson(Tk,Ph,Tc,Pc,w,MW,Liquido);                    %
N_CO2 = Pb_CO2*4/3*pi.*a.^3/R/Tk/Z_CO2;       %mols
%
%%%%%%%%%%%%%%%%%%%%%%%%%%%%%%%%%%%%%%%%%%%%%%%%%%

% N_Total = N_O2 + N_N2 + N_CH4 + N_CO2;       % total number of moles

%% prealocate some variables
i = 1;
t(i) = 0;
a(2:1e6) = 0;
N_O2(2:1e6) = 0;
N_N2(2:1e6) = 0;
N_CH4(2:1e6) = 0;
N_CO2(2:1e6) = 0;
y(2:1e6) = 0;
t(2:1e6) = 0;
%% %%%%%%%%% calculate a rate of change for the bubble %%%%%%%%%%%%%%%%
N_Total = 1;
% while (a(i) > 1e-5) & (y(i) > 1)
while  (N_Total(i)>0)
   %% time step, larger time step increases error
    if a(i) > .001
        dt = .1;
    else
        dt = .1;

    end

    %%       bubble rise speeds
```

Pillsbury 2015

```matlab
        %%%%% [REF: Jamialahmadi et al 1994, McGinnis et al 2006]
    if a(i)*2<2.6e-3

            v=0.001;
            [ vbub ] = MCGINNIS_Vbub( T,S,a(i),y(i),v );

            while v<vbub
                v=v+.001;
                [ vbub] = MCGINNIS_Vbub( T,S,a(i),y(i),v );
                %               keyboard
            end
            vb(i) = vbub;
            vv(i) = v;
            clear v
        else
            [ vb(i)] = MCGINNIS_Vbub( T,S,a(i),y(i),0 );
    end
        wb=vb(i);


        %% local aqueous concentrations
        C_O2 = .29;%6*43.3*1027/1e6;    % aqueous concentration of O2 in liquid
surrounding bubble
        C_N2 = .6021;%0.5;%6*43.3*1027/1e6*(0.79/.21);    % aqueous concentration
of N2 in liquid surrounding bubble
        C_CH4 = 3e-06;    % aqueous concentration of CH4 in liquid surrounding
bubble
        C_CO2 = .01;    % aqueous concentration of CO2 in liquid surrounding
bubble %mmol/L or mol/m^3



        %% rates of change

[da_dt,dN_dt_O2,dN_dt_N2,dN_dt_CH4,dN_dt_CO2,Pb_CH4(i),Pb_CO2(i),Pb_N2(i),Pb_
O2(i),X_CH4,X_CO2,X_O2,X_N2] =
radii_rateofchange2(wb,a(i),y(i),T,S,N_O2(i),N_N2(i),N_CH4(i),N_CO2(i),C_O2,C
_N2,C_CH4,C_CO2,Z_CH4,Z_CO2,Z_N2,Z_O2);
        i = i + 1;
        a(i) = a(i-1) + da_dt*dt;




            N_O2(i) = N_O2(i-1) + dN_dt_O2*dt;
            N_N2(i) = N_N2(i-1) + dN_dt_N2*dt;

%           N_CH4(i) = N_CH4(i-1) + dN_dt_CH4*dt;
            N_CO2(i) = N_CO2(i-1) + dN_dt_CO2*dt;
%
N_CH4(i) = Pb_CH4(i-1)*4/3*pi*a(i)^3/Z_CH4/R/Tk;


if i == 2
N_CH4(1) = N_CH4(2)+dN_dt_CH4;
```

69

Pillsbury 2015

```
N_Total(1) = N_O2(1) + N_N2(1) + N_CH4(1) + N_CO2(1);        % total number of
moles
else
%       keyboard
end
          %%
dN_CH4(i) = N_CH4(i-1)-N_CH4(i);
dN_Gas(i) = N_CO2(i-1)-N_CO2(i)+N_O2(i-1)-N_O2(i)+N_N2(i-1)-N_N2(i);

flux_CH4(i) = dN_CH4(i)/(4*pi*a(i)^2)/dt;
flux_Gas(i) = dN_Gas(i)/(4*pi*a(i)^2)/dt;

%%




% if a(i) < 1e-5
%       N_CO2(i) = 0;
%       N_CH4(i) = 0;
%       N_N2(i) = 0;
%       N_O2(i) = 0;
% end
%
    % make sure there are no negative molar concentrations
    N_O2 = max(N_O2,0);
    N_N2 = max(N_N2,0);
    N_CH4 = max(N_CH4,0);
    N_CO2 = max(N_CO2,0);
%     flux_CH4 = max(flux_CH4,0);

        N_Total(i)= N_O2(i) + N_N2(i) + N_CH4(i) + N_CO2(i);        % total
number of moles


    y(i) = y(i-1) - wb*dt;

    t(i) = t(i-1) + dt;

end
a = a(1:i);
N_O2 = N_O2(1:i);
N_N2 = N_N2(1:i);
N_CH4 = N_CH4(1:i);
N_CO2 = N_CO2(1:i);
y = y(1:i);
t = t(1:i);



end
```

Third Code:

Pillsbury 2015

```
function
[da_dt,dN_dt_O2,dN_dt_N2,dN_dt_CH4,dN_dt_CO2,Pb_CH4,Pb_CO2,Pb_N2,Pb_O2,X_CH4,
X_CO2,X_O2,X_N2] =
radii_rateofchange2(wb,a,y,T,S,N_O2,N_N2,N_CH4,N_CO2,C_O2,C_N2,C_CH4,C_CO2,Z_
CH4,Z_CO2,Z_N2,Z_O2 );

%%%%%%%%%%%%%%%%%%%%%%%%%%%%%%%%%%%%%%%%%%%%%%%%%%%%%%%%%%%%%%%%%%%%
% calculate new bubble radius rate of change
%%%%%%%%%%%%%%%%%%%%%%%%%%%%%%%%%%%%%%%%%%%%%%%%%%%%%%%%%%%%%%%%%%%%

%%%%INPUTS%%%%%
% wb - rise velocity - m/s
% a - bubble radius - m
% y - depth - m
% T - Temp - Celsius
% S - Salinity - PSU
% N_GAS - # of moles of gas constituent in bubble
% C_GAS - Aqueous Concentration of gas constituent - mmol/L

Tk = T+273.15;
%%%%OUTPUTS%%%%
% da_dt = rate of change of bubble radius (w.r.t. time)
% dN_dt_GAS = rate of change of # of moles of gas constiuent (w.r.t time)
%%
%%%% INTERFACIAL SURFACE TENSION %%%%

tau = TAU(N_CH4,N_N2,N_O2,N_CO2,T);      %add contributions from N2 O2 CO2




%%%% internal bubble pressure %%%%
[ Pb,rho_seawater ] = INTbubPRESSURE( y,T,S,a,tau );

%%%% TOTAL # OF MOLS %%%%
N_total = N_O2 + N_N2 + N_CH4 + N_CO2;        %mols




%%%% calculate  individual molar concentrations %%%%
X_O2 = N_O2./N_total;                 % initial molar fraction of oxygen
X_N2 = N_N2./N_total;                  % initial molar fraction of nitrogen
X_CH4 = N_CH4./N_total;             % initial molar fraction of nitrogen
X_CO2 = N_CO2./N_total;             % initial molar fraction of nitrogen


% New rate of change for the gases
% partial pressures
Pb_O2 = X_O2.*Pb;
Pb_N2 = X_N2.*Pb;
Pb_CH4 = X_CH4.*Pb;
```

Pillsbury 2015

```matlab
Pb_CO2 = X_CO2.*Pb;

% if X_O2 ~=0
%     keyboard
% end


%% Z factors
  R = 8.3145;              % universal gas law constant J/(mol K)

Ph = 1.01325e5*(1+0.1*(y));    % hydrostatic pressure (see White, Fluid
Mechanics)
% if isnan(Pb_CH4)
% %     keyboard
% Pb_CH4 = Pb;
% Pb_CO2 = Pb;
% Pb_N2 = Pb;
% Pb_O2= Pb;
% else
% end

%% Henry's Law constants (m^3 Pa)/mol

 %%%% METHANE %%%%%
    H_CH4= HenrysLaw(T,S,Pb,a,N_CH4,Z_CH4 ,1/1.4e-5);
%     C_sat = Pb/H_CH4;
%     keyboard
% %%%% OXYGEN %%%%
% H_O2 = 9.6576e4;                                        % Henry's
constant for O2 see Weiss 1970
H_O2 = 2.125-0.05021*T+5.77e-4*T^2; %mol/(m^3*bar) from Wuest et al 1974
H_O2 = 1/H_O2*1e5; %(m^3*bar)/mol converted to (m^3*Pa)/mol


% % %%%% NITROGEN %%%%
% H_N2 = 1.9433e5;                                        % Henry's constant for
N2 see Weiss 1970
H_N2 = 1.042-0.0245*T+3.171e-4*T^2; %mol/(m^3*bar)  from Wuest et al 1974
H_N2 = 1/H_N2*1e5; %(m^3*bar)/mol converted to (m^3*Pa)/mol

% % %%%% CO2 %%%%
H_CO2 = 1/3.3e-4;                                        % Henry's
constant for CO2 see Weiss 1970

%% Diffusion Coefficients
[D_O2,D_N2,D_CH4,D_CO2] = diffusionConstants(T,S);

%% %%%% molar quantities %%%%%%%
%%%%%%%%%%%%%% Methane %%%%%%%%%%%%%%%%%%%%%%%%%%%
Tc = 191.15; %kelvin critical temperature
%
Pc = 4641000; %Pa critical pressure
%
MW = 16.043; %molecular weight
%
```

72

```matlab
Liquido = 0;
%
w = 0.0115; %accentric factor
%
% [Z_CH4] = PengRobinson(Tk,Ph,Tc,Pc,w,MW,Liquido);
%
N_CH4 = Pb_CH4*4/3*pi.*a.^3/R/Tk/Z_CH4;
%


%%%%%%%%%%%%%%%%%%%%%%%%%%%%%%%%%%%%%%%%%%%%%%%%

%%%%%%%%%%%%%% Oxygen %%%%%%%%%%%%%%%%%%%%%%%%%%%%%%%%%%
Tc = 273.15-118.6; %kelvin critical temperature
%
Pc = 5050000; %Pa critical pressure
%
MW = 16; %molecular weight
%
Liquido = 0;
%
w = 0.021; %accentric factor
%
% [Z_O2] = PengRobinson(Tk,Ph,Tc,Pc,w,MW,Liquido);
%
N_O2 = Pb_O2*4/3*pi.*a.^3/R/Tk/Z_O2;
%
%%%%%%%%%%%%%%%%%%%%%%%%%%%%%%%%%%%%%%%%%%%%%%%%

%%%%%%%%%%%%%% Nitrogen %%%%%%%%%%%%%%%%%%%%%%%%%%%%%%%%%
Tc = 273.15-146.9; %kelvin critical temperature
%
Pc = 3390000; %Pa critical pressure
%
MW = 28.0134; %molecular weight
%
Liquido = 0;
%
w = 0.038; %accentric factor
%
% [Z_N2] = PengRobinson(Tk,Ph,Tc,Pc,w,MW,Liquido);
%
N_N2 = Pb_N2*4/3*pi.*a.^3/R/Tk/Z_N2;   %mols
%
%%%%%%%%%%%%%%%%%%%%%%%%%%%%%%%%%%%%%%%%%%%%%%%%%

%%%%%%%%%%%%%%%%%%%%%%%NITROGEN%%%%%%%%%%%%%%%%%%%%%%%%
Tc = 273.15+31.04; %kelvin critical temperature
%
Pc =7380000; %Pa critical pressure
%
MW = 44.01; %molecular weight
%
Liquido = 0;
%
```

73

Pillsbury 2015

```matlab
w = 0.225; %accentric factor
%
% [Z_CO2] = PengRobinson(Tk,Ph,Tc,Pc,w,MW,Liquido);                    %
N_CO2 = Pb_CO2*4/3*pi.*a.^3/R/Tk/Z_CO2;        %mols
%
%%%%%%%%%%%%%%%%%%%%%%%%%%%%%%%%%%%%%%%%%%%%
    N_Total= N_O2 + N_N2 + N_CH4 + N_CO2;        % total number of moles
% if N_Total >0
% else
%     keyboard
% end
Z_CH4 = 0.75;
Z_CO2 = 1;
Z_N2 = 1;
Z_CO2 = 1;
%%
%%%%%%%%%%%%%%%%%%%%%%%%%%%%%%%%%%%%%%%%%%%%%%%%%%%%%%%%%%%%%%%%%%%%%%%%
% individual gas transfer rates
%%%%%%%%%%%%%%%%%%%%%%%%%%%%%%%%%%%%%%%%%%%%%%%%%%%%%%%%%%%%%%%%%%%%%%%%

 [ kbub_CH4 ] = MCGINNIS_Kbub( wb,a,D_CH4,y )/100;  %[cm/s] converted to
[m/s]
 [ kbub_CO2 ] = MCGINNIS_Kbub( wb,a,D_CO2,y )/100;  %[cm/s] converted to
[m/s]
 [ kbub_N2 ] = MCGINNIS_Kbub( wb,a,D_N2,y )/100;   %[cm/s] converted to [m/s]
 [ kbub_O2 ] = MCGINNIS_Kbub( wb,a,D_O2,y )/100;   %[cm/s] converted to [m/s]

%%   % rate of change of gas inside bubble
dN_dt_O2 = kbub_O2*4*pi.*a.^2.*(C_O2-Pb_O2/H_O2);
dN_dt_N2 = kbub_N2*4*pi.*a.^2.*(C_N2-Pb_N2/H_N2);
dN_dt_CH4 = kbub_CH4*4*pi.*a.^2.*(C_CH4-Pb_CH4/H_CH4);
dN_dt_CO2 = kbub_CO2*4*pi.*a.^2.*(C_CO2-Pb_CO2/H_CO2);
%%

  R = 8.3145;           % universal gas law constant J/(mol K)
g = 9.81;                % gravity constant
Tk = T+273;
%% total rate of change of gas in the bubble
%dN_dt =  X_O2.*dN_dt_O2 + X_N2.*dN_dt_N2 + X_CH4.*dN_dt_CH4 +
X_CO2.*dN_dt_CO2;
% dN_dt =  dN_dt_O2 + dN_dt_N2 + dN_dt_CH4 + dN_dt_CO2;
dN_dt_CH4_p = R*Tk*dN_dt_CH4*Z_CH4;
dN_dt_CO2_p = R*Tk*dN_dt_CO2*Z_CO2;
dN_dt_N2_p = R*Tk*dN_dt_N2*Z_N2;
dN_dt_O2_p = R*Tk*dN_dt_O2*Z_O2;
dN_dt =  dN_dt_CH4_p + (dN_dt_O2_p + dN_dt_N2_p +  dN_dt_CO2_p);

%% new rate of change of bubble radius
dz_dt = -wb; %m/s  % z is defined positive downwards, a bubble rising upward
should get larger with increasing hydrostatic pressure
da_dt = (dN_dt - 4/3*pi*a.^3.*rho_seawater*g.*dz_dt )./(4*pi*a.^2.*Pb -
8/3*pi*a*tau);
```

Those are the three major sections of Matlab code used in the Pillsbury Dissolution Model

Pillsbury 2015

The next section of code is the change in Jerram (2014) code including the Rayleigh mixture model

```matlab
%% Working Seep Directory

clc; clear all; close all

%% 46 load ('C:\Users\lpillsbury\Desktop\WAMS\Plumes and Noise MAT
Files\EX1205L1_46_Plume_and_Noise.mat')
%
load('C:\Users\lpillsbury\Desktop\WAMS\EX1205L1_46_Plume_Params_andANGLES_25b
in.mat')
% load('C:\Users\lpillsbury\Desktop\WAMS\Plumes and Noise MAT
Files\EX1205L1_46_Plume_and_Noise.mat');
%% seep of choice


% load('C:\Users\lpillsbury\Desktop\WAMS\Plumes and Noise MAT
Files\EX1205L1_64_Plume_and_Noise.mat');
%% First
uiopen
Alongship_e= targs.subset.alongship_e;
Athwartship_e= targs.subset.athwartship_e;
Range = targs.subset.r_default;
Sp_noise =targs.subset.Sp_noise;
Sp_plume =double(targs.subset.Sp_plume);
[plume_param, AlAngle_fin, AtAngle_fin] =
SeepRayleighEstimator(Alongship_e,Athwartship_e,Range,Sp_noise,Sp_plume,5);
% save('C:\Users\lpillsbury\Documents\Graduate School\Assistantship\3.
Data\Working_Seep_Directory\Output_MAT_files\EX1204_12_data_out_10bin.mat') %
this
% step can take forever so run once and save

%% Calibration Routine/ TS Correction
% uiopen
pulse = targs.cal.pulselength(1)

% data = load('C:\Users\lpillsbury\Desktop\WAMS\TS_512ms_Correction.mat'); %
5ms cal file
data = load('C:\Users\lpillsbury\Desktop\WAMS\TS_4096ms_Correction.mat') %
TS_corr_vq = data.TS_corr_vq;
[ Plume_DB, TS_Corr_Plume, Plume_DB_corr ]  =
TS_Seep_Corrector(TS_corr_vq,AlAngle_fin,AtAngle_fin,Range,plume_param,Sp_plu
me);

%% transects
figure, imagesc(-128:127,-128:127,TS_corr_vq)
c =colorbar;
set(c,'YColor','white')
xlabel('Alongship','FontSize',14,'FontWeight','bold','Color','white')
ylabel('Athwartship','FontSize',14,'FontWeight','bold','Color','white')
```

Pillsbury 2015

```matlab
set(gca,'Fontsize',14)
set(gca,'YColor','white')
set(gca,'XColor','white')

title('EK60 BeamPattern','Fontsize',14,'FontWeight','bold','Color','White')

ts1 = 1200;
ts2 = 900;
% ts1 = 100;
% ts2 = 300;


figure,
plot(Plume_DB_corr(ts1,:))
hold on
plot(Plume_DB(ts1,:),'r')
% plot(TS_Corr_Plume(1100,:),'g')
xlim([6 13])
legend([],'Corrected','Original','correction','Location','North')
xlabel('Ping')
ylabel('dB')
title('Transect 1')
grid on
% ylim([-40 -10])


figure,
plot(Plume_DB_corr(ts2,:))
hold on
plot(Plume_DB(ts2,:),'r')
% plot(TS_Corr_Plume(960,:),'g')
xlim([6 11])
legend([],'Corrected','Original','correction','Location','North')
xlabel('Ping')
ylabel('dB')
title('Transcect 2')
grid on
% ylim([-40 -10])
%

% TS Profiles
TS_EK = Plume_DB_corr;
[x,y] = size(TS_EK);
x_max =1000; %%%%%%%%%%%%%%%%%%%%%%%%%%%%%% Change for top of seep TS profile
% TS_EK_Pro = zeros(size(TS_EK));
% TS_EK_Pro_mean = TS_EK;
for ii = 1:x
%      if ii>x_max

        for jj = 1:y
            if TS_EK(ii,jj) == 0
                TS_EK(ii,jj) = nan;
            end
        end
        ts_mean(ii) = nanmean(TS_EK(ii,1:y));
```

76

Pillsbury 2015

```matlab
%       else
%           ts_mean(ii) = nan;
%       end

end
range = 0-Range(1:length(TS_EK),2);
ymin = min(targs.subset.Sp_noise_profile_2D);
TS_EK_Pro_mean = ts_mean;
noise_y = 0-
linspace(0,length(targs.subset.Sp_noise_profile_2D),length(targs.subset.Sp_no
ise_profile_2D));
plume_y = 0-
linspace(0,length(targs.subset.Sp_noise_profile_2D),length(targs.subset.Sp_no
ise_profile_2D));
mean_TS_EK = nanmean(TS_EK_Pro_mean);
targ_noise = targs.subset.Sp_noise_profile_2D;
targ_plume = targs.subset.Sp_plume_profile_interp;
del_dif = targ_noise(:,1)-targ_plume(:);
% idx = (800:1376);

figure,
% k=subplot(121);
hold on
 h(:,1) = plot(targs.subset.Sp_noise_profile_2D(:),0-Range(:,2),'k');
h(:,2) = plot(targs.subset.Sp_plume_profile_interp(:),0-Range(:,2),'g');
% h(:,3) = plot(del_dif,0-Range(:,2),'r');
h(:,3) =  plot(TS_EK_Pro_mean,range,'r');
% ylim([min(range) 0])
xlim([ymin(1,1) 0])
set(h(:,1), 'Color','k')
set(h(:,2), 'Color','g')
set(h(:,3), 'Color','r')
legend(h(1,:), {'Noise Floor','Plume Uncorrected','TS Corrected'})
title('Zoom','FontSize',14,'FontWeight','bold','Color','white')

ylabel('Depth [m]','FontSize',14,'FontWeight','bold','Color','white')
xlabel('dB','FontSize',14,'FontWeight','bold','Color','white')
set(gca,'Fontsize',14)
set(gca,'YColor','white')
set(gca,'XColor','white')
grid minor
% save('C:\Users\lpillsbury\Documents\Graduate School\Assistantship\3.
Data\Working_Seep_Directory\Output_MAT_files\EX1205L1_46_TS_profile_HIGHRES.m
at','TS_EK_Pro_mean','range') % this
```

The Rayleigh mixture model code is as follows:

```matlab
function [ plume_param AlAngle_fin AtAngle_fin ] = SeepRayleighEstimator(
Alongship_e,Athwartship_e,Range,Sp_noise,Sp_plume,binz )
%UNTITLED5 Summary of this function goes here
%   Detailed explanation goes here
```

Pillsbury 2015

```matlab
binz=binz;
% binz = 20;

%% BOTTOM DETECTION ALG
[x,y]=size(Sp_noise);



for ii = 1:x
    for jj=1:y
        if Sp_noise(ii,jj)>0 %get rid of bad Sp_noise data that is above 0 dB
and replace with NaN
            Noise_Floor_amp(ii,jj)=NaN;


        else
            Noise_Floor_amp(ii,jj)=10^(Sp_noise(ii,jj)/20);   % dB to amp


        end
    end
end
[x,y]=size(Sp_plume);

% AlAngle=ones(size(Sp_plume));
% AtAngle=ones(size(Sp_plume));
% Sp = Sp_plume;
% clear Sp_plume
% for ii = 1:x
%     for jj=1:y
%         if Sp(ii,jj)>0 %Hopefully improve bottom detect
%             Sp_plume(ii,jj)=NaN;
%             AlAngle(ii,jj)=NaN;
%             AtAngle(ii,jj)=NaN;
%         else
%             Sp_plume(ii,jj)=Sp(ii,jj);   % dB to amp
%             AlAngle(ii,jj)=Alongship_e(ii,jj);
%             AtAngle(ii,jj)=Athwartship_e(ii,jj);
%         end
%     end
% end
[idx,var] = find(Sp_plume>0);
Sp_plume = Sp_plume(1:min(idx),:);
AlAngle = Alongship_e(1:min(idx),:);
AtAngle = Athwartship_e(1:min(idx),:);
Range = Range(1:min(idx),:);
%% NOISE FLOOR BIN

[x,y]=size(Sp_noise);
k=1;
for ii = 0:binz:length(Noise_Floor_amp)-binz

        Noise_Floor_amp_binned(k,1)=nanmean(Noise_Floor_amp(ii+1:ii+(binz-
1)));     %bin noise data in Z direction

    k=k+1;
```

78

```matlab
end
Noise_Floor_amp_binned=Noise_Floor_amp_binned(isfinite(Noise_Floor_amp_binned
));
[x,y]=size(Noise_Floor_amp_binned);
for ii=1:x
%
[Param_MLE(ii)]=mle(Noise_Floor_amp_binned(ii,:),'distribution','rayleigh');
%maximum likelihood estimator
        [Noise_Param(ii,1)]=raylfit(Noise_Floor_amp_binned(ii,:));%estimate
rayleigh parameter
end
%%
[x,y]=size(Sp_plume);

for ii = 0:binz:x-binz-1
    for jj = 1:y
        AlAngle_bin(ii+1:ii+(binz),jj)=nanmean(AlAngle(ii+1:ii+(binz),jj));
        AtAngle_bin(ii+1:ii+(binz),jj)=nanmean(AtAngle(ii+1:ii+(binz),jj));
    end
end

%% synthetic seep
Sp_plume=10.^(Sp_plume/20);
wait=waitbar(0,'Please Wait...');
% figure
[x,y]=size(Sp_plume);
ii=0;
jj=0;
j=0;
for ii=0:binz:x-binz
    j=j+1;
    for jj = 1:1:y
        plume=0;
        %        Noise=0;
        plume(ii+1:ii+binz,jj)=Sp_plume(ii+1:ii+binz,jj);
        plumeloc=plume(ii+1:ii+binz,jj);
        plumeloc=plumeloc(isfinite(plumeloc));
        waitbar((ii)/(length(Sp_plume-binz)),wait,sprintf('percentage =
%2.2f', (ii/(length(Sp_plume-binz)))*100))
        n = raylrnd(Noise_Param(j),100000,1);
        n=n(isfinite(n));
        %        Noise(ii:ii+binz,jj)=Sp_noise(ii:ii+binz,jj);
        %        Noise=Noise_Floor_amp_binned(j);
        %        if kstest2(plumeloc,n)==0
        % %            plume_param(ii:ii+binz,jj)=NaN;
        %        else
        if isnan(plumeloc)==0
            for param = 0.01:.01:.5
                %            bins = .001:.001:1;
                bins = 10.^(-50:.5:0);
                s = raylrnd(param,100000,1);
                sn = s + n;

                if kstest2(plumeloc,sn)==0
                    plume_param(ii+1:ii+binz,jj)=param;
                    break
```

79

Pillsbury 2015

```matlab
                end
            end
        else
            break
        end
    end
end
close(wait)

%% figures

Sp_plume=20*log10(Sp_plume);
[x,y]=size(Sp_plume);
figure
hold on
subplot(131)
ax1=imagesc(Sp_noise(1:x,1:y));
caxis([-60 -10])
title('Noise')
ylabel('Sample #')
xlabel('Ping #')
subplot(132)
ax2=imagesc(Sp_plume);
caxis([-60 -10])
title('Plume')
subplot(133)
ax3=imagesc(plume_param);
title('Plume Rayleigh Parameters')
colorbar

figure
hold on
subplot(141)
imagesc(Sp_plume)
subplot(142)
imagesc(plume_param)
subplot(143)
imagesc(AlAngle_bin)
caxis([-128 128])
subplot(144)
imagesc(AtAngle_bin)
caxis([-128 128])

%%

[x,y]=size(plume_param);
x=length(AlAngle_bin);
AlAngle_fin=zeros(size(plume_param));
AtAngle_fin=zeros(size(plume_param));
[idx] = find(length(plume_param)>length(AlAngle_bin));
if idx == 1
    x=length(AlAngle_bin);
end
```

Pillsbury 2015

```matlab
for ii=1:x
    for jj = 1:y
        if plume_param(ii,jj)==0
            AlAngle_fin(ii,jj)=NaN;
            AtAngle_fin(ii,jj)=NaN;

        else
            AlAngle_fin(ii,jj)=AlAngle_bin(ii,jj);
            AtAngle_fin(ii,jj)=AtAngle_bin(ii,jj);

        end
    end
end

figure
hold on
subplot(141)
imagesc(Range(:,1),Range(:,2),Sp_plume)
subplot(142)
imagesc(Range(:,1),Range(:,2),plume_param)
c =colorbar;
set(c,'YColor','white')
xlabel('Ping','FontSize',14,'FontWeight','bold','Color','white')
ylabel('Depth','FontSize',14,'FontWeight','bold','Color','white')
set(gca,'Fontsize',14)
set(gca,'YColor','white')
set(gca,'XColor','white')
title('plume rayleigh params')

subplot(143)
imagesc(Range(:,1),Range(:,2),AlAngle_fin)
caxis([-128 128])
c =colorbar;
set(c,'YColor','white')
xlabel('Ping','FontSize',14,'FontWeight','bold','Color','white')
ylabel('Depth','FontSize',14,'FontWeight','bold','Color','white')
set(gca,'Fontsize',14)
set(gca,'YColor','white')
set(gca,'XColor','white')

title('Alongship Angles')
subplot(144)
imagesc(AtAngle_fin)
caxis([-128 128])
c =colorbar;
set(c,'YColor','white')
xlabel('Ping','FontSize',14,'FontWeight','bold','Color','white')
ylabel('Depth','FontSize',14,'FontWeight','bold','Color','white')
set(gca,'Fontsize',14)
set(gca,'YColor','white')
set(gca,'XColor','white')

title('Athwartship Angles')
```

81

```
% data_out = [plume_param AlAngle_fin AtAngle_fin];


end
```

And the TS_Seep_Corrector

```matlab
function [ Plume_DB, TS_Corr_Plume, Plume_DB_corr ] = TS_Seep_Corrector(
TS_corr_vq,AlAngle_fin,AtAngle_fin,Range,plume_param,Sp_plume)
%UNTITLED6 Summary of this function goes here
%   Detailed explanation goes here
% TS_corr_vq = data.TS_corr_vq;


%%
[x,y] = size(plume_param);
for ii = 1:x
    for jj = 1:y
        clear At
        clear Al
        if plume_param(ii,jj)~=0

            At = round(AtAngle_fin(ii,jj));
            Al = round(AlAngle_fin(ii,jj));
            At = 126 + At;
            Al = 126 + Al;
%             if TS_corr_vq(At,Al) > 8
%                 TS_Corr_Plume(ii,jj)=0;
%             else
                TS_Corr_Plume(ii,jj) = TS_corr_vq(At,Al);
%             end
%                     end
        end
    end
end

[x,y] = size(TS_Corr_Plume);
for ii = 1:x
    for jj = 1:y
        if TS_Corr_Plume(ii,jj) == 0
            TS_Corr_Plume(ii,jj) = NaN;
        end
    end
end


  figure,

imagesc(min(AtAngle_fin):max(AtAngle_fin),min(AlAngle_fin):max(AlAngle_fin),T
S_corr_vq)
hold all
 c=colorbar;
 title('Beam Pattern')
ylabel('Alongship')
```

82

Pillsbury 2015

```matlab
xlabel('Athwartship')
plot(AtAngle_fin,AlAngle_fin,'.k')
ylabel(c,'dB')
hold off

figure,
subplot(141)
imagesc((TS_Corr_Plume))
title('TS Corrections')
colorbar
subplot(142)
imagesc(plume_param)
title('Rayleigh paramters')
colorbar
subplot(143)
imagesc(AlAngle_fin)
title('Alongship E')
colorbar
caxis([-128 128])
subplot(144)
imagesc(AtAngle_fin)
title('Athwartship E')
colorbar
caxis([-128 128])
%% Estimate Seep Amp/dB from Rayleigh Parameters
[x,y] = size(plume_param);
for ii = 1:x
    for jj = 1:y
        clear y_dist
        clear pd
        if plume_param(ii,jj) ~=0
%                 y_dist=makedist('Rayleigh',plume_param(ii,jj));
%                 pd = pdf(y_dist,0:.01:1);
%                 [pd_max(ii,jj),var(ii,jj)] = max(pd);
            pd_mean(ii,jj) = plume_param(ii,jj) *sqrt(pi/2);
            Plume_DB(ii,jj) = 20*log10((pd_mean(ii,jj)));
            if TS_Corr_Plume(ii,jj)>8
                Plume_DB_corr(ii,jj)=0;
            else
                Plume_DB_corr(ii,jj) = Plume_DB(ii,jj)+TS_Corr_Plume(ii,jj);
            end
        end
    end
end

figure,
subplot(131)
imagesc(Plume_DB)
colorbar
caxis([-35 -20])
title('TS Uncorrected')
subplot(132)
imagesc(TS_Corr_Plume)
colorbar
title('TS Corrections')
subplot(133)
```

83

Pillsbury 2015

```matlab
imagesc(Plume_DB_corr)
colorbar
caxis([-40 -10])
title('TS Corrected')


%%
ping = 1:size(Sp_plume,2);
figure,
imagesc(ping,Range(:,2),Sp_plume)
caxis([-40 0])
c =colorbar;
set(c,'YColor','white')
xlabel('Ping','FontSize',14,'FontWeight','bold','Color','white')
ylabel('Depth [m]','FontSize',14,'FontWeight','bold','Color','white')
set(gca,'Fontsize',14)
set(gca,'YColor','white')
set(gca,'XColor','white')
title('Sp Plume','Fontsize',14,'FontWeight','bold','Color','White')

figure,
hold on

subplot(131)
imagesc(ping,Range(:,2),plume_param)
title('Rayleigh
Parameters','Fontsize',14,'FontWeight','bold','Color','White')
c =colorbar;
set(c,'YColor','white')
xlabel('Ping','FontSize',14,'FontWeight','bold','Color','white')
ylabel('Depth [m]','FontSize',14,'FontWeight','bold','Color','white')
set(gca,'Fontsize',14)
set(gca,'YColor','white')
set(gca,'XColor','white')
subplot(132)
imagesc(ping,Range(:,2),AlAngle_fin)
title('Alongship E','Fontsize',14,'FontWeight','bold','Color','White')
c =colorbar;
set(c,'YColor','white')
xlabel('Ping','FontSize',14,'FontWeight','bold','Color','white')
ylabel('Depth [m]','FontSize',14,'FontWeight','bold','Color','white')
set(gca,'Fontsize',14)
set(gca,'YColor','white')
set(gca,'XColor','white')
caxis([-128 128])
subplot(133)
imagesc(ping,Range(:,2),AtAngle_fin)
title('Athwartship E','Fontsize',14,'FontWeight','bold','Color','White')
c =colorbar;
set(c,'YColor','white')
xlabel('Ping','FontSize',14,'FontWeight','bold','Color','white')
ylabel('Depth [m]','FontSize',14,'FontWeight','bold','Color','white')
set(gca,'Fontsize',14)
set(gca,'YColor','white')
set(gca,'XColor','white')
```

Pillsbury 2015

```matlab
caxis([-128 128])

figure
subplot(131)
imagesc(ping,Range(:,2),Plume_DB)

caxis([-40 -10])
title('TS Uncorrected','Fontsize',14,'FontWeight','bold','Color','White')
c =colorbar;
set(c,'YColor','white')
xlabel('Ping','FontSize',14,'FontWeight','bold','Color','white')
ylabel('Depth [m]','FontSize',14,'FontWeight','bold','Color','white')
set(gca,'Fontsize',14)
set(gca,'YColor','white')
set(gca,'XColor','white')
subplot(132)
imagesc(ping,Range(:,2),TS_Corr_Plume)
c =colorbar;
set(c,'YColor','white')
xlabel('Ping','FontSize',14,'FontWeight','bold','Color','white')
ylabel('Depth [m]','FontSize',14,'FontWeight','bold','Color','white')
set(gca,'Fontsize',14)
set(gca,'YColor','white')
set(gca,'XColor','white')
title('TS Corrections','Fontsize',14,'FontWeight','bold','Color','White')
caxis([0 8])

subplot(133)
imagesc(ping,Range(:,2),Plume_DB_corr)
c =colorbar;
set(c,'YColor','white')
xlabel('Ping','FontSize',14,'FontWeight','bold','Color','white')
ylabel('Depth [m]','FontSize',14,'FontWeight','bold','Color','white')
set(gca,'Fontsize',14)
set(gca,'YColor','white')
set(gca,'XColor','white')
caxis([-40 -10])
title('TS Corrected','Fontsize',14,'FontWeight','bold','Color','White')


data_out = [Plume_DB TS_Corr_Plume Plume_DB_corr];
end
```
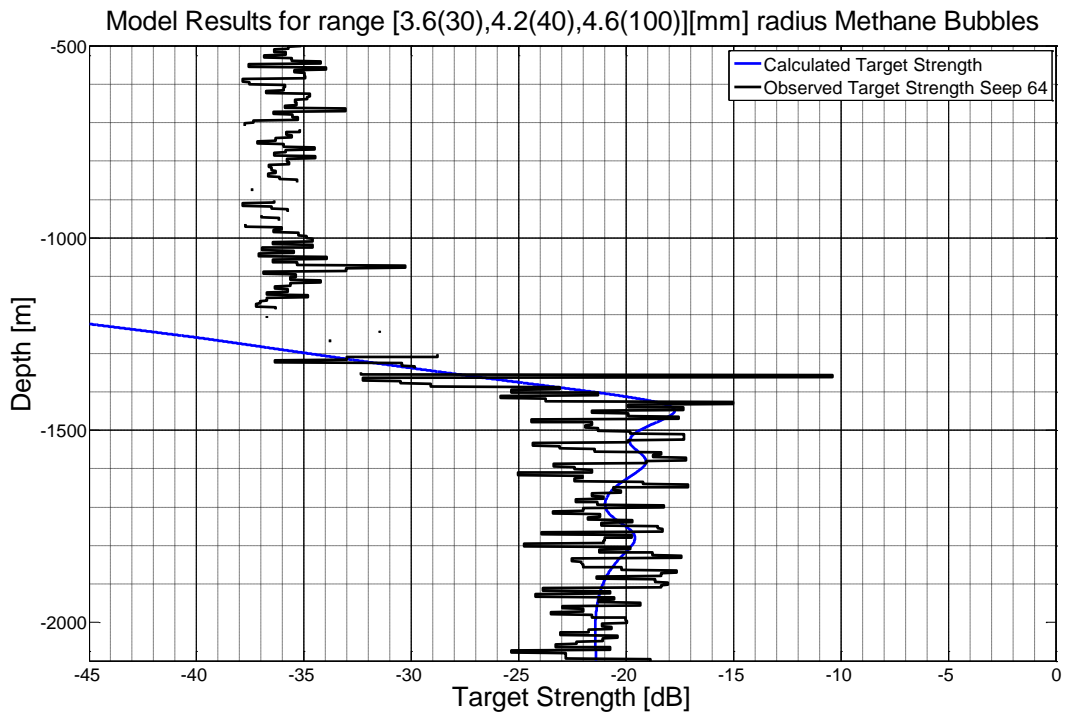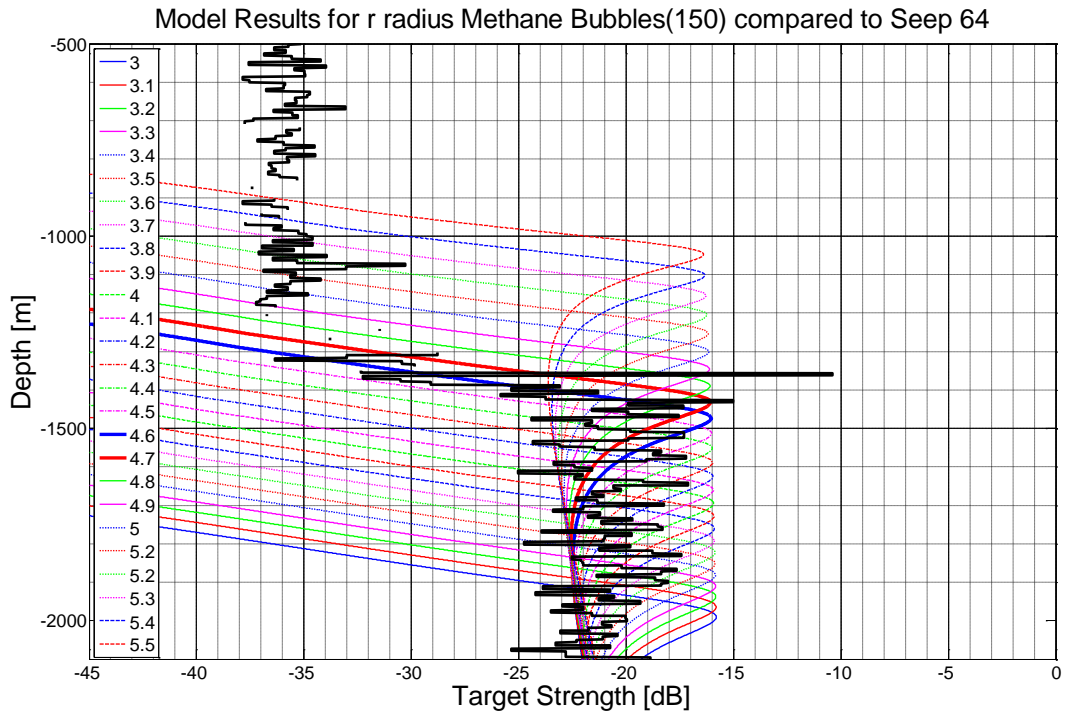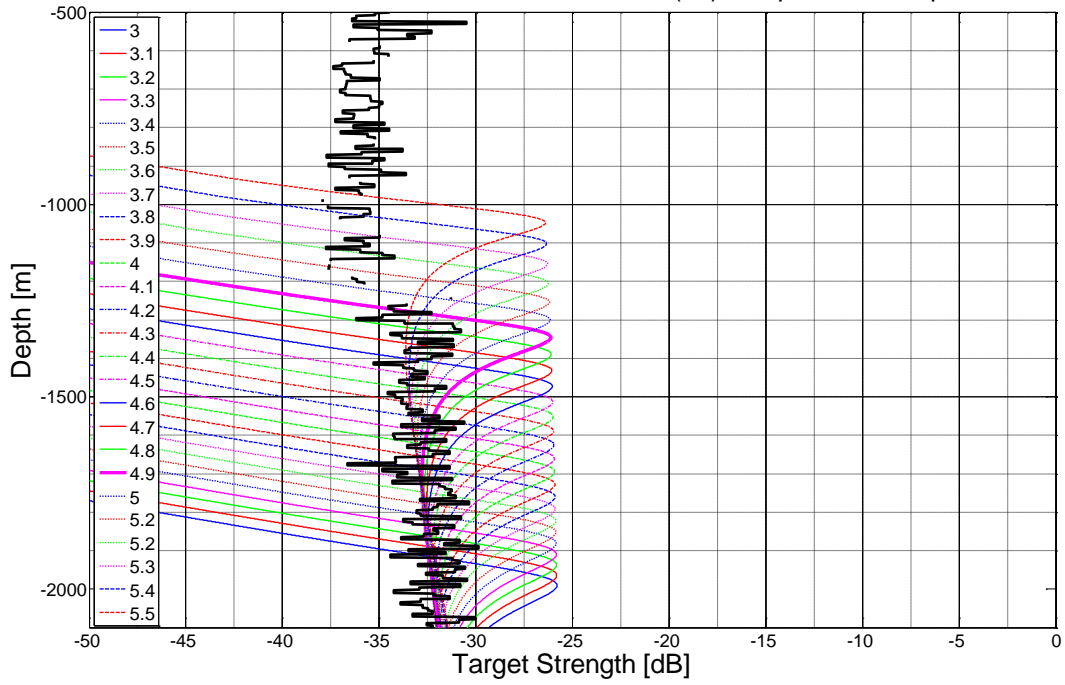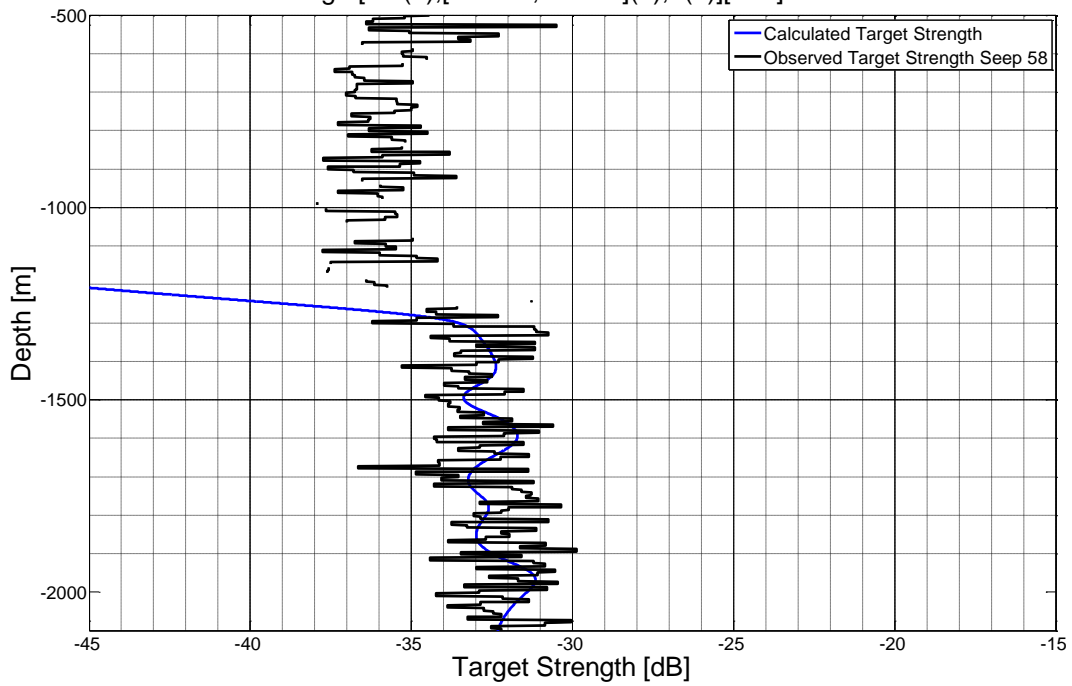
85

Pillsbury 2015

7.3 Extra examples of data/model comparisons

Model Results for r radius Methane Bubbles(150) compared to Seep 64

Model Results for range [3.6(30),4.2(40),4.6(100)][mm] radius Methane Bubbles
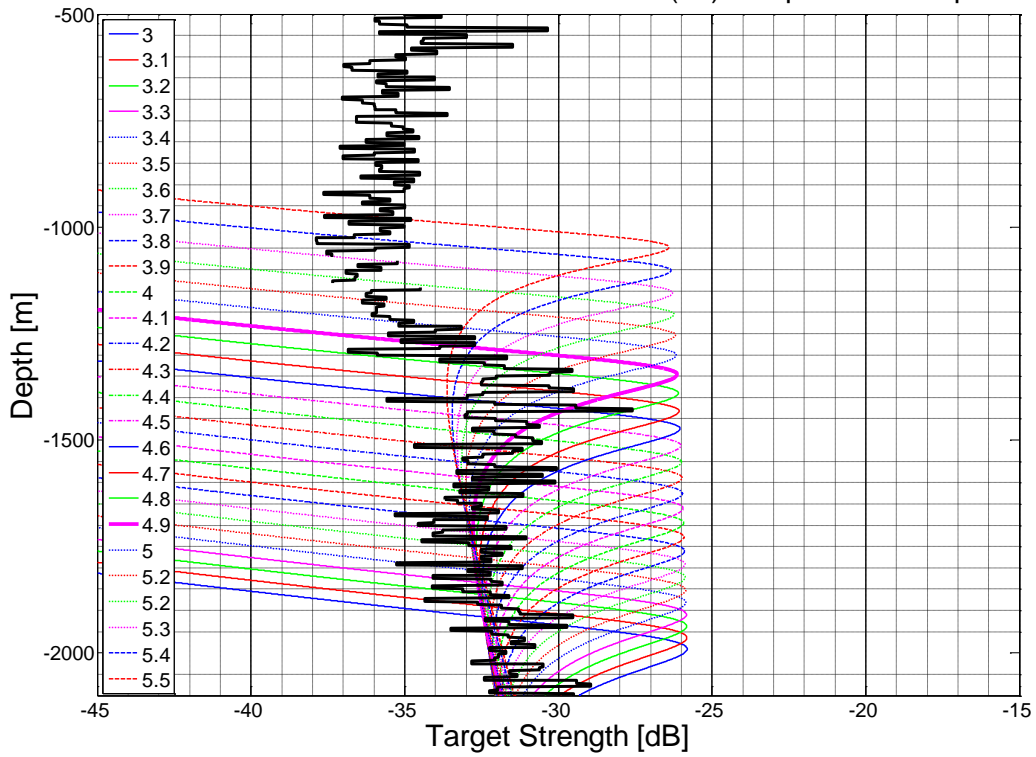
Pillsbury 2015

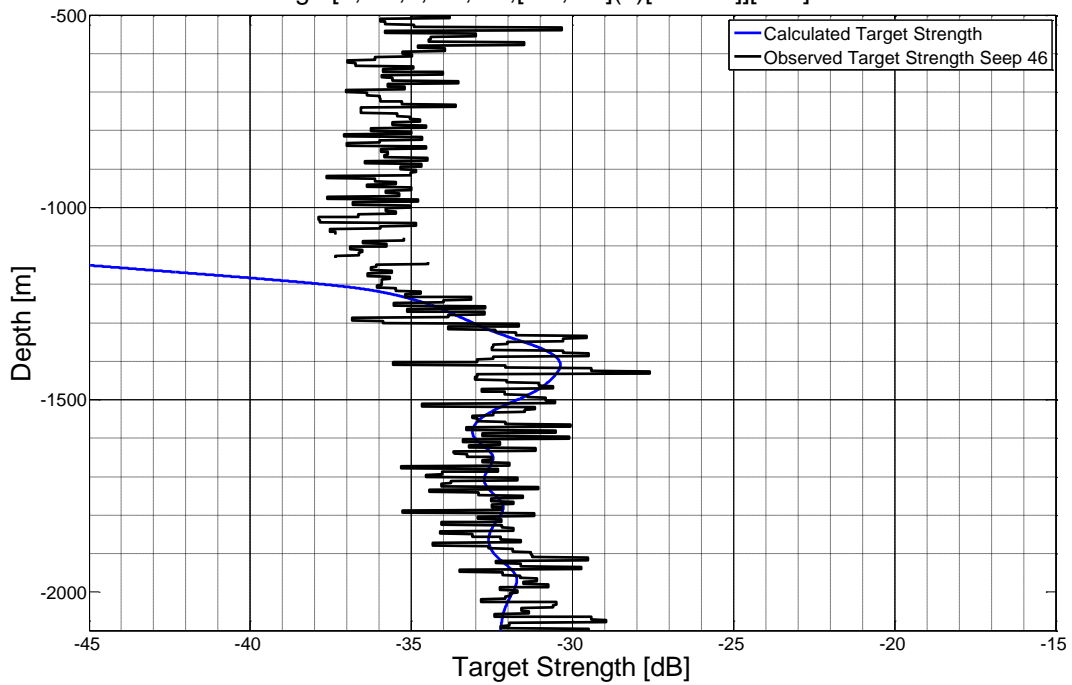## Model Results for r radius Methane Bubbles(15) compared to Seep 58

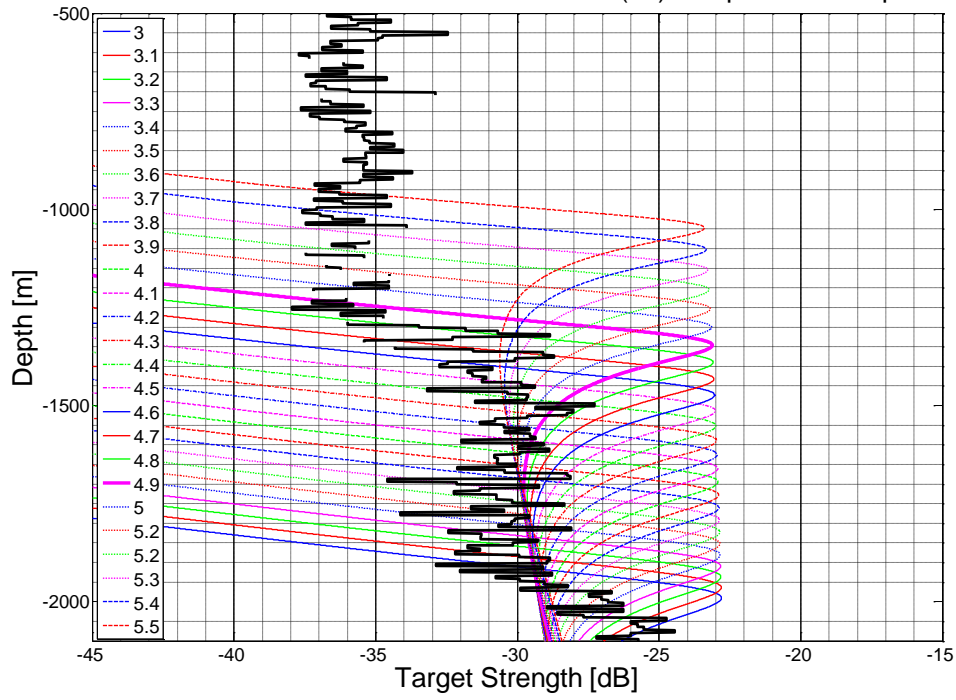## Model Results for range [3.6(2),[4.1-4.3,4.1-4.6](1),5(2)][mm] radius Methane Bubbles

87

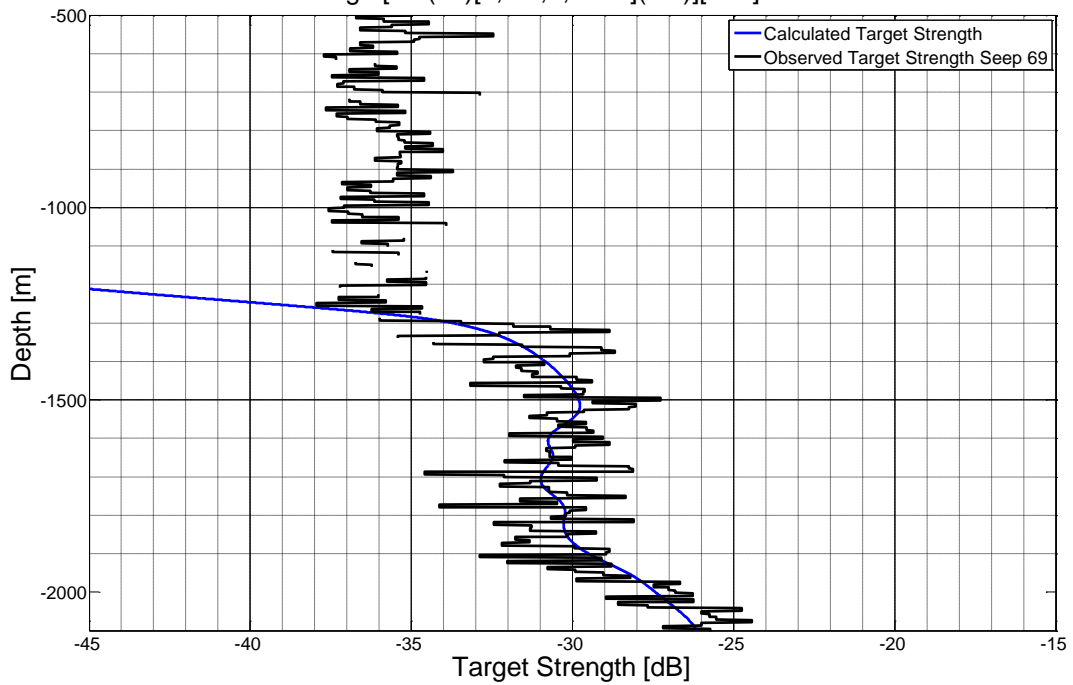## Model Results for r radius Methane Bubbles(15) compared to Seep 46

## Model Results for range [3,3.6,4,4.5,4.6,[4.7,4.8](2)[4.9-5.2]][mm] radius Methane Bubbles
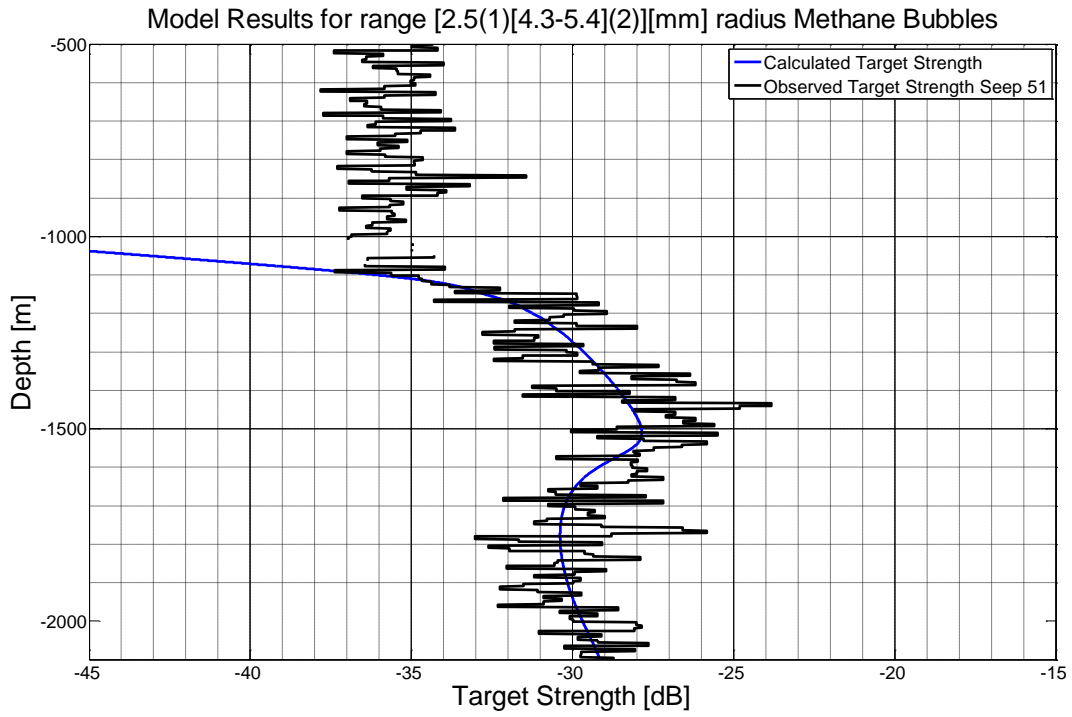
Pillsbury 2015

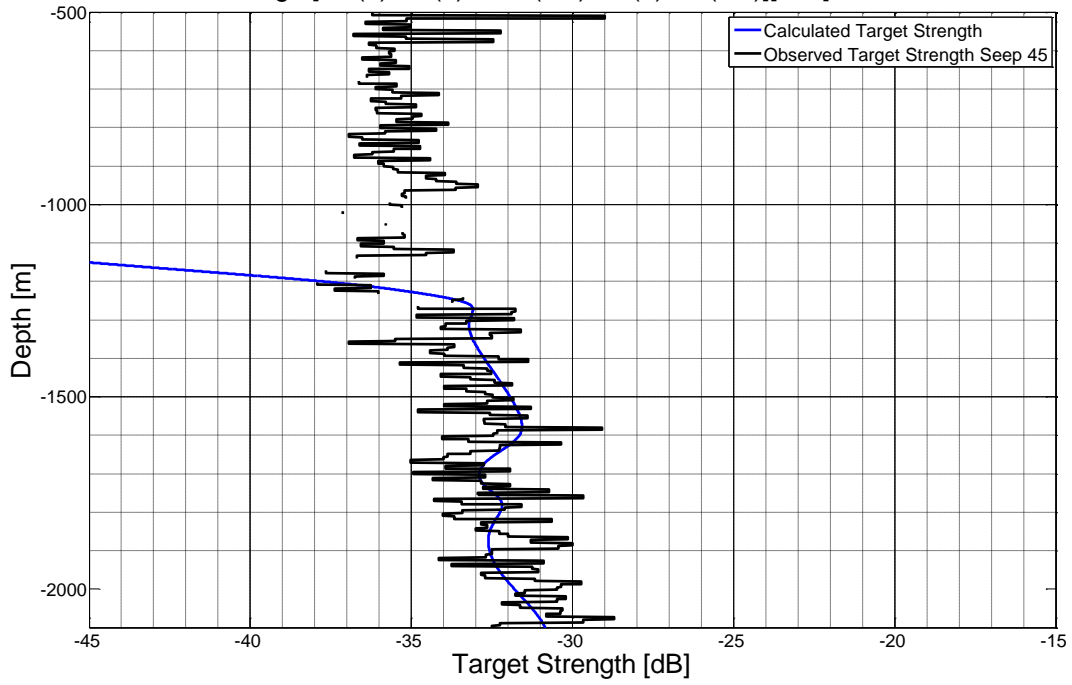Model Results for r radius Methane Bubbles(30) compared to Seep 69

Model Results for range [2.5(10)[3,3.6,4,4.3-5](1.5)][mm] radius Methane Bubbles

89

Pillsbury 2015

Model Results for range [2.5(1)[4.3-5.4](2)][mm] radius Methane Bubbles

Model Results for range [3.6(1),4.4-4.8(1),5(2),5.1(4),5.2(2),5.3(2)][mm] radius Methane Bubbles
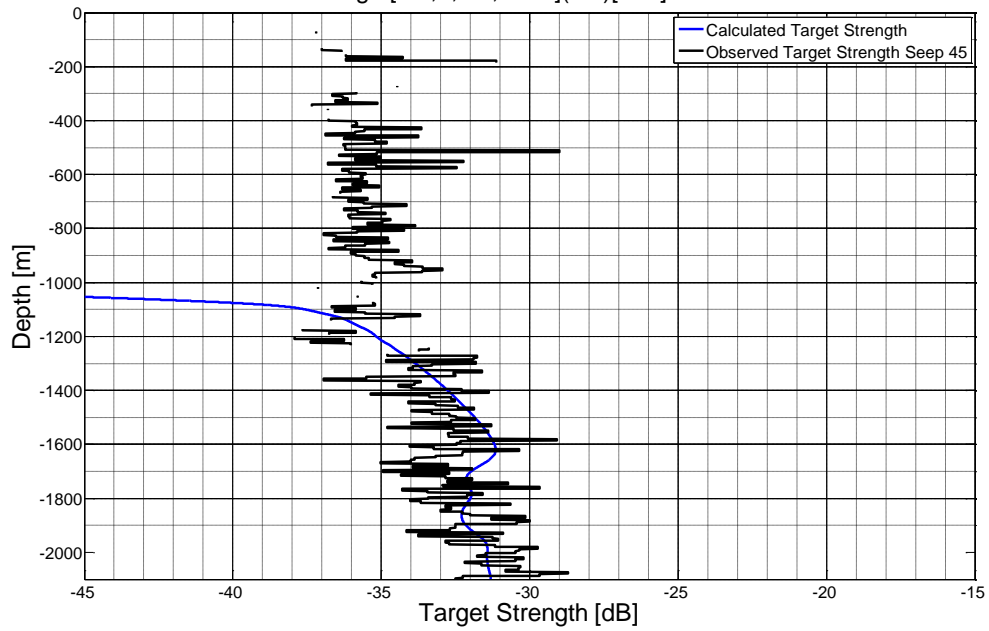
90

Pillsbury 2015
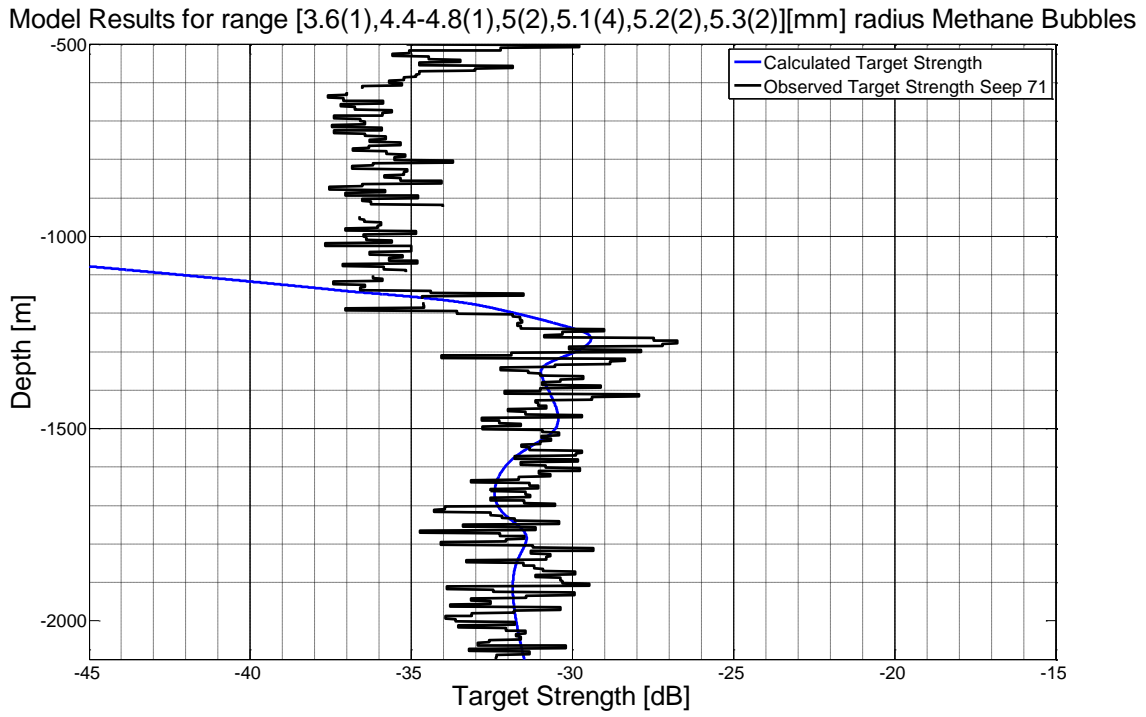
Model Results for range [2.5(2),3.6(1),4.1-5(.75),5.1(2),5.2(.75)][mm] radius Methane Bubbles

Model Results for range [2.5,3.6,4-5.5](.75)[mm] radius Methane Bubbles

91

Model Results for range [2(10),2.5(10),2.75(5),3(50)][mm] radius Methane Bubbles

Pillsbury 2015